Université de Montréal

Structural and Biochemical Characterization of VirB8 Protein in Type IV Secretion Systems

Par

Mahzad Sharifahmadian

Département de biochimie et médecine moléculaire

Faculté de médecine

Thèse présentée à la Faculté de médecine

en vue de l'obtention du grade de PhD en biochimie

July, 2017

Université de Montréal

Faculté des études supérieures

Cette thése intitulée:

Structural and Biochemical Characterization of VirB8 Protein in Type IV Secretion Systems

Présentée par:

Mahzad Sharifahmadian

a été évaluée par un jury composé des personnes suivantes:

Luis Rokeach, président-rapporteur

Christian Baron, directeur de recherche

James Omichinski, codirecteur de recherche

Lea Harrington, membre du jury

Peter Christie, examinateur externe

Bruce Allen, représentant du doyen de la FESP

Table des matiéres

Résumé

La sécrétion est le passage de macromolécules à travers les membranes cellulaires. Chez les bactéries, la sécrétion est essentielle pour la virulence et la survie. Les bactéries à Gram-négatif utilisent le système de sécrétion de type IV (SST4) pour la sécrétion de toxines et de nucléoprotéines. Les SST4 contribuent notamment à la propagation des gènes de résistance aux antibiotiques. Pour cette raison, les composants du SST4 sont des cibles potentielles pour le développement de médicaments antivirulence. Le SST4 est un complexe protéique qui s'étend entre la double membrane de la bactérie à Gram-négatif. Les protéines qui le composent sont insérées dans les membranes cellulaires ou solubles. Bien que la structure du pore central du SST4 ait été résolue récemment, les détails de l'assemblage et la structure de ce complexe ne sont pas connus. VirB8 est une protéine de la membrane interne qui interagit avec de nombreuses autres sous-unités du SST4. Il s'agit d'un acteur central de l'assemblage du SST4. Des études biophysiques, et notamment des expériences de RMN ont ainsi été réalisées pour caractériser les aspects structuraux des interactions avec VirB8. Des regions dynamiques dans la structure de VirB8 ont été identifiées par spectroscopie RMN lors de la transition entre la forme monomérique et dimérique. Les analyses de cristallographie et de RMN ont révélé des différences structurales dans les régions hélicoïdales (α1 et α4) de VirB8 *wild-type* et du variant monomérique VirB8^{M102R}. Le criblage de fragments a permis d'identifier de petites molécules capables de se lier à VirB8 ainsi qu'au variant monomérique. Les analyses d'arrimage moléculaire *in silico* suggèrent que la rainure de surface dans la structure VirB8 est importante pour laliaison de ces petites molécules. Les expériences de RMN et les essais biochimiques révèlent que le feuillet β (β1 en particulier) constitue l'interface d'interaction entre VirB8 et

VirB10. Cette interface d'interaction est d'ailleurs importante pour la conjugaison du SST4. De plus, j'ai identifié des changements dans la structure de VirB8 lors de l'interaction avec VirB5. Les études sur la protéine VirB8 nous ont permis de caractériser la séquence d'événements entre VirB8 et d'autres protéines VirB, régulant l'assemblage et la fonction du SST4.

Mots clés: le système de sécrétion de type IV, résistance aux antibiotiques, VirB8, RMN, cristallographie

Abstract

Secretion is the passage of macromolecules across cellular membranes. In bacteria, secretion is essential for virulence and survival. Gram-negative bacteria use specialized envelope-spanning multiprotein complexes to secrete macromolecules called type IV secretion system (T4SS). T4SSs mediate the secretion of monomeric proteins, multisubunit protein toxins and nucleoprotein complexes. Also, they contribute to the horizontal spread of plasmid-encoded antibiotic resistance genes. Consequently, they are potential targets for antivirulence drugs. Gram- negative bacteria have two membranes that the secretion complex spans. As a result, the T4SS consists of proteins inserted in the membranes and of soluble proteins that face into or out of the bacterial cell. The details of channel assembly and structure are not known, although recent advances have revealed the structure of the core secretion channel. VirB8 is an inner membrane protein of the complex that interacts with many other T4SS subunits and works as nucleation factor for T4SS channel assembly. Biophysical studies and NMR experiments in particular were conducted to characterize the structural aspects of VirB8 interactions. Dynamic regions of VirB8 during monomer-to-dimer transition were identified by NMR spectroscopy. X-ray crystal and NMR analyses revealed structural differences at the helical regions (α-1 and α-4) of wild-type VirB8 and its monomeric variant VirB8^{M102R}. Fragment screening identified small molecules binding to the wild-type and monomeric variant. *In silico* docking analyses suggested that the surface groove in the VirB8 structure is important for effective binding of the small molecules. NMR experiments and biochemical assays demonstrated that the β-sheet domain (β1 in particular) is the binding interface of VirB8 for the interaction with VirB10. The identified interface has functional importance for T4SS-mediated conjugation. In addition, I

8

used NMR spectroscopy to identify changes in the structure of VirB8 upon interaction with VirB5. Altogether, structural and biochemical studies on periplasmic and full length VirB8 enabled us to characterize the sequence of interactions between VirB8 and other VirB proteins during T4SS complex assembly and function. The results of this research may lead to an innovative strategy for the development of novel antimicrobial drugs.

Liste des figures

Figure 18. Cartoon representation of the VirB8sp dimer in complex with 2-(butylamino)-8-quinolinol, the dimerization inhibitor.

Figure 19. Surface plasmon resonance (SPR) analysis of VirB8sp.

Figure 20. The structure of B8I-2 a salicylidene acylhydrazide and Fragment II a salicylanilide.

Figure 21. Mapping of chemical shift changes of VirB8sp in the presence of VirB5s.

Figure 22. A model for the dynamics of VirB8 during T4SS assembly.

Liste des abréviations

ABC transporter ATP-binding cassette transporter

B. suis   *Brucella suis*

BMRB   Biological Magnetic Resonance Bank

BTH   Bacterial two hybrid assay

CFU   Colony forming units

CHAPS   3-[(3-Cholamidopropyl)dimethylammonio]-1-propanesulfonate

CSI   Chemical shift index

CTD   C-terminal domain

DMSO   Dimethyl sulfoxide

DSF   Differential scanning fluorimetry

ECM   Extracellular matrix

E. coli   *Escherichia coli*

ENP   Extracellular nucleation-precipitation

GlcNAc   N-acetylglucosamine

Gsp   General secretory pathway

HCM   Host cell membrane

HEPES   4-(2-hydroxyethyl)-1-piperazineethanesulfonic acid

H. pylori   *Helicobacter pylori*

HSQC   Heteronuclear single quantum correlation

IM   Inner membrane

IMC   Inner membrane component

IPTG	Isopropyl β-D-1-thiogalactopyranoside
IRIC	Institut de Recherche en Immunologie et Cancérologie
LB	Luria broth
MFP	Membrane fusion protein
MurNAc	N-acetylmuramic acid
NEB	New England Biolabs
NMR	Nuclear magnetic resonance
NTD	N-terminal domain
OM	Outer membrane
ONPG	2-nitrophenyl-β-D-galactopyranoside
PDB	Protein Data Bank
RND	Resistance–nodulation–division
SPR	Surface plasmon resonance
T1SS	Type 1 secretion system
T2SS	Type 2 secretion system
T3SS	Type 3 secretion system
T4SS	Type 4 secretion system
T4ASS	Type 4A secretion system
T4BSS	Type 4B secretion system
T5SS	Type 5 secretion system
T6SS	Type 6 secretion system
T7SS	Type 7 secretion system
T8SS	Type 8 secretion system

Tm	Melting temperature
VirB8s	VirB8 from *Brucells suis*
VirB8sp	Periplasmic domain of VirB8 from *Brucells suis*
WHO	World health organization

Acknowledgements

First and foremost, I would like to thank my family and friends for their undying support and encouragement over the years. I thank my supervisor Dr. Christian Baron for his support and his scientific insights, which has been instrumental in my progress as a graduate student. I thank my co-supervisor Dr. James Omichinski for his generous support and would also like to thank my past and present colleagues and collaborators for their support, without whom none of the work that I have accomplished during my Ph.D. would have been possible.

Chapter 1: Introduction

1.1   Secretion systems in bacteria

Secretion is a process of transporting molecules across biological membranes and bacteria have developed several ways to secret molecules from the cytoplasm into the environment, into other bacteria or eukaryotic host cells. Bacterial secretion is accomplished using multiprotein complexes called secretion systems and bacteria use these systems to secrete different type of substrates including small molecules, proteins, nucleoprotein-complexes and DNA. These substrates play roles in adaptation to the environment, adhesion to cells or abiotic surfaces, survival and pathogenicity of bacteria (Marlovits et al., 2009; Alvarez-Martinez & Christie, 2009; Mudrak et al., 2010; Rambow-Larsen et al., 2009). Transfer of virulence factors to host cells also depends on secretion systems and some other secretion systems are involved in transfer of antibiotic resistance genes between bacteria. There are eight known classes of secretion systems in Gram-positive and Gram-negative bacteria and these secretion systems differ based on their localization in cellular compartments, overall structure as well as their mechanism of function (Desvaux et al., 2009; Green & Mecsas, 2016; Costa et al., 2015).

1.2 Types of secretion systems

Secretion systems are categorized based on their genomic organization and overall sequence similarity and eight types of bacterial secretion systems have been identified. Gram-positive and Gram-negative bacteria have different types of cell envelopes (Fig. 1) and as a result of this difference their secretion system architecture is different (Gerlach & Hensel, 2007; Lycklama & Driessen, 2012; Palmer & Berks, 2012).
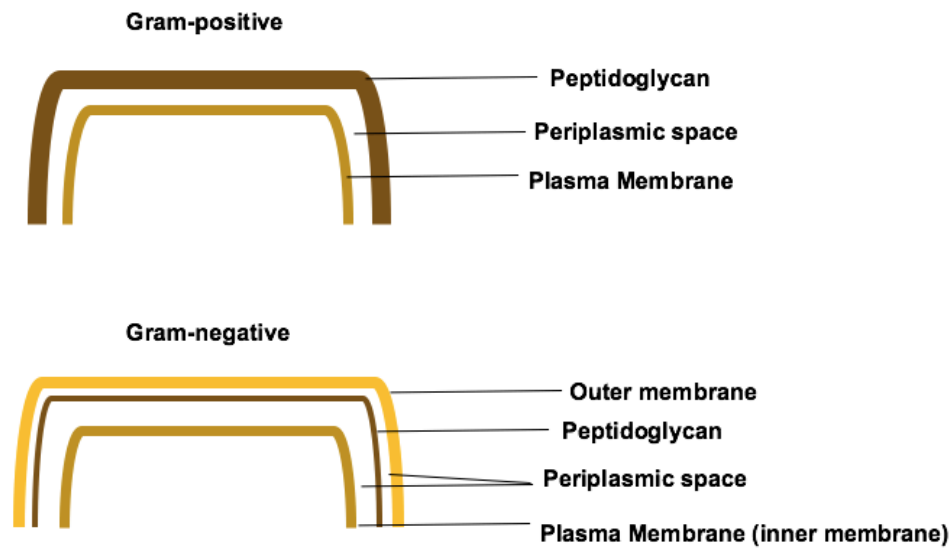
Figure 1. Schematic representation of cell wall composition in Gram-positive and Gram-negative bacteria. The outer membrane in Gram-negative bacteria includes lipopolysaccharides and proteins.

The differences in the organization of the cell envelope result in two major categories of secretion system complexes in bacteria. In the first group, the secretion complex spans both inner and outer membranes, which includes type I secretion system (T1SS), T2SS, T3SS, T4SS and T6SS. In the second group, the secretion system complex locates in the outer membrane, and this is observed in the type V secretion systems (T5SS) (Desvaux et al., 2009). In addition to T5SS, the bacterial chaperone–usher secretion system locates at the outer membrane, where it assembles non-flagellar cell surface appendages identified as type 1 and P pili (Fig. 2). These multiprotein appendages are involved in virulence and biofilm formation of Gram-negative bacteria through host cell recognition and adhesion (Wright, Seed, & Hultgren, 2007;

Lillington, Geibel & Waksman, 2014 ; Hospenthal, Costa & Waksman, 2017). The T7SS have been found only in Gram-positive bacteria such as *Mycobacterium* and *Staphylococcus*. Despite the fact that they are Gram-positive, the cell envelope structure of mycobacteria is similar to that of Gram-negative bacteria and the T7SS complex spans the entire envelope (Houben, Korotkov & Bitter, 2014). Finally, T8SS also called the extracellular nucleation-precipitation (ENP) pathway in Gram-negative bacteria mediates the biogenesis of fimbriae. Fimbriae are cell appendages involved in cell-to-surface attachment of bacteria (Gibson, White, Rajotte & Kay, 2007; Hospenthal, Costa & Waksman, 2017).
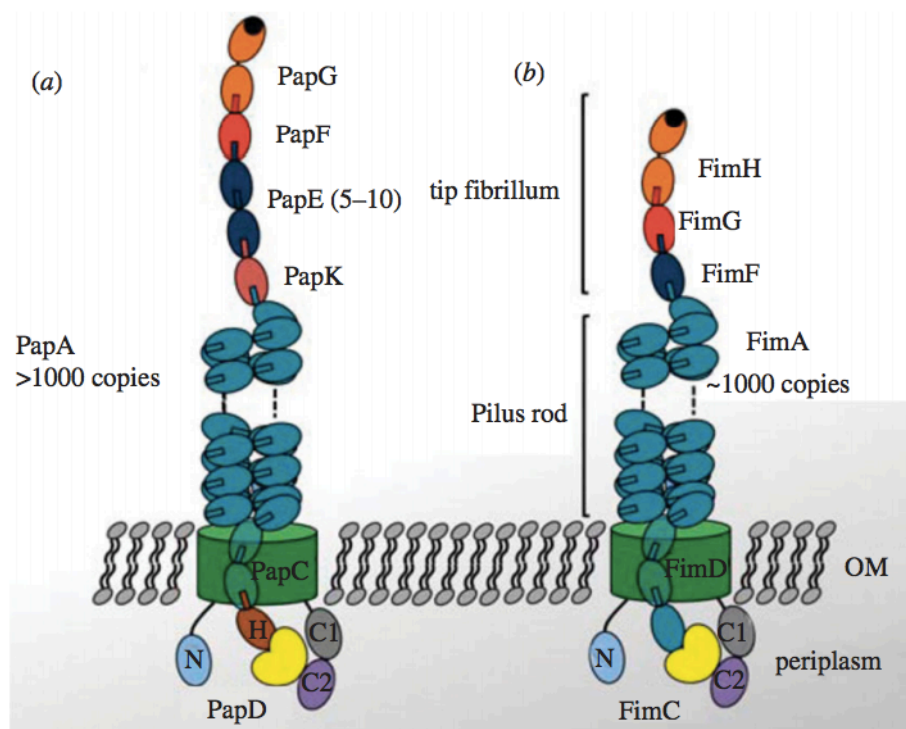
Figure 2. A schematic representation of (a) P and (b) type 1 pili assembled by chaperone-usher pathways; the Pap and Fim systems. The chaperones are located in the periplasm and shown in

yellow. The periplasmic N-terminal and C-terminal domains of the usher are labelled as N and C, respectively. The image is adapted from (Busch & Waksman, 2012).

1.2.1 Type I secretion systems

Type I secretion systems secrete substrates from the cytoplasm into the extracellular environment. The T1SS complex is composed of an inner membrane component (IMC), which is an ATP-binding cassette transporter (ABC transporter), a periplasmic protein identified as membrane fusion protein (MFP) and TolC, an outer membrane protein channel (Fig. 3). Hydrolysis of ATP mediated by the T1SS ABC transporter energizes the translocation of substrates through the complex (Balakrishnan, Hughes & Koronakis, 2001). The architecture of T1S systems is closely related to the resistance–nodulation–division (RND) family of multidrug efflux pumps. The RND efflux complexes pump molecules out of the cell and are important for antibiotic resistance in Gram-negative bacteria (Murakami, Nakashima, Yamashita & Yamaguchi, 2002; Piddock, 2006; Nakashima, Sakurai, Yamasaki, Nishino & Yamaguchi, 2011). Recently, a cryo-EM structure of a complete T1SS complex was determined at 16Å resolution (Du et al., 2014). The EM structure revealed a continuous channel and confirmed the double-membrane-spanning model for T1SS. Fitting the X-ray crystal structures of subunits into the EM envelope suggested that the complex has a 3-6-3 stoichiometry for IMC, MFP and TolC, respectively (Fig. 3).
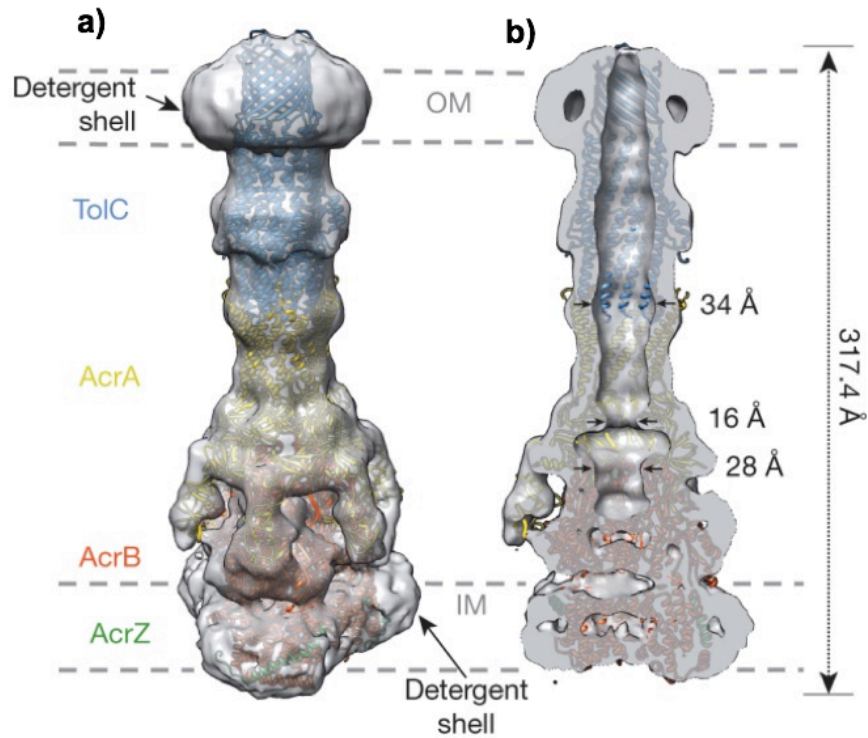
Figure 3. A pseudo-atomic model of the AcrAB–TolC multidrug efflux pump. a) An electron microscopy map of the AcrA–AcrB–TolC RND efflux pump fitted using X-ray structures of subunits TolC (PDB code: 2XMN), AcrA (PDB code: 2F1M) and AcrB (PDB code: 4CDI). AcrA is a membrane fusion protein (MFP). b) View through the reconstruction and model showing the continuous channel through the cell wall. The image is adapted from (Du et al., 2014).

1.2.2 Type II secretion systems

Type II secretion systems are double-membrane spanning complexes composed of 12 to 15 components. T2SS are found in Gram-negative bacteria and secrete substrates from the

periplasm into the extracellular environment. T2SS secretes a diverse array of substrates important for pathogenicity and survival in either the host or for adaptation to various environments (Nivaskumarm & Francetic, 2014). Secretion through T2SS occurs in two steps. First, the substrate is transferred into the periplasm by inner membrane translocation systems (Sec or Tat). In the second step, the substrate is translocated to the outer membrane or into the extracellular space by the T2SS complex. A cryo-EM structure of a T2SS outer membrane complex from *Vibrio cholera* at 19Å resolution is available and consists of a dodecameric structure with a channel at the center, which contains a periplasmic gate (Fig. 4a). The GspD protein, the main component of the outer membrane complex, forms a vestibule on the periplasmic side of the channel which binds to exoproteins and to the tip of the T2SS pseudopilus. On the extracellular side a chamber with a cap structure is detected (Fig. 4b). Despite the fact that most of the T2SS components have been characterized individually, the stoichiometry of several protein components is not known, and the structures of the inner membrane complex and of the cytoplasmic compartment of the T2SS system have not been determined yet (Korotkov, Sandkvist & Hol, 2012; Nivaskumarm & Francetic, 2014).
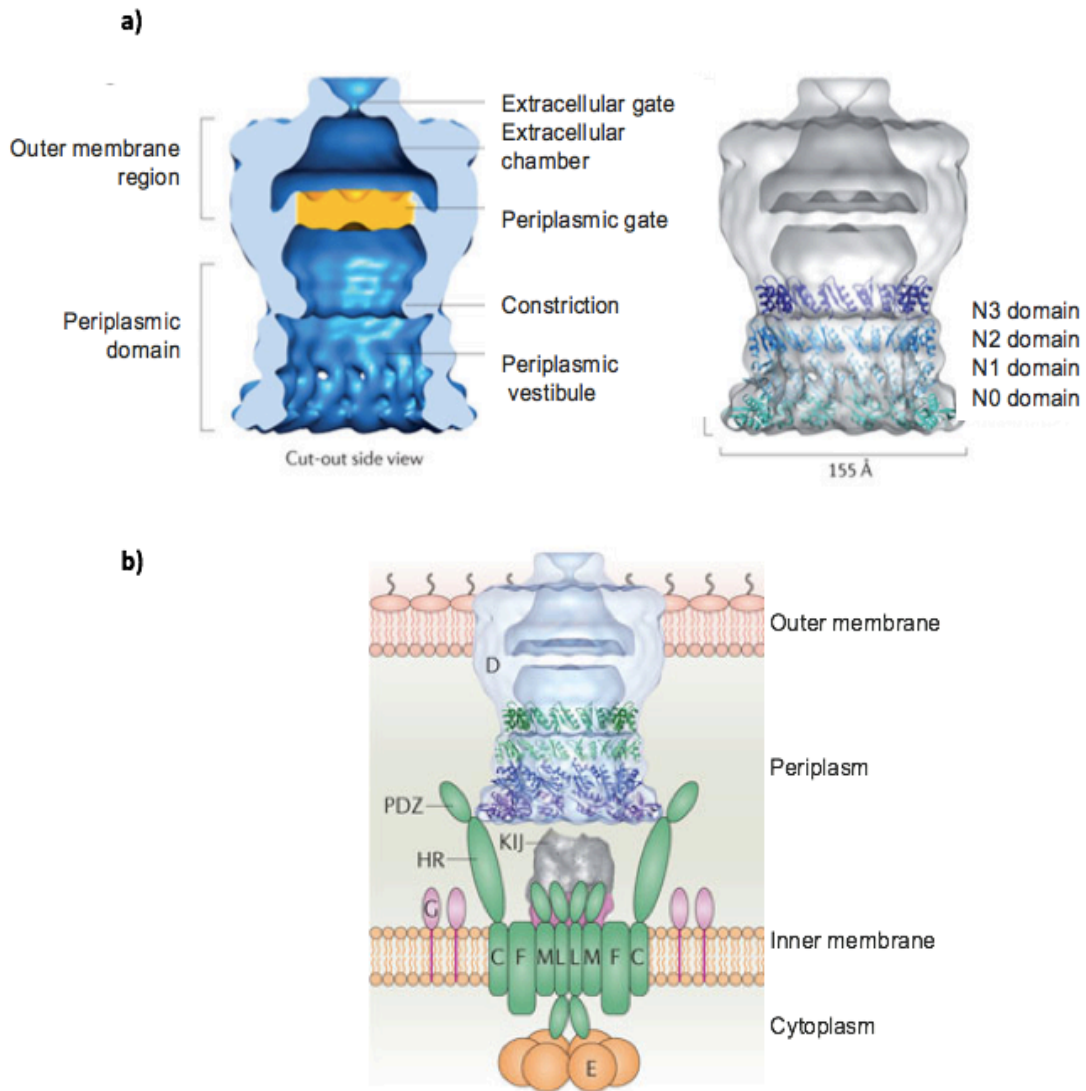
Figure 4. Structural architecture of type II secretion system complex. a) Cryo-EM reconstruction of the *Vibrio cholerae* T2SS secretin GspD. The slice view through the channel (left panel) shows the periplasmic vestibule, a constriction, the periplasmic gate, an extracellular chamber and an extracellular gate. The right panel shows the fit of the ring models for the N-terminal domains of GspD in the structure. Image adapted from (Reichow, Korotkov, Hol & Gonen, 2010). b) A molecular model of the type II secretion system. General secretory pathway (Gsp) proteins are labelled with their capital-letter identifiers. Components are presented as secretion ATPase (E) in orange, the inner-membrane protein platform in green, the

pseudopilus (KIJ) in silver, the major pseudopilin (G) in pink and the outer-membrane secretin (D) channel in blue, cyan and purple. Image adapted from (Korotkov, Sandkvist & Hol, 2012).

1.2.3 Type III secretion systems

Type III secretion systems mediate the transfer of virulence proteins into the cytoplasm of eukaryotic target cells. Various Gram-negative animal and plant pathogens use T3SS to secrete their effector proteins (Mota & Cornelis, 2005). The T3SS is a multiprotein complex that spans the entire cell envelope forming a syringe-like structure with an extracellular needle-like appendage that are collectively responsible for the delivery of effector proteins (Kubori et al., 1998; Blocker et al., 2001; Deng et al., 2017). An intact and *in situ* structure of a T3SS secretion complex from *Chlamydia trachomatis* was reported in free state and after contact with host cells using cryo-electron tomography (Fig. 5). The study revealed coordinated changes in the T3SS compartments comprising needle, basal body and cytoplasmic sorting–ATPase complex. The analysis suggested that the T3SS complex works as a molecular syringe and the basal body will tightly pack when the needle tip contacts the host cell membrane. This compaction is coupled to stabilization of the cytosolic sorting platform–ATPase and eventually will initiate transfer of the substrates into the complex for secretion (Nans et al., 2015).
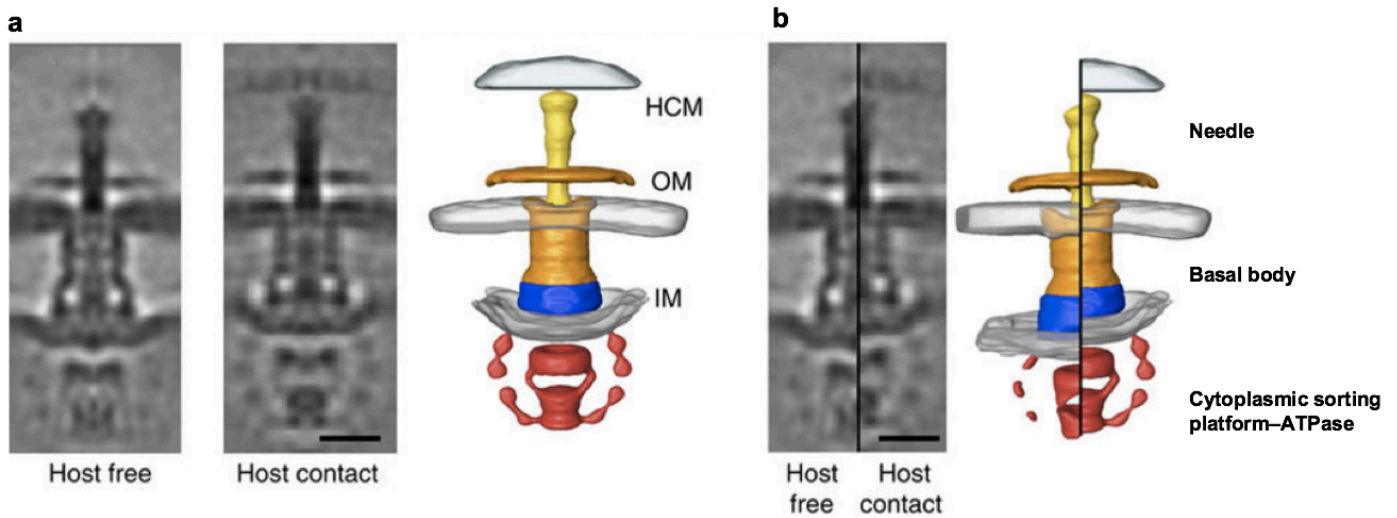
Figure 5. *In situ* structure of host free and host-contact *Chlamydia* T3SS. a) *In situ* cryo-electron subtomogram averages of the *Chlamydia trachomatis* T3SS and the corresponding three-dimensional surface rendering model (right). Outer (OM), inner (IM) and host membranes (HCM) are indicated along with type III secretion complex. b) Comparison of host-free and host-contact *Chlamydia* T3SSs and the corresponding renderings models. The T3SS compartments are labelled on the model (right). Scale bars are 15 nm. The image is adapted from (Nans et al.*,* 2015).

1.2.4 Type IV secretion systems

The type IV secretion system (T4SS) spans across the inner and outer membranes to transfer a variety of substrates into host cells. In addition to protein substrates, T4SS are the

only secretion systems that translocate DNA and DNA-protein complexes across the cell envelope. T4SS are also involved in conjugative transfer of plasmids and play an important role for spreading antibiotic resistance genes (Kuldau, De Vos, Owen, McCaffrey & Zambryski, 1990; Alvarez-Martinez & Christie, 2009). The T4SS will be discussed in detail in the following sections.

1.2.5 Type V secretion systems

Type V secretion systems span only one membrane and are involved in transport of virulence factors across the outer membrane. They comprise a β-barrel domain forming a pore for the secretion of the effector proteins. Those are part of the secretion system that is also called "autotransporter" for this reason. Since T5SSs locate in the outer membrane the substrates are first transported across the inner membrane into the periplasm, e.g. by the Sec transport system. T5SSs can be divided into three groups based on the number of protein components: type Va pathway, type Vb or two-partner secretion pathway, and type Vc (AT-2) pathway (Fig. 6). The type Va system is encoded on one transcript and it contains all the necessary domains for secretion including its proper Sec signal sequence, a passenger domain, a linker domain and a β-barrel domain. The passenger domain either protrudes or gets released outside of the cell. In the case of two-partner secretion systems, one of the proteins contains the β-barrel domain and the other protein is the secreted protein. For the type Vc systems, translocation to the outer membrane occurs following trimerization of the subunits and the C-terminal regions form the β-barrel domain of the pore (Roggenkamp, 2003; Henderson, Navarro-Garcia, Desvaux, Fernandez & Ala'Aldeen, 2004; Leo, Grin& Linke, 2012; Roman-Hernandez, Peterson & Bernstein, 2014).
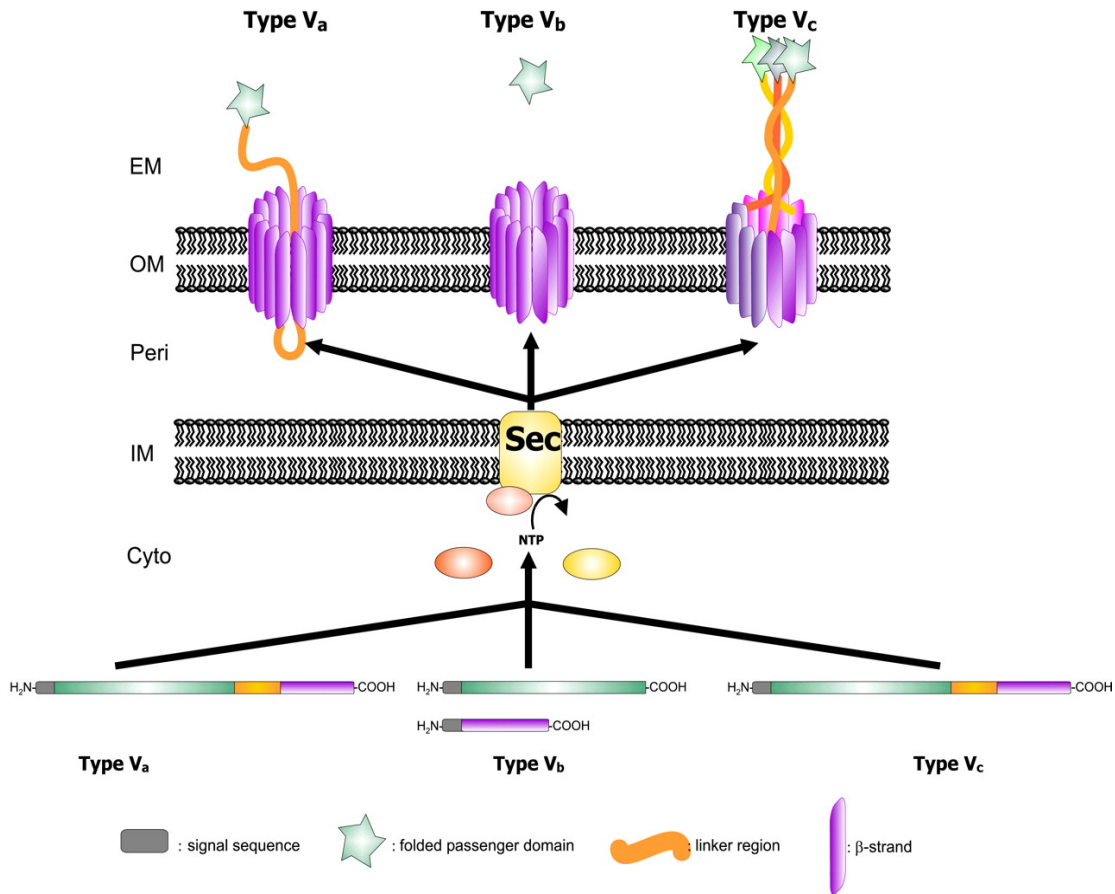
Figure 6. A schematic diagram of the type V autotransporter secretion systems. The autotransporter secretion (type Va) on the left, the two-partner system (type Vb), and the type Vc or AT-2 family is depicted on the right. The functional domains of the proteins are shown: the N-terminal Sec signal sequence, the passenger domain, the linker region, and the β-barrel domain. The translocation of the the autotransporter proteins through the cytoplasm are mediated by the Sec machinery. The β-barrel domain forms a pore in the outer membrane. After the pore formation, the passenger domain inserts into the pore and is translocated to the

cell surface where it may undergo further processing. The image is adapted from (Henderson, Navarro-Garcia, Desvaux, Fernandez & Ala'Aldeen, 2004).

1.2.6 Type VI secretion systems

Type VI secretion systems span the cell envelope and are involved in the secretion of virulence factors to host cells. The T6SS are mainly found in Gram-negative proteobacteria (Boyer, Fichant, Berthod, Vandenbrouck & Attree, 2009). The T6SS consists of an inner-membrane complex and a tubular tail, which is similar to bacteriophage tail assembly complexes and it extends across the cell and into the cytoplasm (Ma, Lin & Lai, 2009; Ho, Dong & Mekalanos, 2014; Cianfanelli, Monlezun & Coulthurst, 2016). A cryo-electron microscopy structure of the cytoplasmic core of the tail (sheath) domain of the *Vibrio cholera* T6SS suggests that the mechanism of T6SS secretion across membranes is similar to the mechanism of contraction of phage tails (Kube et al*.,* 2014). The sheath domain contracts, propels the tubular tail across the cell wall towards the target cell and induces membrane perforation for delivery of the effector proteins. Upon effector protein delivery into the target cell, the contracted sheath will disassemble which is mediated by cytoplasmic ATPase ClpV (Fig. 7) (Cianfanelli, Monlezun & Coulthurst, 2016).
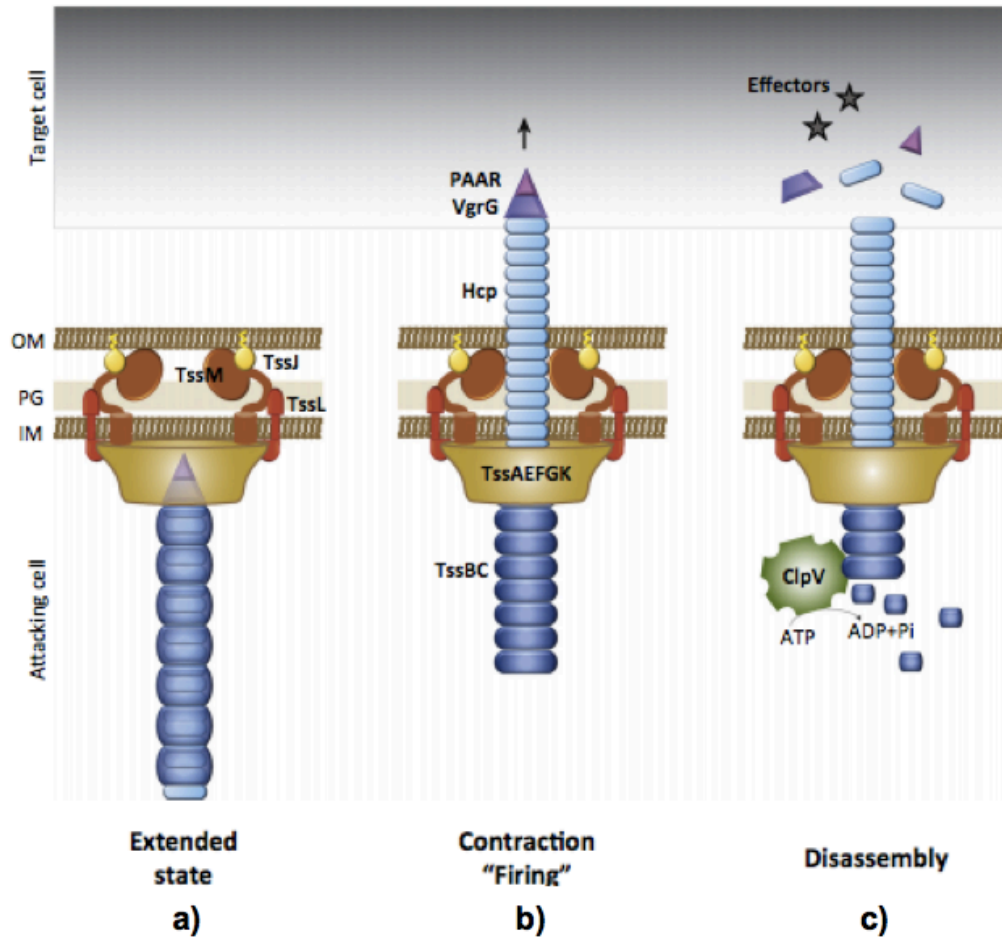
Figure 7. Schematic representation of virulence factor secretion into target cells by the T6SS complex. a) In the extended state, the protein complex (sheath, blue) is assembled from cytoplasmic and membrane components. b) At the second step, the sheath contracts moving the elongated inner tubular structure (light blue) towards the target cell and breaches the membrane. c) The contracted sheath will be disassembled by ClpV (green) when the effector proteins are delivered. The image is adapted from (Cianfanelli, Monlezun & Coulthurst, 2016).

1.2.7 Type VII secretion systems

Type VII secretion systems (T7SS) were first identified in mycobacteria and are essential for their virulence (i.e. *Mycobacterium tuberculosis*). *Mycobacterium* species have unique cell envelopes consisting of an inner membrane, a periplasmic space and a highly hydrophobic outer membrane that contains mycolic acids a major component (Stanley, Raghavan, Hwang & Cox, 2003). The T7SSs consist of a cytoplasmic apparatus that mediates delivery of the substrates to the secretion complex, a highly conserved inner membrane core complex, a membrane-bound protease with a periplasmic domain (MycP), which associates with the core complex to process substrates and an outer membrane channel for secretion of the substrates (Fig. 8) (Korotkova et al., 2014; Houben, Korotkov & Bitter, 2014).
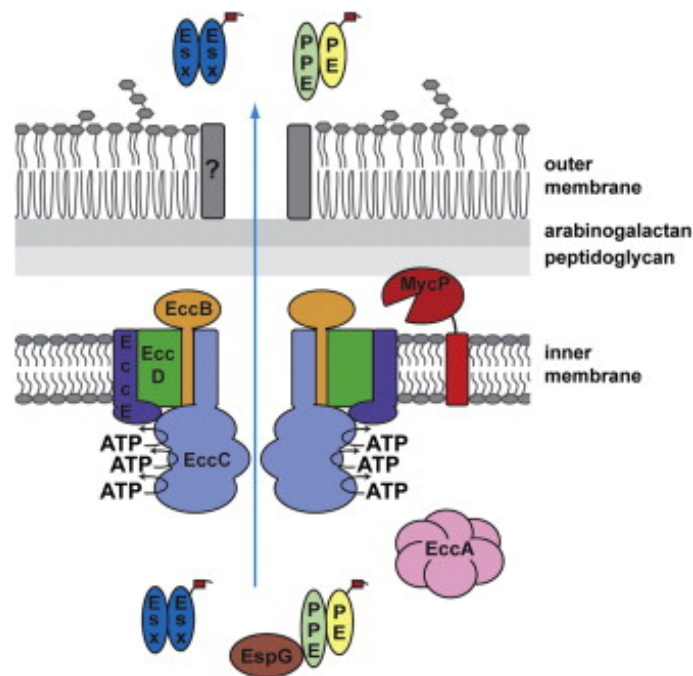
Figure 8. A model for type VII secretion system from *Mycobacterium*. Esx and PE/PPE proteins are substrates, EspG is a cytoplasmic component involved in recognition and translocation of the substrates into the complex. EccB, EccC, EccD and EccE are the inner-membrane components. The EccC protein with three nucleotide binding domains is likely energizing translocation of substrates through the complex. Components of the outer membrane complex are still not defined. The figure is adapted from (Houben, Korotkov & Bitter, 2014)

1.2.8 Type VIII secretion systems

The final system, the type VIII secretion system (T8SS), also called the extracellular nucleation-precipitation pathway, is comprised of surface protein assemblies that mediate adhesion to surfaces and biofilm formation. These assemblies are called curli (fimbriae) (Austin, Sanders, Kay, & Collinson, 1998). In biofilm formation, the bacterial population embeds in an endogenously produced extracellular matrix (ECM), which enables adhesion to abiotic (e.g. glass) or biotic surfaces (e.g. epithelial cells). The ECM is generally comprised of polysaccharides, proteins, and nucleic acids and curli fibers are the main protein component (Adcox et al., 2016). The curli subunits form a channel in the outer membrane that is open toward the periplasm (Fig. 9). The curli major and minor subunits (CsgA and CsgB) nucleate on the outer membrane complex and one is oriented toward the extracellular environment (Hammer et al., 2012; Hospenthal, Costa & Waksman 2017).
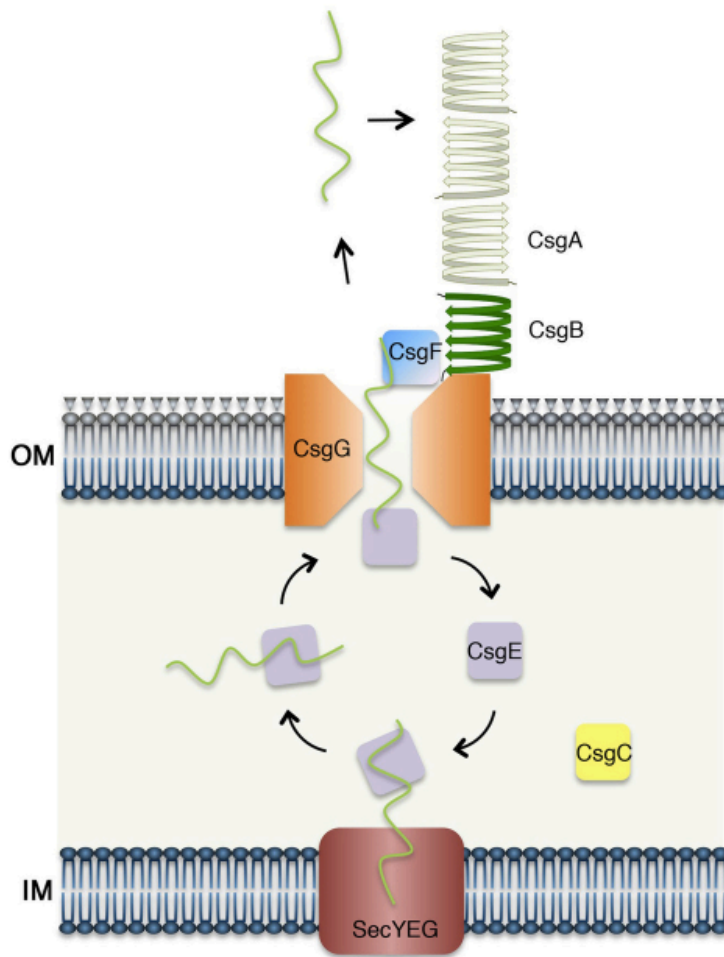
Figure 9. An integrated model for the mechanism of secretion of curli subunit CsgA. CsgA is the major curli subunit and enters the periplasm through the SecYEG translocon. The curli transporter CsgG assembles into an oligomeric translocation channel in the outer membrane and translocates CsgA to the cell surface. CsgB is the minor curli subunit and is associated with the outer membrane (OM). CsgE and CsgF proteins are involved in the transport of CsgA and CsgB. CsgC function is still not defined. The figure is adapted from (Goyal et al., 2014).

This thesis is focused on the type IV secretion system and accordingly, the rest of the introduction will provide a more thorough overview of type IV secretion components and functions.

1.3 Overview of type IV secretion systems

Type IV secretion systems (T4SS) span the inner and outer membrane of the bacteria. The T4SSs are used for various functions such as exchange of DNA with other bacteria and transfer of oncogenic DNA and proteins into host cells (Fig. 10). T4SSs are evolutionarily related to conjugative systems present in Gram-negative bacteria (Christie, 2004) and they mediate the spread of antibiotic resistance genes. R388 (IncW), pKM101 (IncN), R64 (IncI) and RP4 (IncP) are some examples of conjugative plasmids that are transferred by plasmid-encoded T4SS (Christie, 2001; Seubert, Hiestand, de la Cruz, & Dehio, 2003). T4SSs are classified in to three categories based on their functions. The first group comprises T4SSs that mediate conjugation and transfer of DNA between cells by direct cell-to-cell contact (Alvarez-Martinez and Christie, 2009). This type of T4SS is found in both Gram-negative and Gram-positive bacteria and it plays a major role in survival of bacteria since the exchange of genes enables them to adapt to environmental changes. Some pathogenic bacteria such as *Agrobacterium tumefaciens* use this type of T4SS to transport oncogenic T-DNA/protein complexes into plant cells. Upon transfer, the T-DNA is incorporated into the plant chromosome and encodes enzymes (e.g. determining synthesis of plant growth hormones) responsible for tumor formation (Alvarez- Martinez & Christie, 2009; Zupan, Muth, Draper, & Zambryski, 2000). The second type of T4SS transfers proteins used by pathogenic bacteria to

bind host cells and transfer virulence factor proteins into the cytoplasm of the host cell. For example, *Brucella suis* is a mammalian pathogen that uses the *virB* operon-encoded T4SS to deliver effector proteins into host cells (O´Callaghan et al., 1999). Several major human pathogens use this type of T4SS for their virulence, such as *Helicobacter pylori*, *Bordetella pertussis* and *Legionella pneumophila*. The third type of T4SSs is involved in uptake and release of DNA from and into the extracellular environment. *Helicobacter pylori* and *Neisseria gonorrhoeae* are known to use this type of T4SS (Alvarez- Martinez & Christie, 2009).
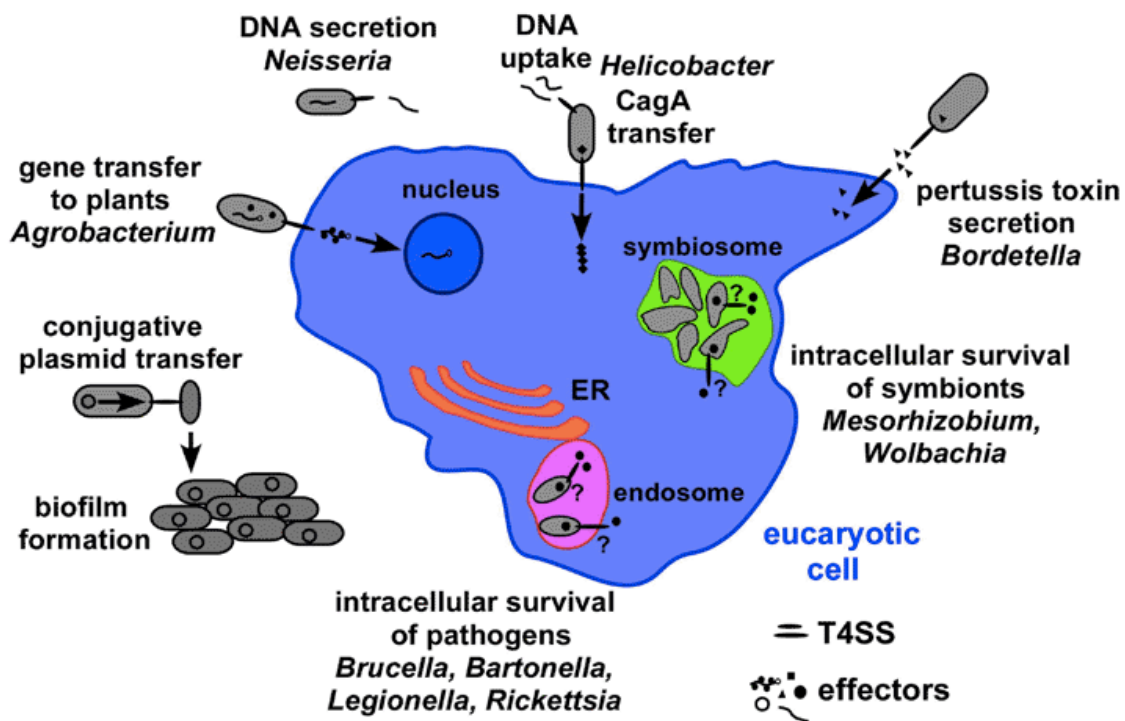

Figure 10. Schematic representation of various functions of T4SS in bacteria. The figure is adapted from (Baron, 2005).

T4SSs are also classified based on their sequence similarity to conjugative systems. T4SSs are divided as type IVA (T4ASS) whether their structural components resemble the VirB/D4 complex of the plant pathogen *A. tumefaciens*. Similarity of structural components to the conjugation system of IncI plasmid has led to the designation of another class of T4SSs, called type IVB (T4BSS) (Voth, Broederdorf, & Graham, 2012). The T4BSS was first identified in the human pathogen *L. pneumophila*. It was found that pathogenicity of *L. pneumophila* depends on the functional Dot/Icm T4BSS complex. Animal pathogens such as *Coxiella burnetii* and *Rickettsiella grylli* use T4BSS complexes similar to the *Legionella* Dot/Icm system. The Dot/Icm T4BSS contains ~27 components. It is suggested that the *Legionella* Dot/Icm system has a core complex comprised of DotC, DotD, DotF, DotG, and DotH proteins that spans both inner and outer membranes. DotC, DotD and DotH/IcmK proteins are localized in the outer-membrane and DotF and DotG are intrinsically inner membrane proteins (Fig. 11). (Vincent et al., 2006; Nagai & Kubori, 2011; Kubori et al., 2014). The type IVA secretion system and VirB/D4 complex will be extensively discussed in the following sections.
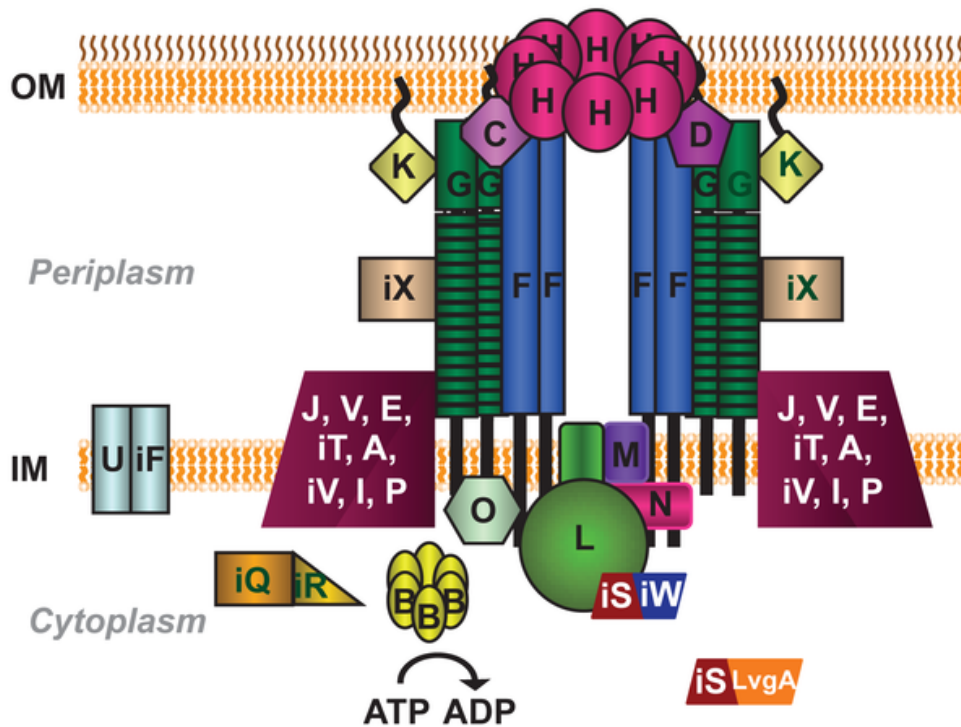
Figure 11. Schematic model of the *Legionella* type IVB secretion system. The 27 protein components are represented in the outer membrane (OM), periplasm, inner membrane (IM) and cytoplasm. Dot proteins are labeled with the last letter of their name. Icm proteins are labeled with 'i' and the last letter of their name. The model was generated based on the predicted or experimentally determined subcomplex localization of the components. Image is adapted from (Sutherland, Binder, Cualing & Vogel, 2013).

1.3.1 Overview of T4SS structure

Despite the above mentioned functional diversity, many T4SSs resemble to the type IVA VirB/VirD4 system from the Gram-negative *A. tumefaciens*. The VirB/VirD4 system from this organism is composed of 12 components (Fig. 12). The VirB1-VirB11 proteins translated from the *virB* operon and the VirD4 protein from the *virD* operon. Among the VirB/VirD4 complex protein components, VirB3, VirB6, VirB7, VirB8, VirB9 and VirB10 form the core complex of the translocation machinery (Christie, Whitaker & González-Rivera, 2014). The ATPases VirB4, VirB11 and VirD4 energize the functions of the complex and VirB2 and VirB5 are the subunits of the pilus believed to make contact with host cells.
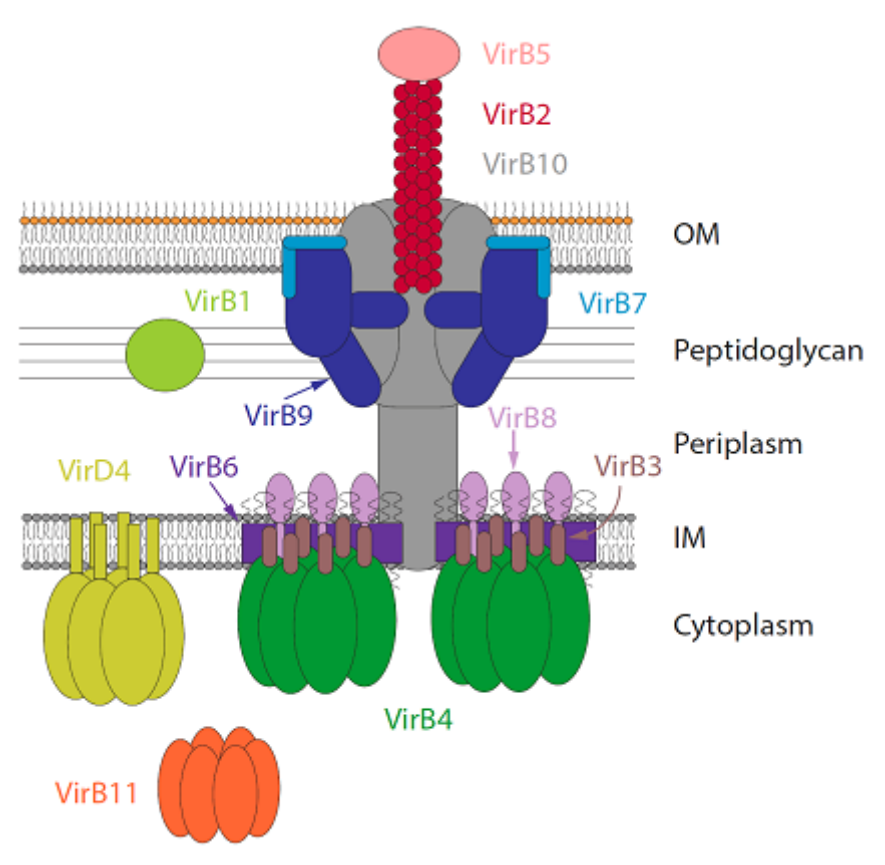
Figure 12. Schematic representation of the T4SS VirB components. Subunits localize in the cell envelope outer and inner membranes, periplasm and cytoplasm. The image adapted from (Redzej, Waksman & Orlova, 2015).

1.3.2 Description of individual T4SS protein components

VirB1 is a lytic transglycosylase that degrades the periplasmic peptidoglycan (murein) and facilitates assembly of the T4SS across the cell wall (Höppner et al., 2004). Lytic transglycosylases cleave β-1,4 glycosidic bonds between N-acetylmuramic acid (MurNAc) and N-acetylglucosamine (GlcNAc). The evidence for VirB1s lytic transglycosylase activity has been reported (Zahrl et al., 2005). VirB1 associates with the secretion channel and was found to interact with VirB8, VirB9 and VirB11 (Höppner et al., 2005). It was shown that changes at the active site of VirB1 led to reduction of virulence (Höppner et al., 2004).

VirB2 and **VirB5** are major and minor pilins, respectively, and are subunits for the pilus assembly at the cell surface (Fullner, Lara & Nester, 1996 ; Eisenbrandt et al., 1999 ; Lai et al., 2002; Aly & Baron, 2007). Pili are cell appendages that are crucial for adhesion of bacteria to surfaces or host cells and also for interaction with other bacteria (Thanassi, Bliska & Christie, 2012). For the biogenesis of pili, the VirB2 propilin is cleaved at the N-terminus and processed to a cyclic form (Eisenbrandt et al., 1999). VirB5 whether serves as an adhesion at the pilus tip, which is also essential for the incorporation of the major component VirB2 into pili (Lai et al., 2000 ; Schmidt-Eisenlohr et al., 1999).

VirB3 is a membrane protein and part of the inner membrane complex (VirB3, VirB6 and VirB8). Previous studies showed that VirB3 co-localizes in the inner membrane with VirB6 (Judd, Kumar, & Das, 2005b) and its level of accumulation is affected by VirB4 (Jones et al., 1994; Yuan et al., 2005). VirB3 is involved in the assembly of protein complexes with the pilus proteins VirB2 and VirB5 (Yuan et al., 2005).

VirB4 is an ATPase that is essential for pilus biogenesis and substrate secretion (Berger & Christie, 1993 ; Fullner, Lara & Nester, 1996). VirB4 proteins are localized on the cytoplasmic side of the inner membrane and comprise a C-terminal domain (CTD) with the ATPase activity and a N-terminal domain (NTD), which interacts with the membrane (Middleton et al., 2005). A negative stain electron microscopy study identified the structure of VirB4 free and bound underneath the core complex of VirB7-VirB9-VirB10 encoded by the pKM101 plasmid (Walldén et al., 2012).

VirB6 is a polytopic inner membrane protein comprising six transmembrane domains and a large central periplasmic loop. VirB6 is involved in substrate secretion and directly contacts the DNA substrate during translocation across the inner membrane (Cascales & Christie, 2004a). The levels of VirB5 and VirB3 in the cell are affected in the absence of VirB6 (Hapfelmeier, Domke, Zambryski, & Baron, 2000). VirB6 likely interacts with VirB8 to transfer DNA substrate from VirB11 into the secretion channel (Cascales & Christie, 2004a ; Jakubowski et al., 2004). VirB6 may interact with VirB8 via the periplasmic loop of VirB6 (Villamil Giraldo et al., 2015).

VirB7 is a small lipoprotein that associates with VirB9 and VirB10 to form the T4SS complex in the outer membrane. In *A. tumefaciens*, VirB7 forms a disulfide linkage with VirB9 (Baron, Thorstenson, & Zambryski, 1997; Fernandez, Dang et al., 1996) and formation of the VirB7-VirB9 heterodimers stabilizes other T4SS components (Fernandez, Spudich, Zhou, & Christie, 1996).

VirB8 is a single transmembrane protein with a large periplasmic domain that is part of the T4SS inner-membrane complex. In the following section, VirB8 and its interactions with other components of the T4SS are extensively reviewed.

VirB9 protein is associated with the outer membrane and interacts with VirB7 and VirB10 to form the T4SS outer membrane core complex consisting of 14 copies of each protein. VirB9 forms the outer sheath of the core complex that is stabilized by VirB7 (Guglielmini et al., 2014; Low et al., 2014). VirB9 also interacts with VirB8 and disruption of VirB8-VirB9 interactions abolishes DNA transfer in *A. tumefaciens* (Das & Xie, 2000). VirB9 is involved in translocation of substrates in the secretion channel and pilus biogenesis as found in *Agrobacterium* (Jakubowski, Cascales, Krishnamoorthy & Christie, 2005).

VirB10 locates at the inner surface of the outer membrane complex, spans the entire length of the T4SS complex and is linked to the inner membrane complex. In addition to this central role as a scaffold of the complex, VirB10 is essential for the transfer of substrates from the inner to the outer membrane. VirB10 does not directly contact the substrate, but likely

works as an energy-sensing gate that transmits ATP-induced conformational changes derived from the cytoplasmic ATPases (Cascales & Christie, 2004b).

VirB11 is an ATPase located in the cytoplasm that energizes the functions of the complex. VirB11 is essential for channel assembly, for substrate transfer and pilus assembly (Sagulenko, Sagulenko, Chen, & Christie, 2001). ATP hydrolysis by VirB11 also induces conformational changes in VirB10 (Cascales & Christie, 2004b). VirB11 assists VirB4 during pilus biogenesis by translocating pilin subunits from the inner membrane to the periplasmic space (Kerr & Christie, 2010).

VirD4 is an ATPase and plays a role of type IV secretion system "coupling protein" (T4CP) that translocates substrates to the VirB1-11 complex. VirD4 is present in most T4SSs and has the function of recognizing and translocating the substrates (Tato, Zunzunegui, de la Cruz & Cabezon, 2005). In *A. tumefaciens* VirD4 directs the transfer of the T-DNA to VirB4 and VirB11. Collectively, the transfer of substrates to the secretion channel is mediated by the ATPase components of the T4SS complex (Atmakuri, Cascales, & Christie 2004).

1.4 Structural insights into the T4SS architecture

The VirB/VirD4 system structure has been thoroughly studied using models from different homologs of the archetypical *Agrobacterium* system. Using cryo-electron microscopy and X-ray crystallography of a subset of co-expressed pKM101 core components (TraN, TraE, TraO and TraF, homologs of VirB7 to VirB10), the first high-resolution structure of the T4SS outer membrane core complex was obtained (Fronzes et al., 2009; Chandran et al., 2009; Trokter et al., 2014). The cryo-EM structure of the core complex showed a 1.05 MDa complex spannig the cell envelope and composed of two layers, the O and I layers, that is formed by 14 copies of VirB7, VirB9 and VirB10 homologues. The I layer consists of the N-terminal domains of VirB9 and VirB10 anchoring in the inner membrane via the N-terminal transmembrane domain of VirB10. The O layer comprises VirB7 and domains of VirB9 and VirB10 forming a main body and a cap (Fig. 13a). Co-expression of TraE, the VirB8 homologue, was not necessary for the formation of the TraN-TraO-TraF complex (Fronzes et al., 2009). X-ray crystal structure analysis of an outer membrane subcomplex of T4SS revealed that 14 copies of the C-terminal domain of VirB10, the C-terminal domain of VirB9 and full length VirB7 create the complex in which VirB10 forms a helical barrel surrounded by VirB9 and VirB7 (Fig. 13 b&c) (Chandran et al., 2009).
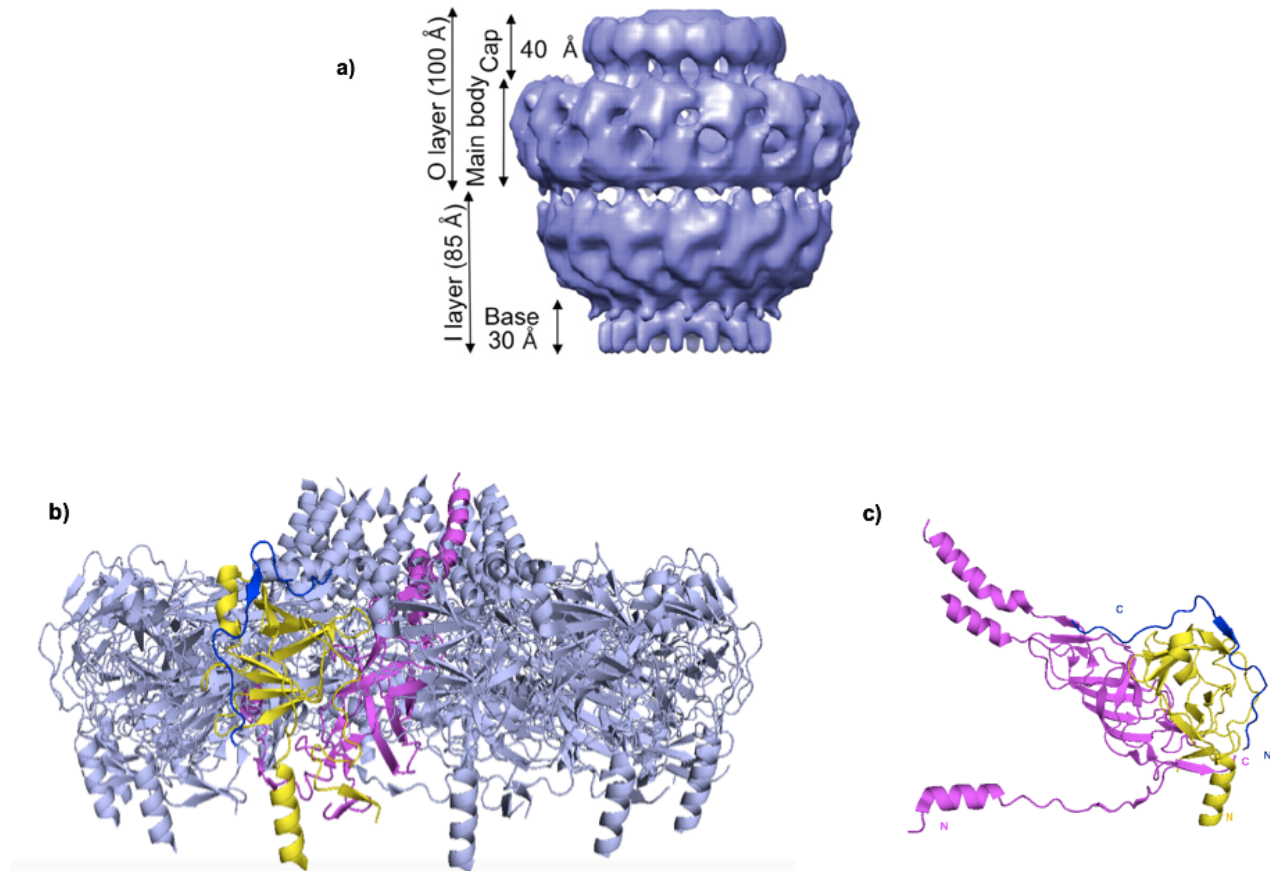
Figure 13. The structure of T4SS outer membrane complex. a) Cryo-EM structure of the TraN/VirB7, TraO/VirB9, and TraF/ VirB10 core complex with compartments and dimensions labelled. Image adapted from (Fronzes et al., 2009) b) Cartoon representation of the outer membrane tetradecameric complex. c) Representation of the heterotrimeric units of the complex. Subunits are shown as $TraF_{CT}$ in magenta, $TraO_{CT}$ in yellow and TraN in blue. Image generated from PDB code 3JQO.

An overall view of a T4SS complex structure was obtained by co-expression and purification of VirB3–VirB10 from conjugative R388 plasmid in *E. coli* (Low et al*.,* 2014). Electron microscopy analysis showed a 3 MDa protein complex spanning the cell envelope. This T4SS structure includes the outer membrane complex, the inner membrane complex, a stalk that connects these complexes and two hexameric barrel-like structures in the inner membrane that protrude toward the cytoplasm. The results suggest that the outer membrane complex includes 14 copies of VirB7, VirB9 and VirB10 as shown in previous studies (Fronzes et al., 2009; Chandran et al., 2009). VirB7 and the C-terminal domains of VirB9 and VirB10 form the upper part of the outer membrane complex (O-layer) and the N-terminal domains of VirB9 and VirB10 form the inner part of this complex (I-layer). VirB7 and VirB9 wrap around VirB10 in this complex, which is similar to the arrangement of the pKM101 TraN-TraO-TraF subcomplex (Chandran et al., 2009; Low et al., 2014). The composition of the stalk that connects outer and inner membrane complexes has not been identified yet. VirB3, VirB4, VirB6, VirB8 and the N-terminus of VirB10 form the inner membrane complex and a part of the inner membrane-associated complex locates in the cytoplasm. The cytoplasmic part of the complex consists of two barrels that each contains six VirB4 ATPase subunits. According to this study (Low et al., 2014), the inner membrane complex contains 12 copies of VirB8, 24 copies of VirB6 and 14 copies of the VirB10 N-terminus. VirB10 is the only T4SS protein that spans the entire cell envelope and interacts with inner and outer membrane T4SS components of the system (Fig. 14).
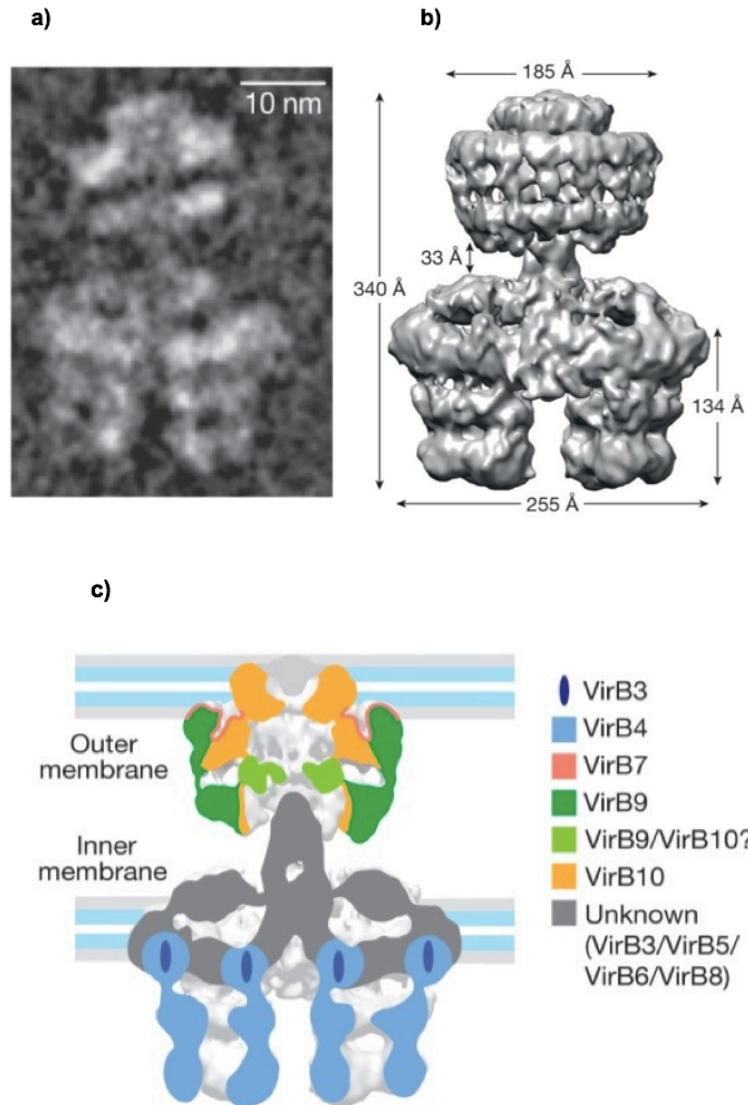
Figure 14. Overview of T4S complex structure. a) Negative-stain electron microscopy image of the $T4SS_{3-10}$ complex. b) Reconstituted structure of the $T4SS_{3-10}$ complex expressed from the R388 plasmid in *E. coli*. The map was generated based on electron densities and merging independently the core complex and the inner membrane complex reconstructions. c) A schematic diagram describing the localization of identified subunits in the T4SS complex. The image is adapted from (Low et al,. 2014).

The overall T4SS architecture appears to be similar in all Gram-negative bacteria. A recent *in situ* study revealed the structure of the type IVB T4SS from *L. pneumophila* in its natural biological context using electron cryotomography (Ghosal et al.*,* 2017). The sequence of the DotG protein at the C-terminus is similar to the sequence of VirB10 at the C-terminus (Nagai & Kubori, 2011), but this is the only sequence similarity found between components of T4BSS and T4ASS. Despite the limited sequence similarity of the components, the electron cryotomography analyses suggest structural similarities between T4ASS and T4BSS at the outer membrane complex and the two barrel like structures in the cytoplasm (Fig. 15). In addition to these similarities, there are drastic differences observed in size (length and width) between the T4ASS from the R388 plasmid and the T4BSS Dot/Icm system from *L. pneumophila* (Ghosal et al.*,* 2017).
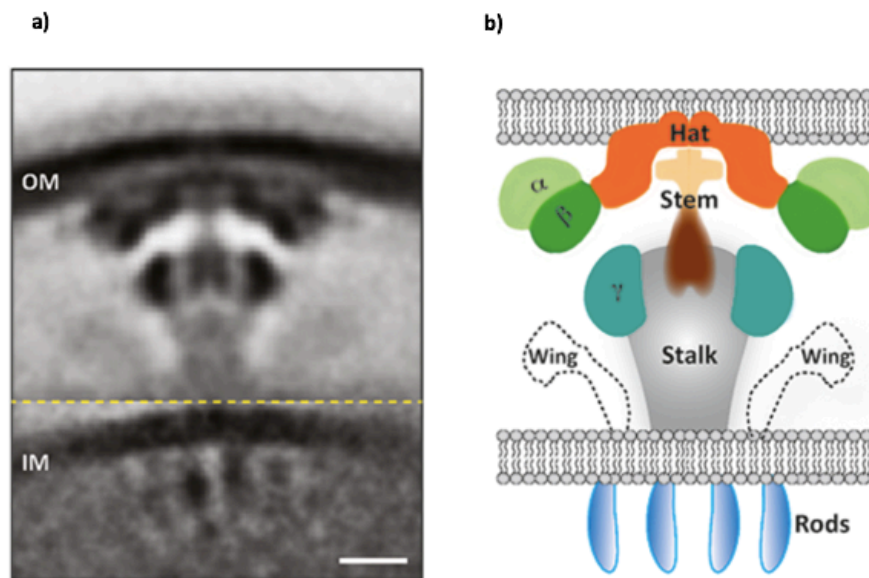

Figure 15. *In situ* structure of Dot/Icm T4BSS. a) Cryo-electron microscopy tomogram average of wild-type Dot/Icm particles from *L. pneumophila*. Abbreviations OM and IM correspond to

outer membrane and inner membrane. The scale bar indicates 10 nm. b) Schematic representation of the complex compartments with labeling of the prominent densities. The image is adapted from (Ghosal et al., 2017)

1.5 The T4SS core component VirB8

VirB8 from *B. suis* is a bitopic inner membrane protein comprising a 5 kDa cytoplasmic N-terminal domain (42 amino acids), followed by a transmembrane helix (20 amino acids) and a 18 kDa C-terminal domain in the periplasm (175 amino acids). Analysis of the crystal structure of VirB8 from *Brucella* showed that it consists of four β-sheets and five α-helices (Terradot et al., 2005). Despite differences in amino acid sequences, VirB8-like proteins possess an overall similar fold, comprising one large α-helical domain and one β-sheet domain. The similarity was observed in crystal structures of the periplasmic domains of VirB8 homologs from *Brucella*, *Agrobacterium*, the IncN plasmid pKM101 (TraE) in Gram-negative bacteria (Fig. 16) and Enterococcus (TraM) and Clostridium (TcpC) in Gram-positive bacteria (Terradot et al., 2005 ; Bailey et al., 2006 ; Casu et al., 2016; Porter et al., 2012 ; Goessweiner-Mohr et al., 2013).
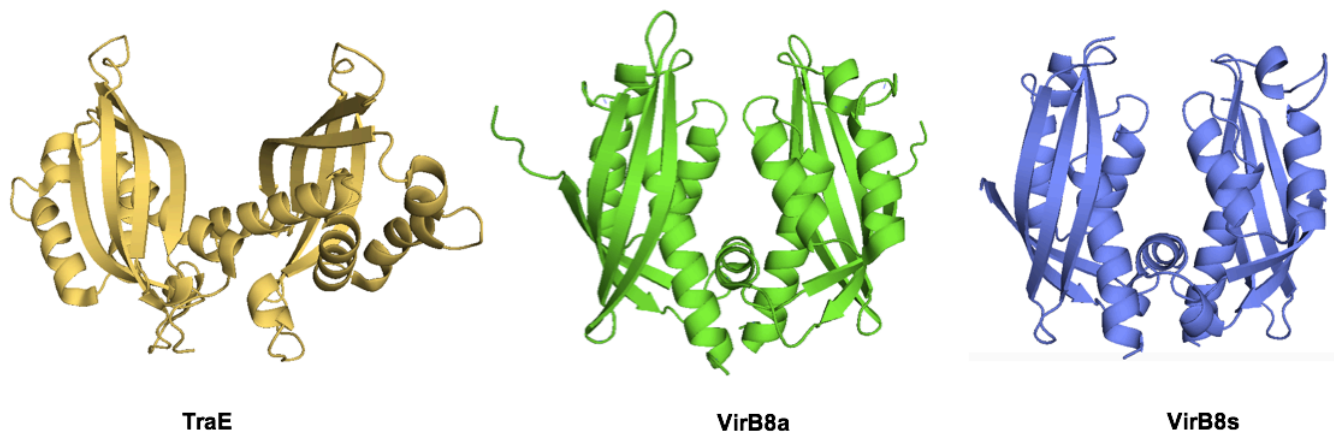
Figure 16. Overall geometry of the periplasmic VirB8s homodimer crystal structure (from *B. suis*, PDB code 2BHM) as compared to VirB8a (from *Agrobacterium*, PDB code 2CC3) and TraE (PDB code 5I97).

1.5.1. VirB8 interactions in the T4SS complex

VirB8 is a crucial component for the structure and function of the T4SS. VirB8 in *A. tumefaciens* is essential for the passage of substrates from the cytoplasm to the periplasm (Sivanesan & Baron, 2011). It was also reported that VirB8 in *A. tumefaciens* is essential for spatial localization of the T4SS complex (Judd, Kumar & Das, 2005a). VirB8 interacts with several components of the T4SS complex. Transfer DNA immunoprecipitation (TrIP) studies showed that VirB8 can be cross-linked to the transferred DNA (T-DNA) complex, which is comprised of single-stranded DNA and the virulence proteins VirD2 and VirE2 (Cascales & Christie, 2004a). The transfer of substrates from VirB11 to the secretion channel is dependent

on VirB8 and VirB6 (Cascales & Christie, 2004a; Jakubowski et al., 2004). Studies of detergent-extracted VirB protein complexes from *A. tumefaciens* showed that interaction of VirB4 with VirB8 is essential for the incorporation of VirB5 and VirB2 into pili (Yuan et al., 2005). VirB8 is an inner membrane protein while the final localization of VirB5 is on the cell surface, which may be explained by transient interactions with VirB8 during pilus assembly (Yeo et al., 2003; Yuan et al., 2005). Previous studies showed that VirB8 also interacts with VirB1 (Yuan et al., 2005), VirB9 (Das & Xie, 2000), VirB10 (Ding et al., 2002 ; Das & Xie, 2000), and VirB11 (Ward, Draper, Zupan & Zambryski, 2002). VirB8 interactions with other T4SS proteins are generally transient, but essential for the functionality of the complex. Accordingly, VirB8 acts as a nucleating factor for the assembly of the secretion system complex.

1.5.2. VirB8 self-dimerization

VirB8 undergoes self-dimerization (Ding et al., 2002 ; Das & Xie, 2000 ; Ward, Draper, Zupan & Zambryski, 2002). The Gram-positive homologue of VirB8 (TraM) is purified as trimers, however trimerization or higher-order homoligomers are not observed in Gram-negative VirB8s. The sequence similarity is very limited between VirB8 homologs while the overall crystal conformation is similar. The low sequence similarity and the difference in purification techniques can lead to different type of interactions and trimerization in purified TraM (Goessweiner-Mohr et al., 2013).

Analysis of the crystal structures of VirB8 from *Agrobacterium, Brucella* and pKM101 plasmid (TraE) and also *in vitro* analyses of purified proteins predicted that VirB8 forms dimers (Bailey et al., 2006 ; Paschos et al., 2006, Casu et al., 2016). The proteins dimerize via an α-helical domain. The purified periplasmic domains of VirB8 form concentration-dependent dimers (Paschos et al., 2006 ; Sivanesan & Baron, 2011, Casu et al., 2016). VirB8 residues at the dimerization site are important for survival of *Brucella* in macrophages, suggesting that VirB8 dimerization has functional importance (Paschos et al., 2006). *In vitro* and *in vivo* analyses of variants of VirB8 at the dimer site in *Agrobacterium* showed the importance of the dimer site for T-pilus assembly and T4SS functions (Sivanesan & Baron, 2011).

It was shown that two residues (M102 and Y105) localized at the dimer interface of *B. suis* VirB8 have a major role for its dimerization. A variant of VirB8 (M102R) exhibited reduced dimerization as shown by analytical gel filtration and analytical ultracentrifugation (Paschos et al., 2006). As shown by complementation experiments, the equivalent residues of *Brucella* VirB8 M102 and Y105 in *A. tumefaciens* (V97 and A100) are required for VirB8 functions. Studies of the periplasmic domain of VirB8 from *B. suis* (VirB8sp) *in vitro* showed that VirB8sp exists in a monomer-dimer equilibrium. The dissociation constant of VirB8sp was determined by analytical ultracentrifugation as 116 μM (Paschos et al., 2006). X-ray structure analysis of VirB8sp identified the dimer interface that includes residues mainly located in the helices α-1 and α-4 including Y98, V101, M102, K104, Y105, L218, P221, L222, and E214 (Terradot et al., 2005). Variants M102R (helix α1), Y105R (helix α1) and E214R (helix α4) had reduced levels of self-association as compared to the wild type (Fig. 17) (Paschos et al., 2006 ; Sivanesan, Hancock, Villamil Giraldo & Baron, 2010). A study of the functional importance of

the interface residues showed that changes of *Agrobacterium* VirB8 residue A100 were similar to a deletion of the *virB8* gene (Kumar & Das, 2001 ; Sivanesan & Baron, 2011). Variations at the predicted dimer interface of TraE from pKM101 conjugative plasmid (E97, K168, Q105, Y214 and their adjacent residues) significantly disrupted the dimerization *in vitro* and reduced or abolished conjugation *in vivo* (Casu et al., 2016). Taken together, this information suggests that residues involved in dimerization of VirB8-like proteins play an important role in T4SS complex functions.
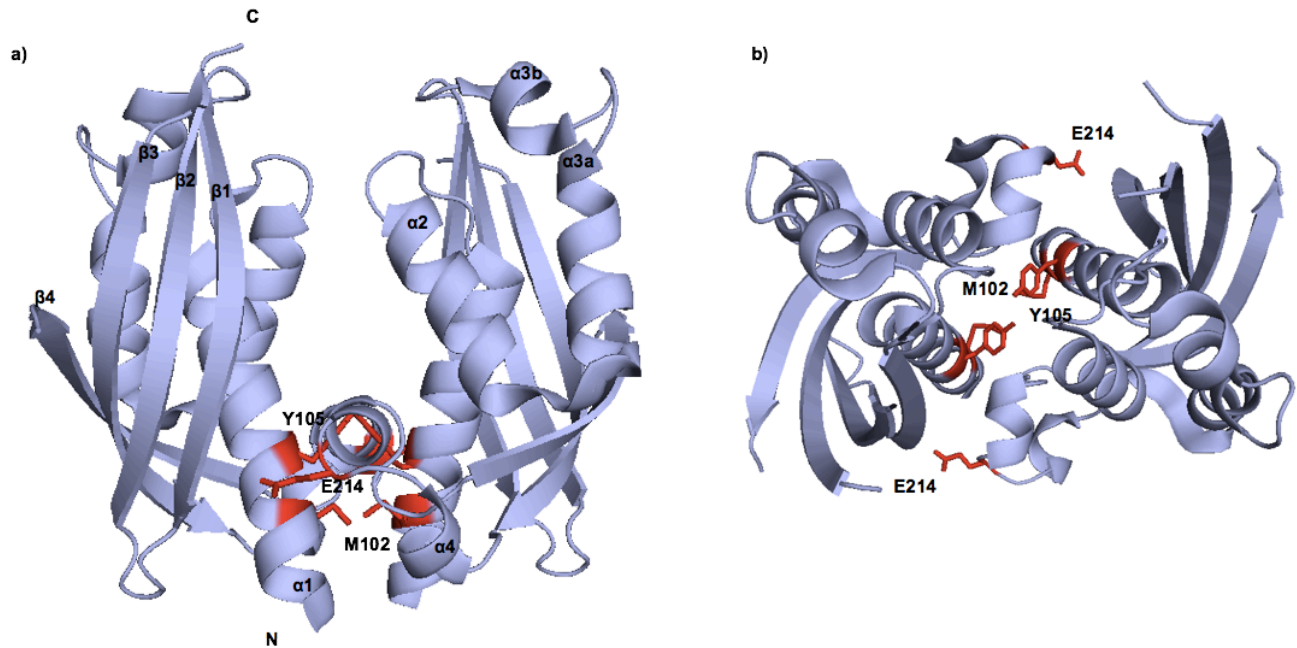
Figure 17. Cartoon representation of the VirB8sp dimer (generated from PDB code 2BHM). Residues M102 (helix α1), Y105 (helix α1) and E214 (helix α4) are identified in red. Changes of these residues reduced the level of VirB8 self-association (Paschos et al., 2006 ; Sivanesan, Hancock, Villamil Giraldo & Baron, 2010).

1.5.3. VirB8 interactions with VirB10 in the T4SS complex

It was reported that the expression of TraE (VirB8 homologue) was not crucial for the over-expression, assembly and co-crystallization of TraN-TraF-TraO (homologes of VirB7-VirB9-VirB10) complex, the core of the T4SS outer membrane complex (Chandran et al., 2009). However, different previous studies had shown that VirB8 does interact with VirB10 in T4SS complexes (Das & Xie, 2000; Paschos et al., 2006). A dynamic model has been proposed for the interactions between VirB8, VirB9 and VirB10 suggesting that VirB8 acts as a scaffolding protein that interacts with VirB9 and VirB10 (Sivanesan, Hancock, Villamil Giraldo & Baron, 2010). Also, studies on variants of VirB8 showed that residue T201 located on the β-sheet surface of *Brucella* VirB8 is the potential site of interaction with VirB10 (Paschos et al., 2006). Therefore, most of the available data suggest that VirB8 and VirB10 interact and in this thesis I have provided additional direct evidence for this interaction and its importance for T4SS functions.

1.5.4. Inhibition of VirB8-like proteins by small molecules

Several studies have focused on finding compounds that will not affect the vitality of pathogenic bacteria but will target their virulence functions. This approach disarms the bacteria and facilitates their elimination through the immune system. Disarming bacteria will reduce the selection pressure for the development of resistance. Since Gram-negative bacteria use T3SS for pathogenicity, this secretion system has been a major target for developing antivirulance drugs. Most of the active molecules inhibiting T3SS belong to salicylidene acylhydrazides and thiazolidinones classes of small molecules (McShan et al., 2015). However, the specific targets

within the T3SS complex for most of these inhibitors have not been identified. Similar classes of small molecules are studied for inhibition of the type IV secretion systems (Paschos et al., 2011). To disarm many T4SS pathogens and reduce antibiotic resistance gene spread, the dimer interface of *Brucella* VirB8 was targeted for the development of these small-molecule inhibitors. Screening a small-molecule library led to the identification of specific VirB8 inhibitors that reduced the intracellular proliferation of *B. abortus* 2308 (Paschos et al., 2011). Inhibitor screening identified molecules that inhibited the dimerization of *Brucella* VirB8 and affected functionality of the T4SS (Paschos et al., 2011; Smith et al., 2012). Derivatives of these molecules also inhibited dimerization of TraE suggesting that VirB8-like proteins have conserved sites that can be targeted by small molecule inhibitors (Casu et al., 2016). Co-crystallization of an inhibitor of VirB8sp dimerization (2-(butylamino)-8-quinolinol) in complex with VirB8sp revealed the binding site of the inhibitor (Fig. 18). The inhibitor was localized in a groove on the side of the VirB8sp molecule, in proximity to the α-1 helix and residues E115, K182, R114 and Y229. The identified inhibitor binding site was distant from the dimerization site leading to the hypothesis that the inhibition was a consequence of conformational changes in VirB8sp (Smith et al., 2012).
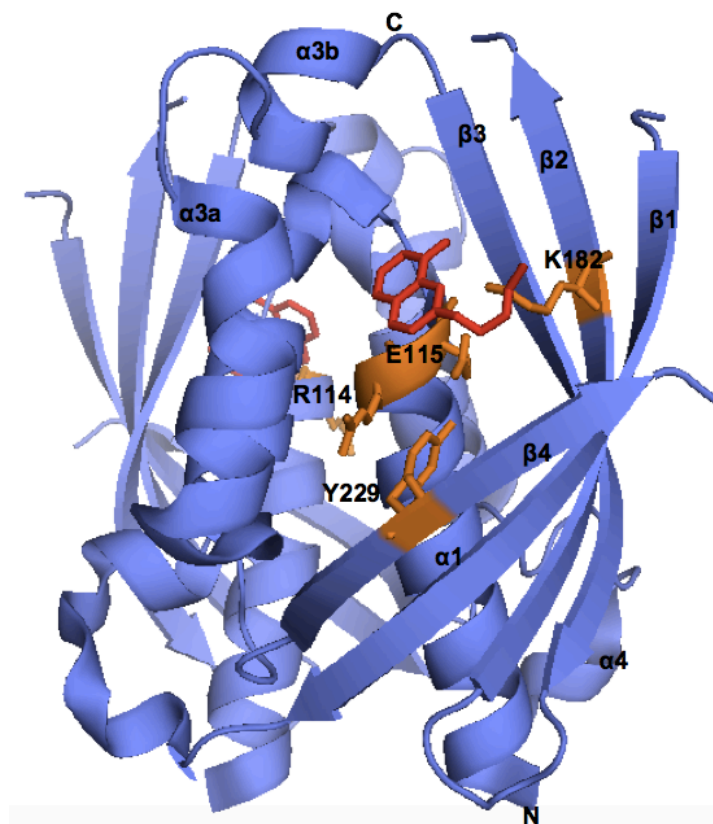
Figure 18. Cartoon representation of the VirB8sp dimer in complex with 2-(butylamino)-8-quinolinol, the dimerization inhibitor (red). The inhibitor locates in the side groove in proximity to the α-1 helix and residues E115, K182, R114 and Y229 (orange). The image was generated from the PDB (4AKY).

1.6 Hypothesis and Objectives

The preliminary data show that VirB8 participates in a series of dynamic interactions with several other VirB proteins and mediates the assembly of the type IV secretion system. Understanding the role of VirB8 as the key factor in the T4SS complex, will lead us to understand T4SS's mechanism of function and alternatives to inhibit the antibiotic resistant infections.

1.6.1 Objectives

The objectives of this thesis were to use NMR analysis to study the dynamics of VirB8 from *B. suis* in solution. First, conformational changes of VirB8 interactions were identified during the monomer-to-dimer transition. Second, structural characteristics of the monomeric variant of VirB8 (M102R) were identified by NMR and crystal structure analyses. Third, molecular binding of VirB8 and VirB8^{M102R} to inhibitors were assessed *in vitro*. Fourth, NMR analyses identified conformational changes of periplasmic VirB8 upon interaction with periplasmic VirB10. Fifth, the interaction site of full length VirB8 with full length VirB10 was identified using phage display and bacterial two hybrid assays. Sixth, the importance of the interaction site of VirB8 with VirB10 for the functionality of T4SS secretion was identified by conjugation assays. Seventh, the interaction of periplasmic VirB8 with VirB5 was characterized by NMR spectroscopy. The results are presented in the two following manuscripts (Chapters 2 and 3) and in chapter 5 comprising the non-published work. The first article presents our findings on the self-association of VirB8 and analyses of the binding site of VirB8 dimerization inhibitors. The second article describes our findings on the interaction of VirB8 with VirB10 and its functional importance. Altogether, the results of the thesis provide new insights into the interactions of VirB8 with other components of the T4SS complex.

1.7 Experimental techniques

1.7.1 Overview of experimental techniques used to identify the dynamics of VirB8 structure and interactions

I have used a variety of structural and biochemical assays to conduct the research presented in this thesis. I used solution state Nuclear Magnetic Resonance (NMR) spectroscopy as the main technique to investigate dynamic properties of the periplasmic domain of VirB8 from *B. suis* (VirB8sp). Using this approach, I obtained a nearly complete backbone assignment of VirB8sp. Through NMR analysis, I was able to examine conformational changes in VirB8sp upon homo-dimerization. In addition, I assessed VirB8sp interaction with the T4SS components VirB10sp and VirB5 as well as with binding fragments. I also used NMR spectroscopy to investigate structural characteristics and interactions of VirB8sp^{M102R}, the monomeric variant of VirB8sp. For all of the NMR experiments, I collaborated with Lauriane Lecoq from the Omichinski group (Department of Biochemistry and Molecular Medicine, Université de Montréal). X-ray crystallography was used to resolve the structure of VirB8sp^{M102R} and this analysis was conducted by Tarun Arya from the Baron group. To identify the small molecules that bind to VirB8, fragment screening was carried out using the differential scanning fluorimetry (DSF) approach. Changes in melting temperatures determined by DSF were used to probe the binding of small molecules to VirB8sp and VirB8sp^{M102R}. DSF experiments were carried by Benoit Bessette from the Baron group. Phage display analysis was used to identify potential sites on VirB8 for the interaction with VirB10. This analysis was carried out by Ingrid Um-Nlend from Christian Baron's group. I conducted bacterial two hybrid assays to measure the interaction of full-length VirB8 and its variants with full-length VirB10.

Finally, I conducted conjugation assays to study the effects of changes of the VirB8 interaction site with VirB10 on T4SS function. To this effect, I studied TraE from the pKM101 conjugative plasmid T4SS, which is a homologue of VirB8 from *B. suis*.

1.7.2 Solution NMR Spectroscopy of VirB8sp

Solution NMR spectroscopy is suited for identifying dynamics of protein structures and interactions in solution. Despite the fact that high resolution NMR data can be obtained only for small proteins or complexes (<40 kDa), NMR experiments provide invaluable dynamic information about protein-protein interactions in solution. The NMR experiments presented in this thesis were carried on a Bruker 500 MHz spectrometer (at Université de Montréal) and an 800 MHz Varian INOVA spectrometer (Québec/Eastern Canada High Field NMR Facility at McGill) equipped with z-pulsed-field gradient units and triple resonance probes. Sequential backbone assignments were acquired from ^{15}N,^{13}C-labeled VirB8sp through standard heteronuclear NMR experiments including 2D ^{1}H-^{15}N HSQC, 3D HNCA, 3D HNCACB, 3D HNCO, 3D HN(CA)CO, 3D HN(CO)CA, CBCA(CO)NH, and 3D ^{15}N-edited NOESY-HSQC. The chemical shift assignment for H, C and N atoms in the VirB8sp amino acid sequence were analysed based on the corresponding ^{1}H, ^{13}C and ^{15}N NMR resonances. Based on the results, 92% of all atoms were assigned (93% of non-prolines). Following the assignment of VirB8sp, NMR chemical shift perturbation experiments were carried out to assess conformational changes upon different conditions. Perturbations in chemical shifts under different conditions were calculated from ^{1}H-^{15}N HSQC experiments using the formula $\Delta\delta=[(0.17\Delta NH)^2 +(\Delta HN)^2]^{\frac{1}{2}}$. The NMR chemical shifts of VirB8sp have been

deposited in the BioMagResBank, www.bmrb.wisc.edu (accession no. 26852). By mapping those chemical shift changes onto the structure of VirB8sp, we were able to determine the regions responsible for dimerization, interaction with VirB5 and interaction with VirB10.

1.7.3 Differential scanning fluorimetry (DSF) of VirB8sp and VirB8sp[M102R]

Differential scanning fluorimetry is a technique used to assess protein stability. It measures the changes of the melting temperature of proteins by monitoring unfolding in the presence of the fluorescent dye SYPRO Orange that binds non-specifically to hydrophobic surfaces of proteins. SYPRO Orange fluorescence is quenched by water. At a certain temperature when the protein unfolds, SYPRO Orange binds to the exposed hydrophobic surfaces of the protein and excludes water, resulting in an increase of its fluorescence. We have used this technique to identify fragments that bind to VirB8sp and VirB8sp[M102R]. We screened the binding of molecules from a library of 186 fragments and the changes of the melting temperatures of the proteins in the presence of the fragments were determined based on changes of SYPRO Orange fluorescence. The library of fragments was generated by in-house synthesis in collaboration with Edward Ruediger at the Institut de Recherche en Immunologie et Cancérologie (IRIC), Université de Montréal.

1.7.4 X-ray crystallography of VirB8sp[M102R]

X-Ray crystallography is a technique to determine the high-resolution 3D structures of proteins. A diffraction pattern is generated from the X-ray radiation traversing the atoms in the

crystallized state of a protein. The resulting diffraction pattern reveals the electron density profile of the protein, which can be used to determine the protein structure. VirB8-like proteins exist in a monomer-dimer equilibrium and since the structure of the dimer is already known, it was pertinent to also identify the structure of the monomer. VirB8sp^{M102R} is a variant that does not form dimers and we used X-ray crystallography to determine its structure and to complement the result of earlier crystal structure analysis of VirB8sp. The protein was crystalized using the hanging drop vapour diffusion method. VirB8sp^{M102R} crystals diffracted to 1.95Å resolution. The structure was solved by molecular replacement and the crystal structure of *B. suis* VirB8sp (PDB code 2BHM) was used as the template. The VirB8sp^{M102R} structural coordinates have been deposited to the RCSB protein data bank (available at http://www.rcsb.org/), PDB code 5JBS.

1.7.5 *In silico* docking of VirB8sp and VirB8sp^{M102R}

In silico docking is a method that is extensively used in virtual drug screening protocols. This procedure is used to identify potential binding sites on a protein structure for small molecule probes. *In silico* docking studies were performed using AutodockTools software (available at http://autodock.scripps.edu/resources/adt). The docking software uses algorithms, which rank the potential protein-small molecule interactions based on predicting the strength of non-covalent interactions. The small molecules used in the docking studies were chosen based on binding results of the DSF experiment. Chemical structure of the small molecules were retrieved from the ZINC compound database (available at http://zinc.docking.org/) and were docked to the structures of VirB8sp (PDB code 2BHM) and VirB8sp^{M102R} (PDB code 5JBS).

The lowest-energy conformations that docking calculations predicted were superimposed on the crystal structures of VirB8sp and VirB8sp^{M102R} to analyze the potential binding sites.

1.7.6 Phage Display

Phage display is a screening technique to identify potential sites of protein-protein interactions. The bacteriophage genome determines the sequence of the surface protein of the phage and libraries of peptides can be generated by phages which are used for screening. The peptides are genetically fused to the pIII coat protein of M13 phage. In this study, purified VirB10sp was immobilized and incubated as prey with two different phage libraries Ph.D.-12 and Ph.D.-C7C (New England Biolabs, NEB). Ph.D.-12 indicates 12 randomized amino acid sequence, while Ph.D.-C7C indicates 7 randomized amino acids displayed in a constrained fashion on the surface of M13 phage. After washing steps to remove non-specifically bound phages, the VirB10sp-bound phages were eluted and amplified. Sequencing of the phage genome identified the peptides on the surface interacting with VirB10sp. In order to identify potential binding sites of VirB8 with VirB10, the peptides were aligned to the VirB8 sequence using RELIC program formerly available at http://relic.bio.anl.gov (Mandava et al., 2004).

1.7.7 Bacterial two-hybrid assay

The bacterial two-hybrid assay was used to test the effects of variations of the β1-strand region of VirB8 on interactions with VirB10. The genes encoding full length VirB8s and full length VirB10s were fused to genes encoding the T18 and T25 fragments of adenylate cyclase

in order to express them as fusion proteins (T18 and T25 are enzymatically inactive catalytic domains of *Bordetella pertussis* adenylate cyclase). VirB8s and VirB10s fusion proteins were co-expressed in adenylate cyclase-deficient *E. coli* strain BTH101. When the fusion proteins interact, T18 and T25 fragments are physically joined restoring adenylate cyclase enzyme activity. The production of cAMP consequently triggers the production of β-galactosidase in the cell via a signalling cascade. The amount of β-galactosidase in the cell depends on the strength of the interaction and is quantified by measuring cleavage of the substrate 2-nitrophenyl-β-D-galactopyranoside (ONPG).

1.7.8 Bacterial conjugation assay

I also conducted *in vivo* bacterial conjugation assays in order to verify the importance of the VirB8-VirB10 interaction site identified by NMR and BTH experiments for T4SS functions. For this assay, the VirB8 homolog TraE from the pKM101 conjugative plasmid was studied. *E. coli* strains FM433 pKM101 (donor, ampicillin-resistant), a non-polar *traE* transposon insertion variant of pKM101 and WL400 (recipient, chloramphenicol-resistant) were used. Complementation of the *traE* insertion was conducted using plasmid pTrc200 expressing TraE and its variants. After incubation of the donor and recipient cells, the number of produced ampicillin-chloramphenicol-resistant WL400 colonies indicated the conjugation frequencies and the capacity of TraE and of its variants to complement the pKM101::traE transposon insertion deletion. The conjugation frequencies were calculated as the mean of three biological replicates.

Chapter 2: Article 1 (Published 2017)

Title : **Monomer-to-dimer transition of *Brucella suis* type IV secretion system component VirB8 induces conformational changes**

Authors : Mahzad Sharifahmadian[1], Tarun Arya[1], Benoit Bessette[1], Lauriane Lecoq[1], Edward Ruediger[2], James G. Omichinski[1] and Christian Baron[1]*

Affiliation : [1]Department of Biochemistry and Molecular Medicine, Faculty of Medicine, [2]Institut de Recherche en Immunologie et Cancer (IRIC), Université de Montréal, Montréal, QC, Canada

Corresponding Author: Christian Baron

E-mail: christian.baron@umontreal.ca Phone: (514) 343- 6300

Abstract

Secretion systems are protein complexes essential for bacterial virulence and potential targets for anti-virulence drugs. In the intracellular pathogen *Brucella suis*, a type IV secretion system mediates the translocation of virulence factors into host cells and it is essential for pathogenicity. VirB8 is a core component of the secretion system and dimerization is important for functionality of the protein complex. We set out to study dimerization and possible conformational changes of VirB8 from *Brucella suis* (VirB8s) using nuclear magnetic resonance, X-ray crystallography and differential scanning fluorimetry. We identified changes of the protein induced by a concentration-dependent monomer-to-dimer transition of the periplasmic domain (VirB8sp). We also show that the presence of the detergent CHAPS alters several signals in the heteronuclear single quantum coherence (HSQC) spectra and some of these chemical shift changes correspond to those observed during monomer-dimer transition. X-ray analysis of a monomeric variant (VirB8sp[M102R]) demonstrates that significant structural changes occur in the protein's α-helical region (α4). We localized chemical shift changes of residues at the dimer interface as well as to the α1 helix that links this interface to a surface groove that binds dimerization inhibitors. Fragment-based screening identified small molecules that bind to VirB8sp and two of them have differential binding affinity for wild-type and the VirB8sp[M102R] variant underlining their different conformations. The observed chemical shift changes suggest conformational changes of VirB8s during monomer-dimer transition that may play a role during secretion system assembly or function and they provide insights into the mechanism of inhibitor action.

Introduction

Type IV secretion systems (T4SS) are protein complexes in the cell envelope of Gram-negative bacteria and examples in Gram-positive bacteria are also known [1-4]. These cell envelope-bound protein complexes typically comprise 12 proteins that form a high molecular mass complex spanning the inner and the outer membrane of the cell. They assemble surface-exposed pili that are believed to initiate contact with other cells, followed by cell-cell contact and translocation of either proteins or DNA-protein complexes across the cell envelope into recipient cells [5-8]. T4SS are used by many bacteria to translocate virulence factors into eukaryotic cells and they contribute in an important fashion to bacterial pathogenicity.

In this work we have investigated the structural dynamics of VirB8, a component of the *Brucella suis* T4SS that is essential for the virulence of this intracellular pathogen. VirB8 proteins are essential for all type T4SS in which they have been studied [9-12]. They interact with several other T4SS components and these interactions are generally transient, which contributes to the notion that they act as assembly factors for the secretion system [13-18]. VirB8 from *Brucella suis* (VirB8s) is a bitopic membrane protein comprising a 5 kDa cytoplasmic N-terminus, one transmembrane helix and an 18 kDa periplasmic domain. The X-ray structures of the periplasmic domains of VirB8 homologs from *Brucella*, *Agrobacterium*, from the IncN plasmid pKM101 (TraE) in Gram-negative bacteria and *Enterococcus* (TraM) and *Clostridium* (TcpC) in Gram-positive bacterial species have been solved. Their overall folds are very similar, comprising one largely α -helical region and one β -sheet domain of the protein[19-21,52,53] . The proteins dimerize via the α -helical domain, purified periplasmic domains form concentration-dependent dimers, and changes

at the dimer interface were shown to reduce T4SS function *in vivo* [15, 19, 22]. High-throughput inhibitor screening identified molecules that inhibit the dimerization of *Brucella* VirB8s and derivates of these molecules also inhibited dimerization of TraE as well as the function of the respective T4SS [19, 23, 24]. Interestingly, the inhibitors were found to bind to a surface groove on the protein that is distinct from the dimerization interface raising questions on the mechanism of inhibition [19, 23]. The X-ray structure of an inhibitor-VirB8s complex did not reveal any conformational changes in VirB8s that could explain the mechanism of inhibitor action. The X-ray structures provided molecular details on the dimerization interface, but this approach did not provide information on conformational changes that may occur during monomer-to-dimer transition that may be linked to the function of VirB8 as T4SS assembly factor.

To assess whether the VirB8s protein undergoes conformational changes we analyzed the structure of the periplasmic domain of *Brucella suis* VirB8 (VirB8sp) by NMR spectroscopy at concentrations at which the protein was previously shown to be mostly a monomer or mostly a dimer [15]. We found backbone amide chemical shift changes in different parts of the protein. Analysis of a monomeric variant of the protein (VirB8sp^{M102R}) that was characterized by NMR spectroscopy as well as by X-ray crystallography revealed further chemical shift changes and conformational differences. Finally, small molecules were identified that differentially bind to VirB8sp and VirB8sp^{M102R} showing that the different conformations can be monitored with chemical probes.

Results

NMR assignment of the periplasmic domain of VirB8s

We carried out the NMR chemical shift assignments for the periplasmic domain of *B. suis* VirB8 (VirB8sp, residues 77-239) for which the X-ray structure had previously been determined[20]. Preliminary HSQC analysis of VirB8sp in aqueous buffer did not yield spectra with sufficient resolution to obtain the complete chemical shift assignment. The addition of the zwitterionic detergent CHAPS resulted in HSQC spectra with greatly improved resolution and the CHAPS micelle (7 kDa) did not significantly change the apparent molecular weight of the protein. Since the HSQC spectra of VirB8sp in CHAPS had the best resolution among the different conditions tested, we used this condition for the chemical shift assignments. The backbone chemical shift assignments were carried out on $^{15}N/^{13}C$-labeled VirB8sp comprising 163 residues of the protein. The Cα, C$_\beta$, and CO resonances of VirB8sp were used to measure secondary chemical shifts (Fig. 1B). Using this information, 92% of all residues were assigned (93% of non-prolines), encompassing the backbone amides of 145 residues. Six of the non-assigned residues are prolines that cannot be assigned using this approach. The remaining 12 were not assigned due to weak signals in the 3D experiments, particularly the $^{13}C_\beta$ chemical shifts (residues: Y98, V101, M102, L107, S108, V111, S136, D148, A200, L218, N225, V226). The deduced secondary structure, based on chemical shift index (CSI) analysis, indicates that VirB8sp in the CHAPS micelle has a very similar secondary structure when compared to the crystal structure of VirB8sp (Fig. 1). This suggests that CHAPS micelles do not change the overall three-dimensional

structure. Residues 77-97 and 188-194 were identified as intrinsically disordered regions and this is consistent with the absence of clear electron density in the original X-ray structure [20].

Conformational changes during monomer-to-dimer transition

The dimerization of VirB8s is known to occur in a concentration-dependent manner. We performed NMR chemical shift perturbation studies to identify conformational changes during this monomer-to-dimer transition. ^{1}H-^{15}N HSQC spectra were recorded with ^{15}N-labeled VirB8sp both at a mostly monomer (15 μM) and a mostly dimer concentration (200 μM). Changes in both ^{1}H and ^{15}N chemical shifts were observed for a significant number of signals (Fig. 2A). These experiments were carried out in a phosphate buffer without CHAPS. The signals exhibiting the most significant chemical shift changes (δΔ>0.07) correspond to residues D103, Q109, T121, S134, Y141, S157, V166, I199, Q205, V207, S210, A216 and T227 (Fig. 2B). The signals for residues G174 and N208 were only detected at the mostly dimer concentration and therefore maybe in a region stabilized by the dimerization. The residues that changed during monomer-to-dimer transition are primarily located either in the helical regions or at the dimer interface based on the X-ray structure. However, changes in other parts of the protein including the β-sheet face were also observed (Fig. 2C).

Conformational changes in the presence of CHAPS micelles

We next analyzed chemical shift changes to understand the effect of the CHAPS micelles on the conformation of VirB8sp. ^{1}H-^{15}N HSQC spectra were recorded with ^{15}N-labeled VirB8sp (200 μM) either in the absence or presence of 30 mM CHAPS (Fig. 3A). The CHAPS micelle induced

^{1}H and ^{15}N chemical shift changes for many residues, but the most significant changes ($\delta\Delta > 0.2$) were observed for residues L88, S95, Q109, Y110, Y117, L122, K124, Y126, D152, K153, G156, S157, W198, I199, V207, S210 and L211 (Fig. 3B). Residues Q109, S157, I199, V207, S210 also display chemical shift changes during the monomer-to-dimer transition (shown in green in Fig. 3). In addition, signals for residues D118, D125, T190, Y206 and G223 were only detected in the presence of CHAPS, suggesting that their conformations are stabilized by addition of the detergent (Fig. 3B). Whereas the presence of the CHAPS micelles did not change the overall three-dimensional structure of VirB8sp as compared to the X-ray structure (Fig. 1), it affected the chemical shift of several residues on the surface of the protein and at the dimerization interface (Fig. 3C). Interestingly, the HSQC spectrum recorded at the mostly monomer concentration (15 μM) in CHAPS was very similar to that at 200 μM, suggesting that CHAPS has similar effects on VirB8sp at monomeric and dimeric concentrations (Fig. 3D). Similarly, when we compared the elution of VirB8sp at 15 μM and 200 μM concentrations by size exclusion chromatography in the presence and in the absence of CHAPS, we did not observe significant differences (Fig. 3E). This suggests that CHAPS does not impact the dimeric state of the protein.

NMR analysis of the monomer variant VirB8sp^{M102R}

We have previously determined that VirB8sp^{M102R}, a variant carrying an amino acid substitution at the dimer interface, is a monomer in solution [15, 17]. We analyzed chemical shift changes to assess whether the change of the key amino acid M102 led to conformational changes similar to those observed during the monomer-to-dimer transition of the wild-type protein. The following

experiments were carried out in a phosphate buffer without CHAPS. Surprisingly, when we compared the HSQC spectra of ^{15}N-labeled VirB8sp^{M102R} and VirB8sp (at 15 μM, mostly monomeric state), we detected substantial changes of several signals. However, a full assignment of the VirB8sp^{M102R} variant was not obtained for this study.

Changes in chemical shifts of residues are mapped by overlaying HSQC spectra of VirB8sp and M102R (Fig. 4A). Some of the changes could be mapped leading us to the conclusion that N79, Q109, R114, K124, Y126, K173, Q205, V207 and S210 undergo significant chemical shift perturbations ($\delta\Delta > 0.08$, Fig. 4B). Residues Q109, Q205, V207 and S210 also undergo chemical shift changes during the monomer-to-dimer transition (shown in green in Fig. 4), showing that there is partial overlap in the conformational changes observed with the monomer variant (Fig. 2A). However, the changes of chemical shifts for several residues of M102R (29 in total including; A80, T82, S95, S97, I112, A113, D118, Q123, D125, E127, G147, L151, Y155, N158, S162, G174, T177, K182, T183, R186, T187, D188, Y206, N208, S213, T219, N220, G223, F224) could not be determined due to lack of a full assignment (Fig. 4C). This suggests that the chemical shift changes of VirB8^{M102R} are more substantial than those during the monomer-to-dimer transition of the native protein. Among the residues that could be mapped some undergo notable chemical shift changes including; Q109, R114, K124, Y126, T128, K173, G189, Q205, S210, L218, R179, Y229. A number of these residues with chemical shift changes (L151, K182, and E114) locate in the previously identified inhibitor binding site and in the α1 helix leading to the dimerization site. The changes in chemical shifts for VirB8sp^{M102R} are due to a large change in the electronic environment caused by a change of the oligomeric state as well as some distinct structural changes in the loops and α4 helix. This change in the electronic

environment is larger than what is detected in transition from mostly dimeric to mostly monomeric state of the wild-type protein. These results suggest that the structure of the VirB8sp[M102R] monomer variant may reflect an alternative conformational state of the protein.

X-ray crystallographic analysis of the VirB8sp[M102R] variant

To gain further insights into the importance of the M102 residue for the structure of VirB8s, the crystal structure of VirB8sp[M102R] was determined at 1.95Å resolution. The crystals are in the $P2_1$ space group with four molecules in the asymmetric subunit. The overall structure is similar to the wild-type VirB8s (RMSD 0.53 Å) comprising a β-sheet face and an opposite α-helical region (Fig. 5A). However, analysis of the asymmetric unit revealed that the VirB8sp[M102R] molecules do not interact via the dimerization site in the α-helical region that was observed in the wild-type [20, 21] (Fig. 5B). M102 plays a critical role in dimerization of the wild-type protein by forming a van der Waals contact between the respective methionine residues of both subunits. In contrast, in the asymmetric unit of the VirB8sp[M102R] crystals, the R102 residues are oriented in the opposite direction and do not participate in protein-protein (dimer) interactions (Fig. 5B). Comparison of the wild-type and VirB8sp[M102R] variant shows a substantial difference in the orientation of the α4 region. This may be due to the position of the positively charged R102, which is facing towards the α4 region (Fig. 5C). These results are consistent with the changes observed by NMR spectroscopy in the same region (Fig. 4C) adding to the picture of a significant conformational difference of the VirB8sp[M102R] variant.

Differential scanning fluorimetry reveals conformational differences between VirB8sp and VirB8sp^{M102R}

To gain further insights into the conformational differences between the wild-type protein and the dimer site variant, we performed differential scanning fluorimetry. This approach exploits the change of fluorescence of protein-bound Sypro Orange to determine the melting temperatures (T_m) of VirB8sp and VirB8sp^{M102R} at 15 μM (the mostly monomeric concentration of VirB8sp) (Fig. 6A). The T_m of VirB8sp was determined to be 64.1°C as compared to 65.3°C for VirB8sp^{M102R} suggesting overall similar stability. We next conducted fragment-based screening using a library of 186 small molecules (113-350 Da molecular mass) to assess whether such molecules can serve as probes to differentiate the conformations of the two proteins (supplementary table 1). A positive shift in the T_m value is generally considered as an indication for small molecule binding, and this approach is commonly used as first screening step for fragment-based drug design[25]. The fragment library was independently screened against both proteins and a priority list of molecules that displayed the strongest stabilizing effect on the two proteins was established. Binding molecules were selected based on their capacity to shift the T_m value two-times above the standard deviation of the DMSO control. Fig. 6B and 6C show eight molecules that induce the highest positive shifts of VirB8sp. Most of the tested fragments had very similar effects on VirB8sp and VirB8sp^{M102R}, but interestingly, fragments II and VIII had differential effects on the positive shift of T_m-values. Fragment II preferentially increased the T_m value of VirB8sp whereas fragment VIII preferentially increased the T_m of VirB8sp^{M102R} (Fig. 6B).

Docking simulations suggest differential binding of fragments

To identify potential binding sites for the fragments, we performed *in silico* docking studies. For each molecule, the lowest-energy conformation predicted by the docking calculations was superimposed on the VirB8sp and VirB8sp^{M102R} crystal structures. Fragment II was predicted to occupy a similar site in a surface groove of both proteins that has previously been identified as the binding site for other VirB8s dimerization inhibitors (Fig. 7). In contrast, the docking studies predict that fragment VIII binds to this surface groove only in VirB8sp^{M102R} correlating with the stabilizing effect on this protein variant (Fig. 7). These results suggest that the binding of these molecules is sensitive to the conformational differences between the two proteins. The binding effects of these fragments were further studied by NMR experiments, but we did not observe significant chemical shift perturbations in the presence of the fragments.

Discussion

We have assessed whether VirB8sp undergoes conformational changes during its monomer-to-dimer transition. The disruption of dimerization reduces the functionality of VirB8s homologs *in vivo* suggesting that dimerization has functional importance[15, 22]. The K_D value of dimerization of the purified periplasmic domain VirB8sp is relatively high (100 μM) suggesting that dimerization may only be transient [17]. VirB8sp also interacts with the periplasmic domains of VirB9 and VirB10 and K_D values are in the high nanomolar to micromolar range, suggesting that these interactions may also be transient [17]. Since X-ray crystallography is not the most suited technique to detect subtle conformational changes that may accompany the monomer-to-dimer transition, we have applied NMR spectroscopy to approach this question.

Comparative analysis of chemical shift changes in the HSQC spectra of VirB8sp at mostly monomer and mostly dimer concentrations constitutes evidence for a series of subtle conformational changes at different sites on the protein. It was reported that changes of residues M102, Y105 and E214 interrupt dimerization of VirB8s and reduce functionality of the T4SS complex *in vivo*[15]. NMR analysis provides evidence for changes in the local chemical environment of these regions, which is consistent with their role in dimerization. Residue M102 could not be assigned due to the weak quality of the signal. However, we observed a significant chemical shift change of the adjacent residue D103 during monomer-to-dimer transition. Residues adjacent to Y105 and E214 including Q109, S210 and L211 also underwent significant chemical shift changes at monomer-to-dimer transition. Crystal structures of VirB8 proteins from *B. suis*[20], *A. tumefaciens*[21], *Bartonella grahamii*, *Bartonella birtlesii* TrwG[51] and TraE from the

plasmid pKM101[19] share a high level of structural similarity of their periplasmic domains and dimer interface folds. It is therefore possible that the residues we here identified by NMR have similar functions in dimer-to-monomer transition of other VirB proteins. To support this notion, a recent report suggested that equivalents of the residues Q109 and T121 for which we observed shifts in *Brucella suis* VirB8 as well as of M102 are involved in the dimerization of *Bartonella* VirB8 and TrwG proteins[51].

Interestingly, we obtained the highest quality spectra in the presence of the CHAPS micelle. This was somewhat surprising since we analyzed only the periplasmic domain of VirB8 (VirB8sp) and not the full-length protein. Also, the HSQC spectrum at the mostly monomer concentration (15 μM) in presence of CHAPS was very similar to that at 200 μM (mostly dimer) suggesting that the CHAPS micelles have similar effects on the protein at both concentrations. We observed significant chemical shift changes of residues S157 and S210 during monomer-to-dimer transition and in the presence of the CHAPS micelle. These residues locate in dynamic regions of VirB8sp (S157 in a loop and S210 in the α4 helix), suggesting that dimerization and presence of micelle stabilizes the conformation of VirB8sp. The periplasmic domain is most likely close to or in contact with the membrane in the natural biological context. This would help explain the observation that the addition of CHAPS apparently stabilizes the conformation of the protein.

We also analyzed the dimerization variant VirB8sp[M102R] in order to study an entirely monomeric protein ($K_D > 1$ mM [17]). Surprisingly, analysis of the HSQC spectrum revealed a substantial number of differences as compared to the results obtained with VirB8sp at varying concentrations. The chemical shift changes were quite significant and 24 residues could not even

be assigned by comparing with the HSQC spectrum of the wild-type protein. Amino acids that apparently undergo significant chemical shift changes were localized in several different regions of the protein and many of them localize in the α-helical regions. For example, several amino acids localize on the α1 helix that links the dimerization site to the surface groove to which dimerization inhibitors bind, and in the surface groove itself (e.g. L151, K182, and E114). These results are consistent with the hypothesis that VirB8s inhibitors binding to this surface groove may influence dimerization either via induction of or by blocking of structural changes transmitted from the dimerization site via the α1 helix [23]. We were not able to directly test this hypothesis since the addition of inhibitors such as B8I-2 did not lead to changes in the HSQC spectra. This may be due to the fact that their affinities are weak (EC_{50} for inhibition of dimerization in the low micromolar range [23]).

To gain additional insights into the conformation of the VirB8sp^{M102R} variant, the protein was crystallized and the results showed that the overall fold of the protein was similar to the wild-type protein. However, comparison of the wild-type and VirB8sp^{M102R} X-ray structures revealed subtle changes throughout the protein and a significant change in the orientation of the α4 helix. Significant chemical shift changes for amino acids in the α4 helix were also observed by NMR spectroscopy; the results obtained with both analytical techniques are therefore consistent. Interestingly, whereas the M102 residues of both monomers are adjacent to each other in the structure of the wild-type, the R102 residues face away from each other in the structure of the variant. This difference could be due in part to repulsion between the positive charges of the arginine residues, which forces the protein into a different orientation in the crystal packing. The significant structural differences between the wild-type and the dimerization site variant were

observed by NMR spectroscopy as well as by X-ray crystallography, suggesting that we have discovered an alternative conformation for the protein. While the functionality of dimer site variants is reduced, their conformational differences may reflect alternative states of functional importance. The dimer VirB8s may open and close during T4SS assembly or function in substrate transfer to enable interactions with different VirB proteins. This is consistent with its role as assembly factor.

We were particularly interested in conformational changes affecting the surface groove of VirB8s that was previously shown to be the binding site for dimerization inhibitors[23]. To this effect, we pursued a fragment-screening based approach to probe the VirB8sp wild-type and the dimerization variant using a small library of 186 fragments with DSF as the readout. If molecules cause positive shifts of the thermal meting curve this is generally viewed as evidence for binding. Whereas most molecules had no or identical effects on the melting temperatures (ΔTm values) of both proteins, two fragments (II and VIII) had differential effects. Fragment II is a salicylanilide that causes a positive shift of the melting temperature of the wild-type protein. The binding site of this molecule predicted by docking is similar to that of previously analysed VirB8s dimerization inhibitors. Interestingly, the structure of this molecule is similar to the VirB8s dimerization inhibitor B8I-2 [23], which would explain why it has a similar binding site. Subtle differences in this surface groove may reduce binding of molecule II to the VirB8sp^{M102R} variant explaining the reduced thermal stabilization. In fact, we observed significant chemical shift changes of the dimerization inhibitor binding site in the α1 helix close to E114, of L151 and of K182 thereby supporting this notion. In contrast, fragment VIII is a benzimidazole that preferentially shifts the melting temperature of VirB8sp^{M102R}. Docking studies predicts that it

may bind to the same site as fragment II. However, this was only observed for the dimerization variant, which is likely due to a conformational change of the surface groove. Fragment-based screening has therefore identified two molecules that serve as chemical probes for selecting between the different conformations of VirB8sp and of VirB8sp^{M102R}, respectively. Despite this finding, further NMR studies on VirB8sp and VirB8sp^{M102R} in presence of fragments II and VIII did not reveal any significant chemical shift changes. However, molecules of similar chemical structures (salicylanilides and benzimidazoles) are known to possess antibacterial and antiviral properties, and it may be possible to develop the fragments we discovered into inhibitors of VirB8s dimerization in the future by medicinal chemistry[26-28]. Apart from future possibilities to develop these molecules into inhibitors, this work also improves our understanding of the structural dynamics of the monomer-to-dimer transition of VirB8s and provides insights into its functional role in T4SS assembly. Dimerization of the full-length protein was also shown using the bacterial and yeast two-hybrid systems [13, 16, 17]. In future, work on the full-length VirB8s protein will reveal the contribution of membrane association to dimerization of VirB8s.

Materials and Methods

Cloning and protein expression. The strains and plasmids used in this study are presented in Table 2. For cloning experiments, cultures of *E. coli* JM109 were grown at 37°C in LB medium (1% tryptone (w/v), 0.5% yeast extract (w/v), 1% NaCl (w/v)) in the presence of kanamycin (50 mg/ml). Plasmid pHTVirB8sp (for expression of VirB8sp) and its variant pHTM102R (for expression of VirB8sp^{M102R}) were transformed into *E. coli* strain BL21 star (DE3) for protein overproduction. For NMR studies, ^{15}N-labeled and ^{15}N/^{13}C-labeled proteins were expressed in M9 minimal media containing ^{15}NH$_4$Cl and/or ^{13}C6-glucose (Sigma-Aldrich) as the sole nitrogen and carbon sources. 1 liter of M9 minimal media supplemented with 2 g/L ^{13}C-glucose and 1 g/L ^{15}NH$_4$Cl were inoculated to an OD$_{600}$ of 0.05 from an overnight culture grown in LB. Cells were cultivated under aerobic conditions at 37°C to an OD$_{600}$ of 0.7 and gene expression was induced by the addition of 0.5 mM IPTG (isopropyl-β-D-thiogalactopyranoside). Cultivation under aerobic conditions proceeded at 25°C for 16h after induction. For overproduction of VirB8sp^{M102R} for crystallographic experiments an overnight culture in LB was inoculated into 1L of LB media, cultivated under aerobic conditions at 37 °C to an OD$_{600}$ of 0.7, 0.5 mM IPTG was added to induce gene expression and cultivation under aerobic conditions proceeded at 25°C for 16 h.

Protein purification. Hexa-histidine-tagged *B. suis* VirB8sp (residues 77–239) was purified by metal ion affinity chromatography, followed by cleavage of the tag with TEV protease and gel filtration as described [23]. Hexa-histidine-tagged *B. suis* VirB8sp^{M102R} (residues 77–239) was

purified using the same procedure using 25 mM HEPES, 100 mM NaCl (pH 8) as buffer for gel filtration.

NMR experiments. All NMR experiments were carried out at temperature 300 K either on a Bruker 500 MHz spectrometer (at Université de Montréal) or a 800 MHz Varian INOVA spectrometer (Québec/Eastern Canada High Field NMR Facility) equipped with z-pulsed-field gradient units and triple resonance probes. NMR data were processed using NMRPipe[29] and analyzed by CCPNMR[30].–Assignment experiments were carried out using 350 μM ^{15}N,^{13}C-labeled VirB8sp dissolved in 20 mM sodium phosphate at pH 7, 100 mM NaCl, 30 mM CHAPS and 90% (vol/vol) H_2O/10% (vol/vol) D_2O. Sequential backbone assignments were acquired through standard assignment experiments including 2D ^{1}H-^{15}N HSQC[31], 3D HNCA[32], 3D HNCACB[33], 3D HNCO[34], 3D HN(CA)CO[35], 3D HN(CO)CA[36], CBCA(CO)NH[37], and 3D ^{15}N-edited NOESY-HSQC[38] with a 65 ms mixing time. Secondary NMR chemical shifts were calculated by CCPNMR Analysis 2.4[39] and chemical shift index (CSI) values were obtained based on the Wishart and Sykes method[40, 41]. Signal peaks in HSQC experiments without presence of CHAPS micelles were referenced based on the assignment of the sample in CHAPS micelles. To reference the assigned peaks, HSQC spectra of VirB8sp at 200 μM were collected while CHAPS was added to the sample. The final concentration of CHAPS in the sample for data collection at each point was 5 mM, 15 mM and 30 mM, respectively. Changes upon increase of the CHAPS concentration were used to track the chemical shifts of assigned residues in the sample without CHAPS micelles. The NMR chemical shifts of VirB8sp have been deposited in the BioMagResBank, www.bmrb.wisc.edu (accession no. 26852).

NMR chemical shift perturbation experiments. The chemical shifts were calculated from ^{1}H-^{15}N HSQC experiments using the formula $\Delta\delta=[(0.17\Delta NH)^2 +(\Delta HN)^2]^{\frac{1}{2}}$. Significance values in Figures 2-4 are indicated by a horizontal line, which indicates the average change in chemical shifts of residues plus one standard deviation. NMR chemical shift perturbation experiments to assess the effect of dimerization of VirB8sp comprised two samples of ^{15}N-VirB8sp at 15 µM and 200 µM concentration, respectively, in 20 mM sodium phosphate (pH 7) 100 mM NaCl and 90% (vol/vol) H_2O/10% (vol/vol) D_2O. For NMR chemical shift perturbation experiments to assess the effect of CHAPS, the detergent was added into a sample of 0.2 mM ^{15}N-VirB8sp in 20 mM sodium phosphate (pH 7), 100 mM NaCl and 90% (vol/vol) H_2O/10% (vol/vol) D_2O. The final concentrations of CHAPS in the sample for data collection was 30 mM. The effect of CHAPS micelle was also assessed for 15 µM ^{15}N-VirB8sp. NMR chemical shift comparisons of VirB8sp and VirB8sp^{M102R} were acquired from experiments with 15 µM of ^{15}N-VirB8sp and ^{15}N- VirB8sp^{M102R} in 20 mM sodium phosphate (pH 7), 100 mM NaCl and 90% (vol/vol) H_2O/10% (vol/vol) D_2O.

Differential scanning fluorimetry (DSF). A library of 186 fragments was used in this study that followed the 'rule of three' characteristics[42] (listed in supplementary information). DSF experiments were conducted using 20 µM of protein, 15x concentration of SYPRO Orange (from 5000x stock solution, ThermoFisher) in 50 mM Tris (pH 8), 100 mM NaCl and 5% final concentration of DMSO. For fragment-based screening, small molecules were added to final concentrations of 5 mM. SYPRO Orange is a fluorescent dye that binds non-specifically to hydrophobic surfaces of proteins. The melting temperature with highest level of SYPRO Orange fluorescence indicates the complete unfolding and stability of the protein. SYPRO Orange

fluorescence was monitored over 20-95°C with a LightCycler® 480 instrument (Roche). The LightCycler® 480 Software was used to calculate the first derivate of the resulting melting curve, with the steepest point of the slope being the T_m. Due to the nature of the experiment, it is not possible to subtract the potential interference of SYPRO with fragments from calculations. Results show average T_m of triplicates from three independent experiments.

Crystallization of VirB8sp^{M102R} and data collection. Initial crystallization conditions were identified using the MCSG crystallization screen (Microlytic) in 96-well plates and a sitting drop method. Crystallization conditions were optimized and crystals were grown at room temperature using the hanging drop vapour diffusion method in 0.1 M Tris/HCl pH 6.8, 18% PEG-MME 2000. Plate-shaped crystals appeared within three days of crystal setup that diffracted to 1.95 Å at the Canadian Light Source (Saskatchewan, Canada). The collected data were processed with HKL2000 [43] in the P2$_1$ space group. The structure was solved by molecular replacement using the Phoenix suite [44] using the *Brucella* VirB8sp structure as template (PDB ID: 2BHM). Refinements were performed using refmac and COOT [45, 46] and figures were generated using Pymol [47].

***In silico* docking.** Subunit A of VirB8sp structure (PDB 2BHM [20]) and VirB8sp^{M102R} (PDB 5JBS) were used for docking analyses. Docking simulations were conducted using AutodockTools software [48, 49]. Polar hydrogen atoms were added to the protein structures and Gaisteger charges were calculated for each atom. Affinity grids were calculated using autogrid4 for each atom type found in the small molecules for 120 x 120 x 120 A° with 0.3 A° spacing positioned on the center of mass of the protein structures. Chemical structures for each small

molecule were retrieved from the ZINC database[50] in MOL2 format and converted to PDB format using AutodockTools. Hydrogen atoms, Gaisteger charges, and atom types were added to each file using AutodockTools. For docking, the Lamarckian genetic algorithm was used for Autodock 4.0. Search parameters were set to population size of 150 individuals; 25 million energy evaluations; a maximum of 27,000 generations, with one top individual to survive to the next generation; a mutation rate of 0.02; and a crossover rate of 0.8. The local search probability was set to 0.06 with 300 iterations. Docking for each small molecule was run 100 times, a 2 Å RMSD threshold was defined to cluster the docked conformations.

Acknowledgements

Funding

Notes

The authors declare no competing financial interest.

Author Contributions

Mahzad Sharifahmadian – conducted experiments, analysed data, revised manuscript

Tarun Arya – conducted experiments, analysed data, revised manuscript

Benoit Bessette – conducted experiments, analysed data

Lauriane Lecoq – conducted experiments, analysed data

Edward Ruediger – provided resources (fragments), analysed data

James G. Omichinski – analysed data, revised manuscript

Christian Baron – analysed data, wrote and revised manuscript

References

1] Fronzes, R., Christie, P. J., and Waksman, G. (2009) The structural biology of type IV secretion systems, *Nature reviews. Microbiology 7*, 703-714.

[2] Trokter, M., Felisberto-Rodrigues, C., Christie, P. J., and Waksman, G. (2014) Recent advances in the structural and molecular biology of type IV secretion systems, *Current opinion in structural biology 27C*, 16-23.

[3] Chandran Darbari, V., and Waksman, G. (2015) Structural Biology of Bacterial Type IV Secretion Systems, *Annu Rev Biochem 84*, 603-629.

[4] Goessweiner-Mohr, N., Arends, K., Keller, W., and Grohmann, E. (2013) Conjugative type IV secretion systems in Gram-positive bacteria, *Plasmid 70*, 289-302.

[5] Lai, E.-M., and Kado, C. I. (1998) Processed VirB2 is the major subunit of the promiscuous pilus of *Agrobacterium tumefaciens*, *J. Bacteriol. 180*, 2711-2717.

[6] Eisenbrandt, R., Kalkum, M., Lai, E. M., Lurz, R., Kado, C. I., and Lanka, E. (1999) Conjugative pili of IncP plasmids, and the Ti plasmid T pilus are composed of cyclic subunits, *J. Biol. Chem. 274*, 22548-22555.

[7] Aly, K. A., and Baron, C. (2007) The VirB5 protein localizes to the T-pilus tips in *Agrobacterium tumefaciens*, *Microbiology 153*, 3766-3775.

[8] Kwok, T., Zabler, D., Urman, S., Rohde, M., Hartig, R., Wessler, S., Misselwitz, R., Berger, J., Sewald, N., Konig, W., and Backert, S. (2007) Helicobacter exploits integrin for type IV secretion and kinase activation, *Nature 449*, 862-866.

[9] Thorstenson, Y. R., and Zambryski, P. C. (1994) The essential virulence protein VirB8 localizes to the inner membrane of *Agrobacterium tumefaciens*, *J. Bacteriol. 176*, 1711-1717.

[10] Buhrdorf, R., Forster, C., Haas, R., and Fischer, W. (2003) Topological analysis of a putative VirB8 homologue essential for the cag type IV secretion system in *Helicobacter pylori*, *Int. J. Med. Microbiol. 293*, 213-217.

[11] O´Callaghan, D., Cazevieille, C., Allardet-Servent, A., Boschiroli, M. L., Bourg, G., Foulongne, V., Frutos, P., Kulakov, Y., and Ramuz, M. (1999) A homologue of the *Agrobacterium tumefaciens* VirB and *Bordetella pertussis* Ptl type IV secretion systems is essential for intracellular survival of *Brucella suis*, *Mol. Microbiol. 33*, 1210-1220.

[12] Fercher, C., Probst, I., Kohler, V., Goessweiner-Mohr, N., Arends, K., Grohmann, E., Zangger, K., Meyer, N. H., and Keller, W. (2016) VirB8-like protein TraH is crucial for DNA transfer in Enterococcus faecalis, *Sci Rep 6*, 24643.

[13] Das, A., and Xie, Y.-H. (2000) The *Agrobacterium* T-DNA transport pore proteins VirB8, VirB9 and VirB10 interact with one another, *J. Bacteriol. 182*, 758-763.

[14] Yuan, Q., Carle, A., Gao, C., Sivanesan, D., Aly, K., Höppner, C., Krall, L., Domke, N., and Baron, C. (2005) Identification of the VirB4-VirB8-VirB5-VirB2 pilus assembly sequence of type IV secretion systems, *J. Biol. Chem. 280*, 26349-26359.

[15] Paschos, A., Patey, G., Sivanesan, D., Gao, C., Bayliss, R., Waksman, G., O'Callaghan, D., and Baron, C. (2006) Dimerization and interactions of *Brucella suis* VirB8 with VirB4 and VirB10 are required for its biological activity, *Proc. Natl. Acad. Sci. USA 103*, 7252-7257.

[16] Bourg, G., Sube, R., O'Callaghan, D., and Patey, G. (2009) Interactions between *Brucella suis* VirB8 and its homolog TraJ from the plasmid pSB102 underline the dynamic nature of type IV secretion systems, *J Bacteriol 191*, 2985-2992.

[17] Sivanesan, D., Hancock, M. A., Villamil Giraldo, A. M., and Baron, C. (2010) Quantitative analysis of VirB8-VirB9-VirB10 interactions provides a dynamic model of type IV secretion system core complex assembly, *Biochemistry 49*, 4483-4493.

[18] Villamil Giraldo, A. M., Sivanesan, D., Carle, A., Paschos, A., Smith, M. A., Plesa, M., Coulton, J., and Baron, C. (2012) Type IV secretion system core component VirB8 from *Brucella* binds to the globular domain of VirB5 and to a periplasmic domain of VirB6, *Biochemistry 51*, 3881-3890.

[19] Casu, B., Smart, J. P., Hancock, M. A., Smith, M., Sygusch, J., and Baron, C. (2016) Structural analysis and inhibition of TraE from the pKM101 type IV secretion system, *J Biol. Chem.*, PMID: 27634044

[20] Terradot, L., Bayliss, R., Oomen, C., Leonard, G., Baron, C., and Waksman, G. (2005) Crystal Structures of the periplasmic domains of two core subunits of the bacterial type IV secretion system, VirB8 from *Brucella suis* and ComB10 from *Helicobacter pylori*, *Proc. Natl. Acad. Sci. USA 102*, 4596-4601.

[21] Bailey, S., Ward, D., Middleton, R., Grossmann, J. G., and Zambryski, P. (2006) *Agrobacterium tumefaciens* VirB8 structure reveals potential protein-protein interactions sites, *Proc. Natl. Acad. Sci. USA 103*, 2582-2587.

[22] Sivanesan, D., and Baron, C. (2011) The dimer interface of *Agrobacterium tumefaciens* VirB8 is important for type IV secretion system function, stability and for association of VirB2 with the core complex, *J. Bacteriol. 193*, 2097-2106.

[23] Smith, M. A., Coincon, M., Paschos, A., Jolicoeur, B., Lavallee, P., Sygusch, J., and Baron, C. (2012) Identification of the Binding Site of *Brucella* VirB8 Interaction Inhibitors, *Chem Biol 19*, 1041-1048.

[24] Paschos, A., den Hartigh, A., Smith, M. A., Atluri, V. L., Sivanesan, D., Tsolis, R. M., and Baron, C. (2011) An In Vivo High-Throughput Screening Approach Targeting the Type IV Secretion System Component VirB8 Identified Inhibitors of *Brucella abortus 2308* Proliferation, *Infect Immun 79*, 1033-1043.

[25] Delaglio, F., Grzesiek, S., Vuister, G. W., Zhu, G., Pfeifer, J., and Bax, A. (1995) NMRPipe: a multidimensional spectral processing system based on UNIX pipes, *J Biomol NMR 6*, 277-293.

[26] Vranken, W. F., Boucher, W., Stevens, T. J., Fogh, R. H., Pajon, A., Llinas, M., Ulrich, E. L., Markley, J. L., Ionides, J., and Laue, E. D. (2005) The CCPN data model for NMR spectroscopy: development of a software pipeline, *Proteins 59*, 687-696.

[27] Bodenhausen, G., and Ruben, D. J. (1980) Natural abundance nitrogen-15 NMR by enhanced heteronuclear spectroscopy, *Chemical Physics Letters 69*, 185-189.

[28] Bax, A., and Ikura, M. (1991) An efficient 3D NMR technique for correlating the proton and 15N backbone amide resonances with the alpha-carbon of the preceding residue in uniformly 15N/13C enriched proteins, *J Biomol NMR 1*, 99-104.

[29] Wittekind, M., and Mueller, L. (1993) HNCACB, a high-sensitivity 3D NMR experiment to correlate amide-proton and nitrogen resonances with the alpha- and beta-carbon resonances in proteins, *J. Magn. Reson. B 101*, 201-205.

[30] Kay, L. E., Xu, G. Y., and Yamazaki, T. (1994) Enhanced-sensitivity triple-resonance spectroscopy with minimal H2O saturation, *J. Magn. Reson. A 109*, 129-133.

[31] Clubb, R. T., Venkataraman, T., and Wagner, G. (1969) A constant-time three-dimensional triple-resonance pulse scheme to correlate intraresidue 1HN, 15N, and 13C′ chemical shifts in 15N-13C-labelled proteins, *J. Mag. Res. 97*, 213-217.

[32] Bax, A., and Ikura, M. (1991) An efficient 3D NMR technique for correlating the proton and 15N backbone amide resonances with the alpha-carbon of the preceding residue in uniformly 15N/13C enriched proteins, *J. Biomol. NMR 1*, 99-104.

[33] Grzesiek, S., and Bax, A. (1992) Correlating Backbone Amide and Side-Chain Resonances in Larger Proteins by Multiple Relayed Triple Resonance Nmr, *Journal of the American Chemical Society 114*, 6291-6293.

[34] Pascal, S. M., Muhandiram, D. R., Yamazaki, T., Forman-Kay, J. D., and Kay, L. E. (1994) Simultaneous acquisition of 15N- and 13C-edited NOE spectra of proteins dissolved in H2O, *J. Magn. Reson. A 103*, 197-201.

[35] Schwarzinger, S., Kroon, G. J. A., Foss, T. R., Chung, J., Wright, P. E., and Dyson, H. J. (2001) Sequence-Dependent Correlation of Random Coil NMR Chemical Shifts, *J. Am. Chem. Soc. 123*, 2970-2978.

[36] Wishart, D. S., and Sykes, B. D. (1994) The 13C chemical-shift index: a simple method for the identification of protein secondary structure using 13C chemical-shift data, *J. Biomol. NMR. 4*, 171-180.

[37] Wishart, D. S., Sykes, B. D., and Richards, F. M. (1992) The chemical shift index: a fast and simple method for the assignment of protein secondary structure through NMR spectroscopy, *Biochemistry 31*, 1647-1651.

[38] Congreve, M., Carr, R., Murray, C., and Jhoti, H. (2003) A 'rule of three' for fragment-based lead discovery?, *Drug discovery today 8*, 876-877.

[39] Otwinowski, Z., and Minor, W. (1997) Processing of X-ray diffraction data collected in oscillation mode, *Methods Mol Med Methods Enzymol 276*, 307-326.

[40] Adams, P. D., Grosse-Kunstleve, R. W., Hung, L. W., Ioerger, T. R., McCoy, A. J., Moriarty, N. W., Read, R. J., Sacchettini, J. C., Sauter, N. K., and Terwilliger, T. C. (2002) PHENIX: building new software for automated crystallographic structure determination, *Acta crystallographica. Section D, Biological crystallography 58*, 1948-1954.

[41] Murshudov, G. N., Vagin, A. A., and Dodson, E. J. (1997) Refinement of macromolecular structures by the maximum-likelihood method, *Acta crystallographica. Section D, Biological crystallography 53*, 240-255.

[42] Emsley, P., and Cowtan, K. (2004) Coot: model-building tools for molecular graphics, *Acta crystallographica. Section D, Biological crystallography 60*, 2126-2132.

[43] DeLano, W. L. (2002) The PyMOL Molecular Graphics System, DeLano Scientific LLC, San Carlos, CA, USA.

[44] Morris, G. M., Goodsell, D. S., Halliday, R. S., Huey, R., Hart, W. E., Belew, R. K., and Olson, A. J. (1998) Automated docking using a Lamarckian genetic algorithm and an empirical binding free energy function, *J Comput Chem 19*, 1639-1662.

[45] Morris, G. M., Huey, R., and Olson, A. J. (2008) Using AutoDock for ligand-receptor docking, *Curr Protoc Bioinformatics Chapter 8*, Unit 8 14.

[46] Irwin, J. J., Sterling, T., Mysinger, M. M., Bolstad, E. S., and Coleman, R. G. (2012) ZINC: a free tool to discover chemistry for biology, *J Chem Inf Model 52*, 1757-1768.

[47] Mashalidis, E. H., Sledz, P., Lang, S., and Abell, C. (2013) A three-stage biophysical screening cascade for fragment-based drug discovery, *Nature protocols 8*, 2309-2324.

[48] Lee, I. Y., Gruber, T. D., Samuels, A., Yun, M., Nam, B., Kang, M., Crowley, K., Winterroth, B., Boshoff, H. I., and Barry, C. E., 3rd. (2013) Structure-activity relationships of antitubercular salicylanilides consistent with disruption of the proton gradient via proton shuttling, *Bioorg Med Chem 21*, 114-126.

[49] Gong, Y., Somersan Karakaya, S., Guo, X., Zheng, P., Gold, B., Ma, Y., Little, D., Roberts, J., Warrier, T., Jiang, X., Pingle, M., Nathan, C. F., and Liu, G. (2014) Benzimidazole-based compounds kill Mycobacterium tuberculosis, *Eur J Med Chem 75*, 336-353.

[50] Goudreau, N., Lemke, C. T., Faucher, A. M., Grand-Maitre, C., Goulet, S., Lacoste, J. E., Rancourt, J., Malenfant, E., Mercier, J. F., Titolo, S., and Mason, S. W. (2013) Novel inhibitor binding site discovery on HIV-1 capsid N-terminal domain by NMR and X-ray crystallography, *ACS Chem Biol 8*, 1074-1082.

[51] Gillespie, J. J., Phan, I. Q. H., Scheib, H., Subramanian, S., Edwards, T. E., Lehman, S. S., … Pulliainen, A. T. (2015) Structural Insight into How Bacteria Prevent Interference between Multiple Divergent Type IV Secretion Systems. *mBio*, *6*(6), e01867–15.

[52] Porter, C. J., Bantwal, R., Bannam, T. L., Rosado, C. J., Pearce, M. C., Adams, V., Lyras, D., Whisstock, J. C. and Rood, J. I. (2012) The conjugation protein TcpC from *Clostridium perfringens* is structurally related to the type IV secretion system protein VirB8 from Gram-negative bacteria. *Molecular Microbiology, 83*: 275–288.

[53] Goessweiner-Mohr, N., Grumet, L., Arends, K., Pavkov-Keller, T., Gruber, C. C., Gruber, K., ... & Keller, W. (2013) The 2.5 Å structure of the Enterococcus conjugation protein TraM resembles VirB8 type IV secretion proteins. *Journal of Biological Chemistry*, *288*(3), 2018-2028.

[54] Yanisch-Perron, C., Viera, J., and Messing, J. (1985) Improved M13 phage cloning vectors and host strains: nucleotide sequence of the M13mp18 and pUC18 vectors, *Gene 33*, 103-119.

Tables

Table 1. Data collection of the VirB8sp^{M102R} variant.

	VirB8sp^{M102R}
Resolution range (Å)	42.20 - 1.95 (2.02 - 1.95)
Space group	P2$_1$
Unit cell parameters: a (Å), b (Å), c (Å), β	67.5, 78.7, 70.8, 111.56
Total reflections	163793
Unique reflections	48835 (4316)
Multiplicity	3.4 (3.2)
Completeness (%)	97.0 (85.84)
Mean I/σ(I)	17.1 (2.4)
Wilson B-factor	36.05
R-merge	0.072
R-meas	0.086
R-work	0.1909
R-free	0.2409
Number of non-hydrogen atoms	4 679
Macromolecules	4 562
Water	117
Protein residues	558
RMS bonds (Å)	0.018
RMS angles (°)	1.84
Ramachandran favored (%)[c]	97
Ramachandran allowed (%)[c]	2.40
Ramachandran outliers (%)[c]	0.59
Clashscore	3.15
Average B-factor (Å^2)	47.10
PDB ID	5JBS

Table 2: **Bacterial strains and plasmids.**

Strain	Genotype or Description	Source or Reference
JM109	*endA1 gyr96 thi hsdR71 supE44 recA1 relA1 (Δlac-proAB) (F'traD36 proAB+lacIqlacZΔM15)*	[54]
BL21 Star (DE3)	*F– ompT hsdSB(rB–, mB–) gal dcm rne131 (DE3)*	Invitrogen
Plasmids		
pHT	kan[r] pET24d derivative T7 expression vector with N-terminal 6xHis-tag and TEV protease cleavage site	[23]
pHTVirB8sp	kan[r] T7 promoter vector for expression of the 6xHis-tagged periplasmic domain of *B. suis* VirB8	[23]
pHTVirB8sp[M102R]	kan[r] pHTVirB8sp modified to encode VirB8 with amino acid change M102R	[15]

Figures
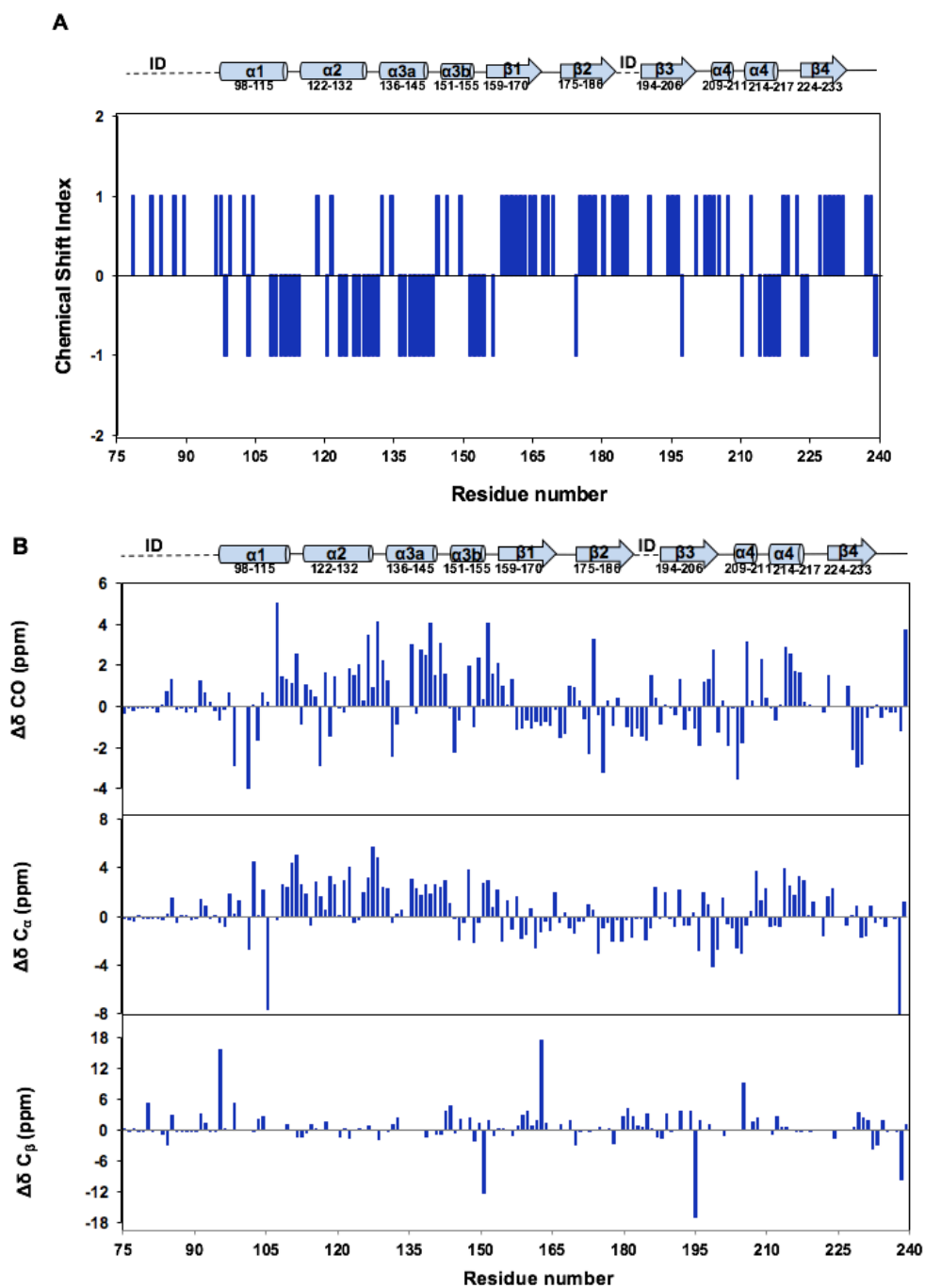
Figure 1. Secondary structure analysis of VirB8sp in solution based on NMR experiments.

(A) Chemical shift index (CSI) consensus values (bars) of VirB8sp in CHAPS micelles were

measured. Negative CSI values indicate helical segments. The secondary structures are indicated corresponding to the secondary structures in the VirB8sp crystal. Intrinsically disordered regions are identified as ID (residues 76-97 and 188-194). These regions were not defined in the crystal structure. A α-helices, β-strands, loops and intrinsically disordered regions are identified as cylinders, arrows, solid lines and dashed lines, respectively. (B) Secondary NMR chemical shifts of CO, C_α and C_β nuclei for VirB8 are presented. The secondary structures based on the crystal structure of VirB8 are shown for comparison[1].

Figure 2. NMR mapping studies of VirB8sp dimerization. (A) Overlay of ^{1}H-^{15}N HSQC spectra of VirB8sp at 15 μM (blue) and 200 μM (red); arrows indicate the signals that display significant chemical shift changes. Common changes are labelled in green in Figures 3 and 4. (B) Histogram of the variation in chemical shifts [Δδ (ppm)] observed in ^{1}H-^{15}N HSQC spectra of ^{15}N-labeled VirB8sp at 15 μM and 200 μM. The chemical shift perturbations were calculated with the formula Δδ=[(0.17ΔNH)^2 +(ΔHN)^2]$^{1/2}$, and are given in parts per million. ΔδHN

values above the horizontal line that indicates the average of changes plus one standard deviation are considered significant. Asterisks indicate residues present only at the mostly dimer concentration. (C) Mapping of residues (shown in red) for which significant chemical shift changes are observed mapped on the cartoon structure of VirB8sp (PDB code 2BHM) [20].
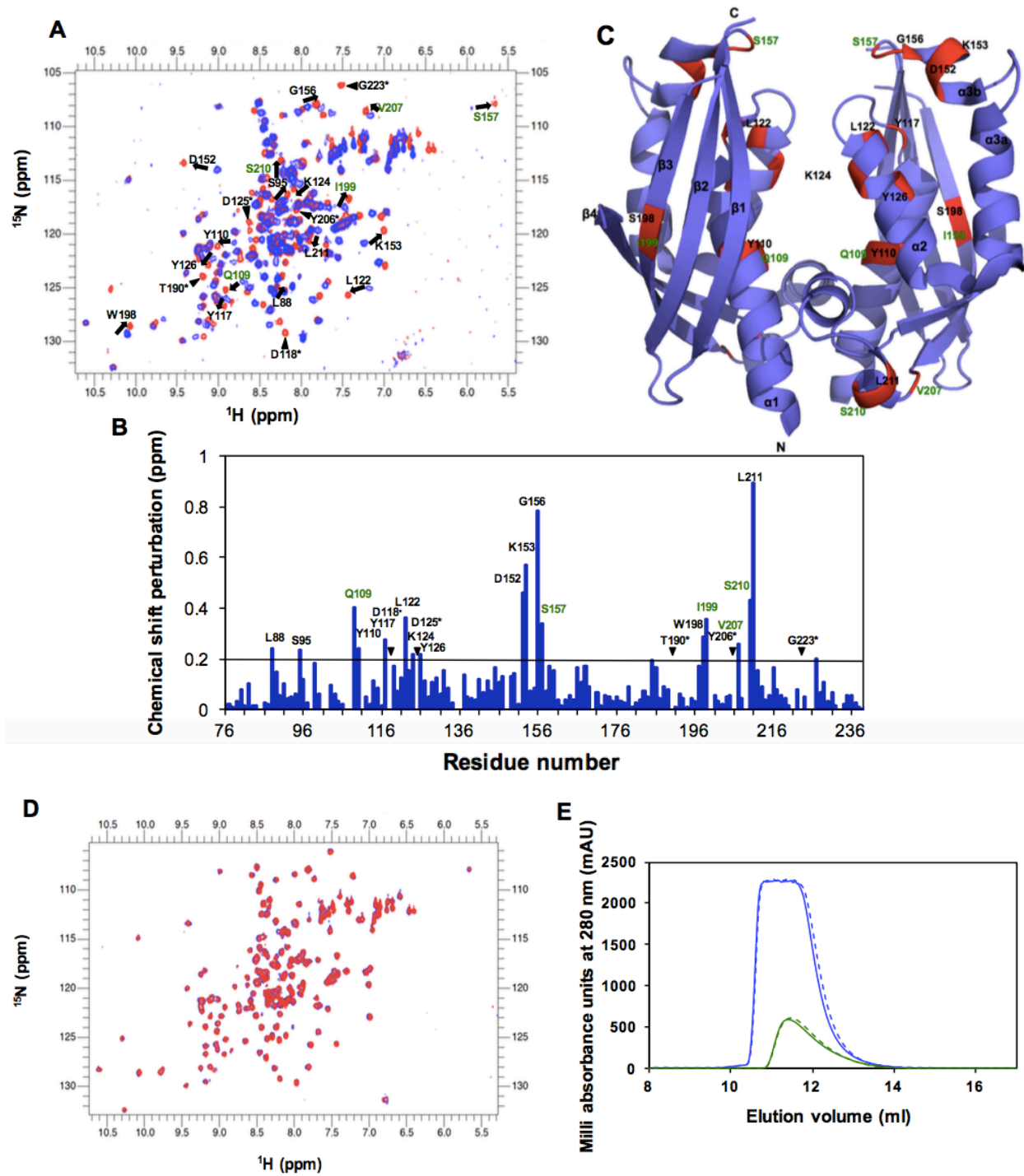
Figure 3. Chemical shift changes following the addition of CHAPS. (A) Overlay of ^{1}H-^{15}N

HSQC spectra of VirB8sp at 200 μM in either the absence (red) or in the presence of 30 mM

CHAPS (blue); arrows indicate the significant chemical shift changes. Residues labelled in green also undergo chemical shift changes during the monomer-to-dimer transition (Figure 2). (B) The chemical shift perturbations in the ^{1}H-^{15}N HSQC spectra of ^{15}N-labeled VirB8sp are presented as $\Delta\delta=[(0.17\Delta NH)^2 +(\Delta HN)^2]^{\frac{1}{2}}$. The values above 0.2 ppm (mean of changes plus one standard deviation) are considered significant. Asterisks in the histogram indicate residues that are detected only in the presence of CHAPS. (C) Mapping of residues (in red) displaying significant chemical shift changes in the presence of CHAPS mapped on a cartoon representation of the crystal structure of VirB8sp[20]. (D) Overlay of ^{1}H-^{15}N HSQC spectra of VirB8sp in presence of 30 mM CHAPS at 15 μM (red) and 200 μM (blue) protein concentrations. (E) Size exclusion chromatography on a S75 gel filtration column of VirB8sp at 200 μM (blue lines) and 15 μM (green lines) concentration in the presence (full lines) or in the absence (dotted lines) of 30 mM CHAPS.
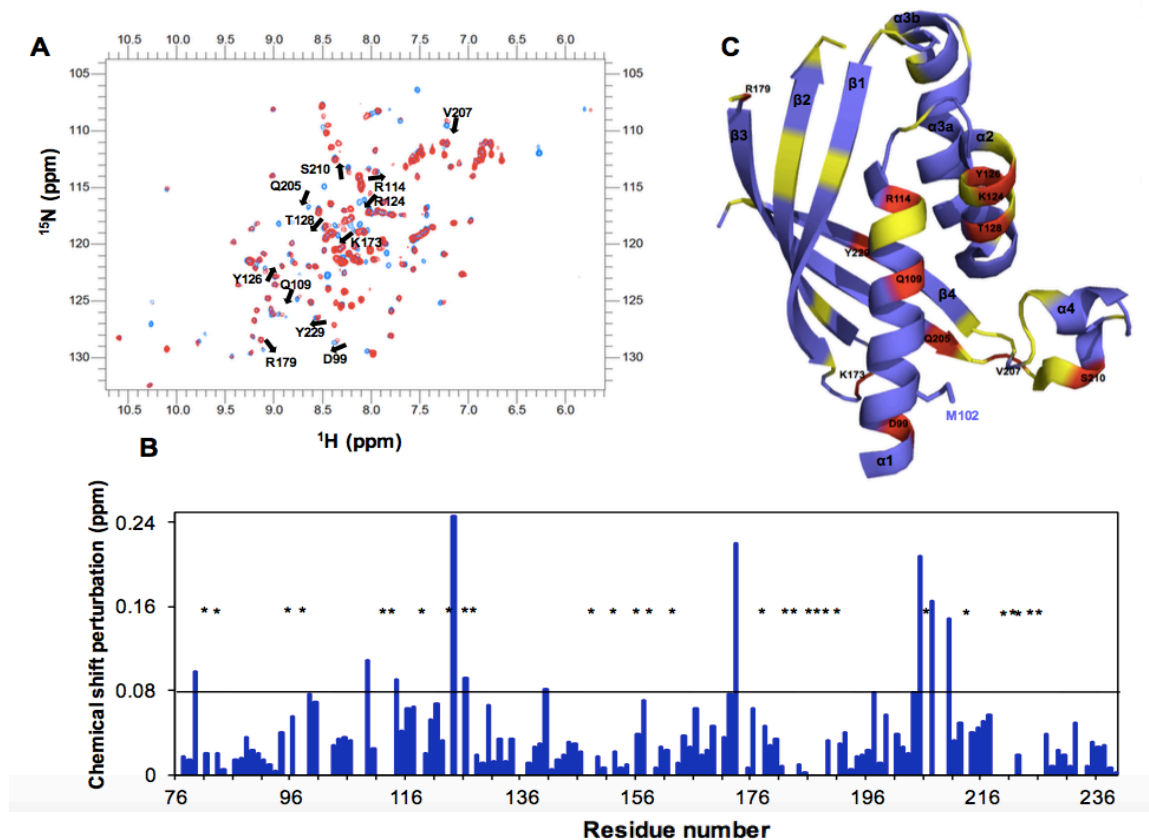
Figure 4. The VirB8sp[M102R] variant has a different conformation than wild-type VirB8sp. (A) Overlay of ^{1}H-^{15}N HSQC spectra of VirB8sp (red) and the VirB8sp[M102R] variant (blue) at 15 μM; arrows indicate the residues undergone significant chemical shift changes. Residues labelled in green also undergo chemical shift changes during the monomer-to-dimer transition (Figure 2). (B) Changes of chemical shifts observed in the ^{1}H-^{15}N HSQC spectrum of VirB8sp[M102R] when compared to VirB8sp. (Δδ was calculated for residues that could be mapped based on the formula; Δδ=[(0.17ΔNH)^2 +(ΔHN)^2]$^{\frac{1}{2}}$). Asterisks in the histogram correspond to the residues of VirB8sp that could not be mapped in the ^{1}H-^{15}N HSQC spectrum of VirB8sp[M102R]. (C) Residues of VirB8sp (red) for which significant chemical shift changes in VirB8sp[M102R] were observed (red) or that could not be mapped (yellow) on the crystal structure of the VirB8sp monomer [20].
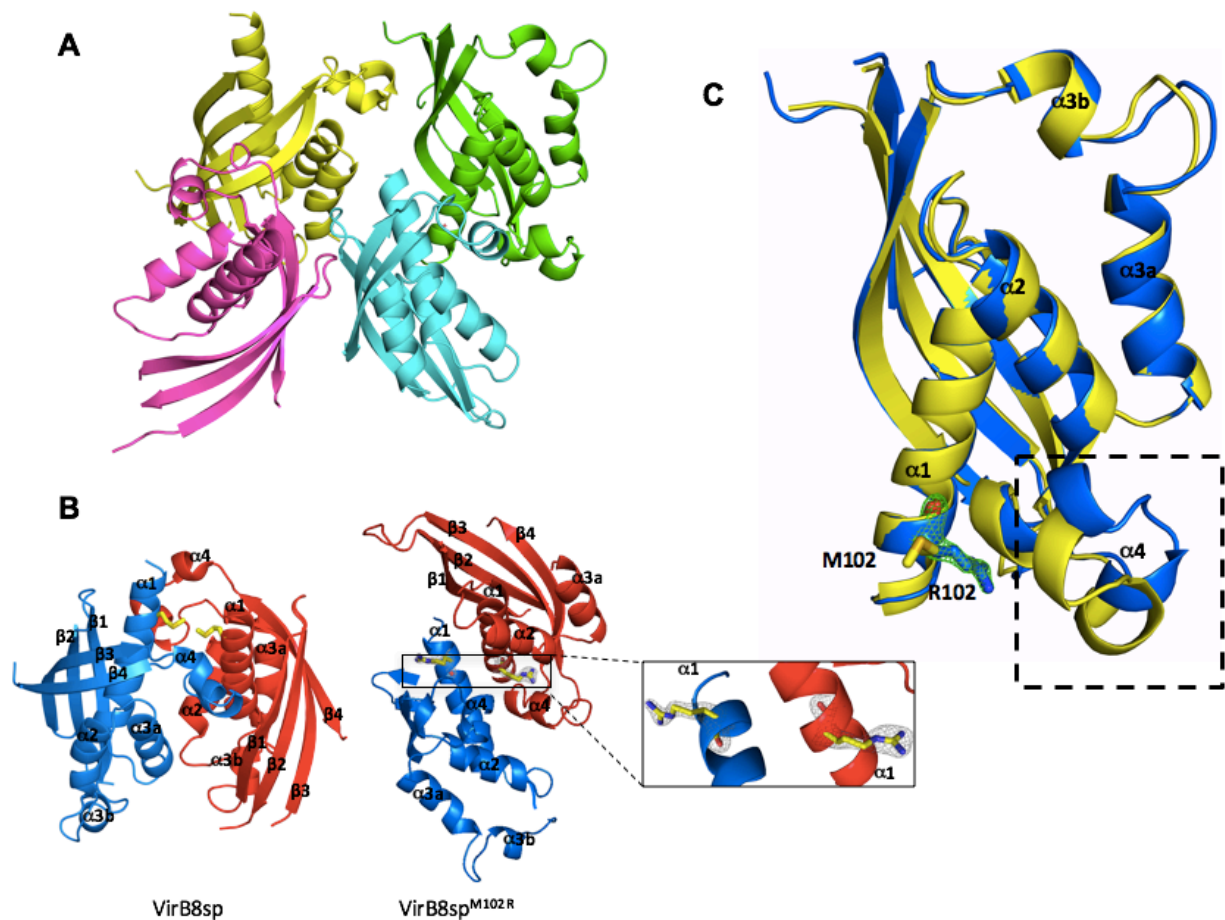
Figure 5. Crystal structure of the VirB8sp^{M102R} variant. (A) Cartoon representation of the crystal structure of VirB8sp^{M102R} having four molecules in the asymmetric unit. (B) Interaction interfaces between two subunits from VirB8sp wild-type and variant VirB8sp^{M102R}. In the VirB8sp crystals, M102 forms a van der Waals interaction with M102 from the second subunit (shown in yellow), while in the VirB8sp^{M102R} crystal structure, the R102 residues are oriented away from each other (shown in yellow). (C) Overlay of the VirB8sp (yellow) and VirB8sp^{M102R} (blue) (RMSD is 0.53 Å) crystal structures, the α4 region with the most pronounced shift of the fold is identified with a box. The 2*F*o-*F*c electron density of R102 is shown at 1.2 σ.
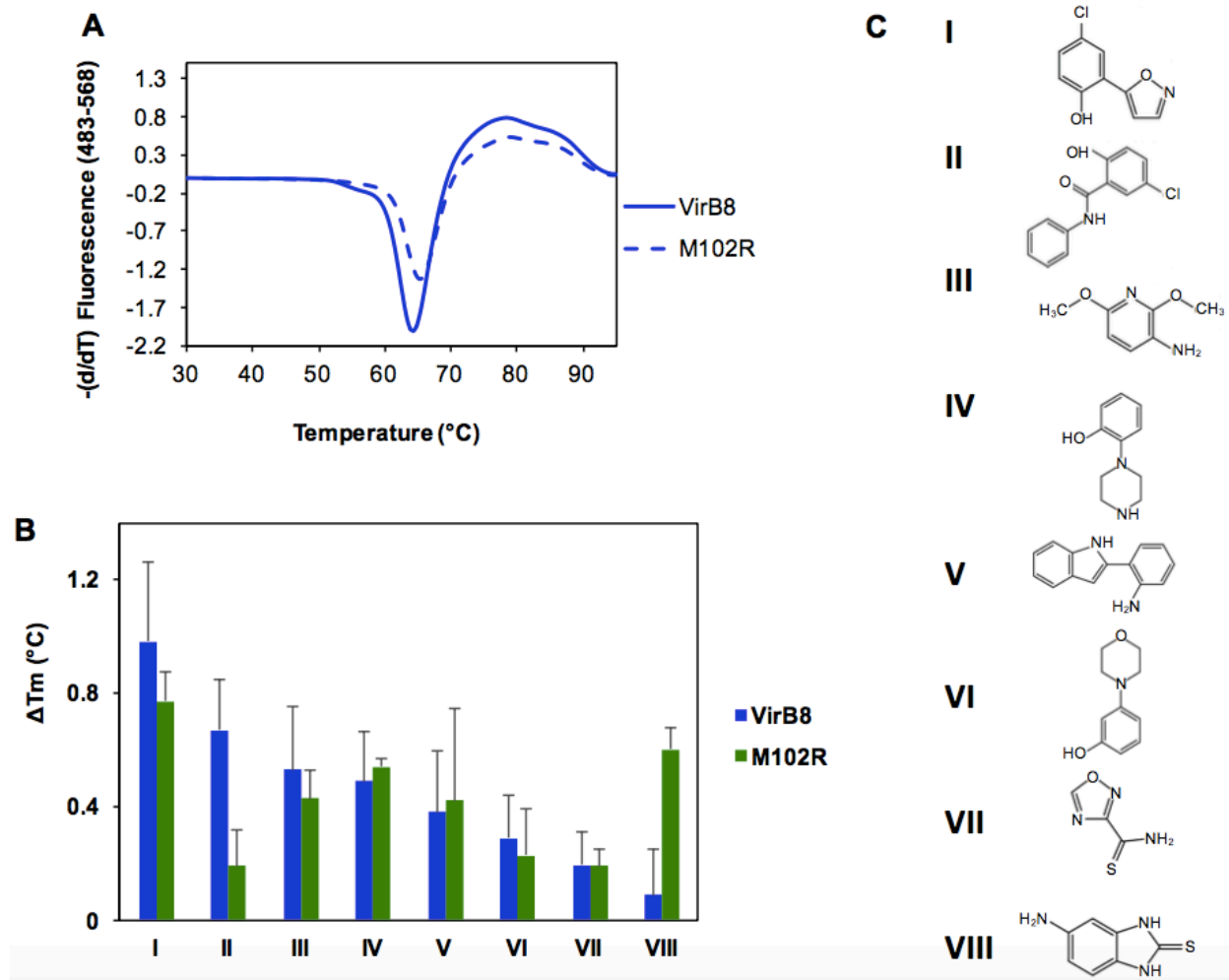
Figure 6. Conformational probing by differential scanning fluorimetry. (A) Determination of the melting temperatures of VirB8sp (line) and of VirB8sp^{M102R} (dotted line) in 5% DMSO by DSF. (B) Effects of eight fragments at 5 mM concentration on the positive shift (ΔT_m) of the melting temperatures of VirB8sp and VirB8sp^{M102R}, respectively. (C) Structures of molecules I, 4-Chloro-2-(5-isoxazolyl)phenol; II, 5-Chlorosalicylanilide; III, 2,6-Dimethoxypyridin-3-amine; IV, N-(2-Hydroxyphenyl)piperazine; V, 2-(2-Aminophenyl)indole; VI, 3-(4-Morpholino)phenol; VII, 1,2,4-Oxadiazole-3-carbothioamide and VIII, 5-Amino-2-mercaptobenzimidazole. Data presented are from three separate experiments conducted in triplicates, error bars reflect the standard deviation.
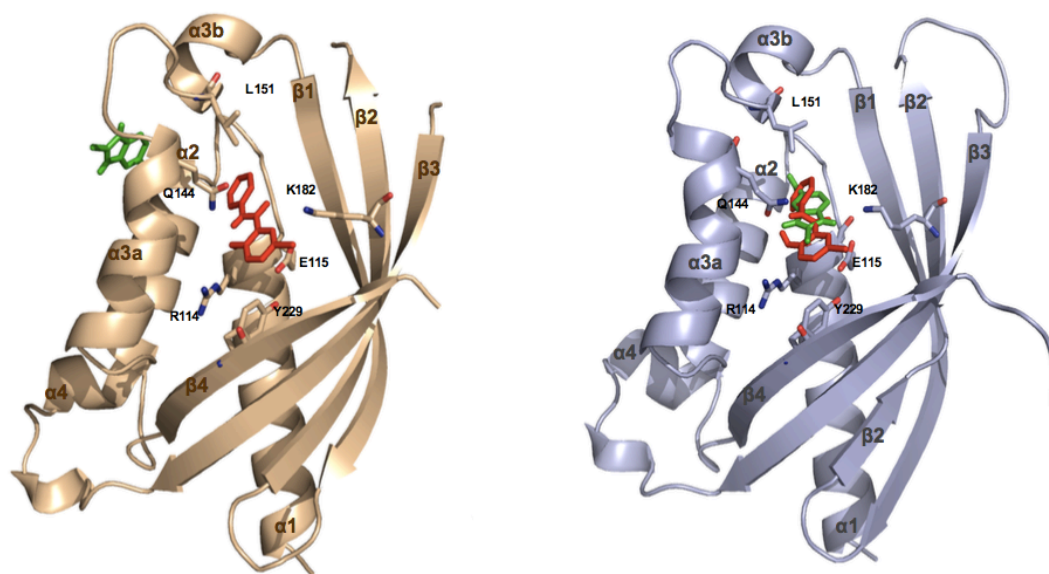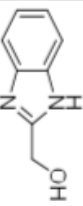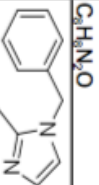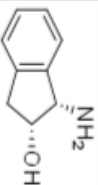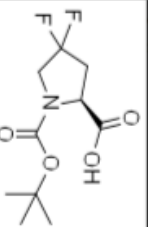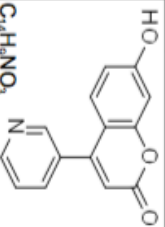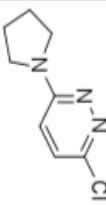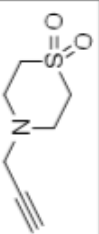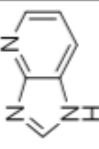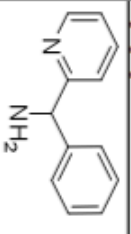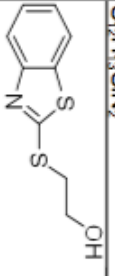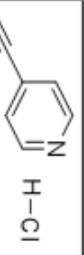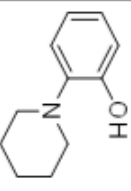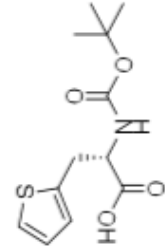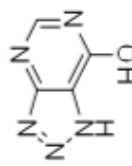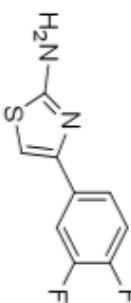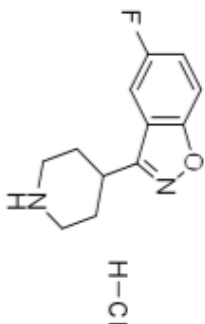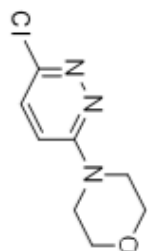
Figure 7. Docking simulation of fragment binding. Docked conformations of the small molecules 5-Chlorosalicylanilide (molecule II, red) and 5-Amino-2-mercaptobenzimidazol (molecule VIII, green) are presented on the crystal structures of VirB8sp subunit A (gold) [20] and VirB8sp[M102R] (blue), amino acids R114, E115, Q144, L151, K182 and Y229 at the inhibitor B8I-2 binding site are shown as stick models.
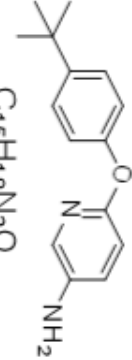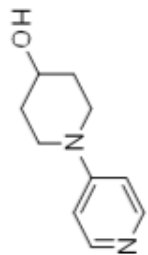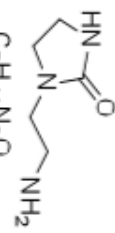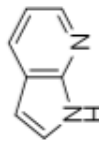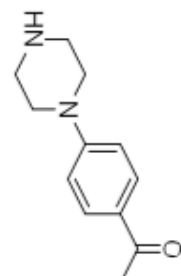
Supplementary Information
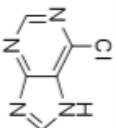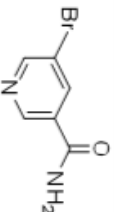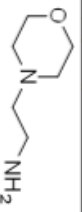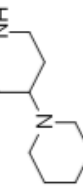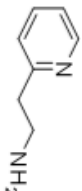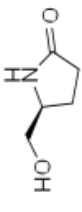
Supplementary table 1: The table of small molecules used of DSF screening with structures and size information.
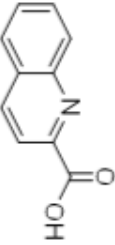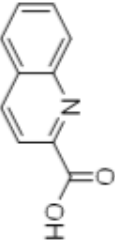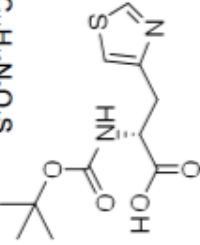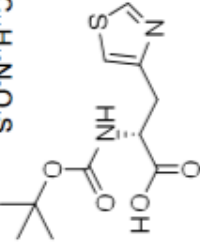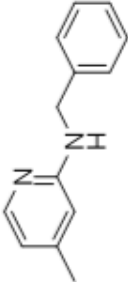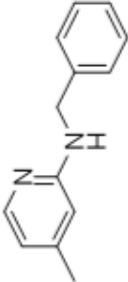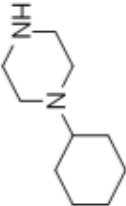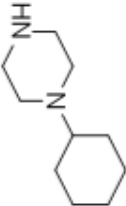
Supplementary Table. Small Molecules

	A		B	C
	Structure		**Name**	**Molecular Weight (Da)**
1	$C_8H_8N_2O$		1H-BENZIMIDAZOLE-2-METHANOL	148.2
2	$C_{11}H_{12}N_2O$		1-BENZYL-2-(HYDROXYMETHYL)IMIDAZOLE	188.2
3	$C_9H_{11}NO$		(1S,2R)-(+)-CIS-1-AMINO-2-INDANOL	149.2
4	$C_{10}H_{15}F_2NO_4$		N-T-BOC-4,4-DIFLUORO-L-PROLINE	251.2
5	$C_8H_{15}NO$		TROPINE	141.2
6	$C_{14}H_9NO_3$		7-HYDROXY-4-(PYRIDIN-3-YL)COUMARIN	239.2
7	$C_8H_{10}ClN_3$		3-CHLORO-6-PYRROLIDIN-1-YL-PYRIDAZINE	183.6
8				

104
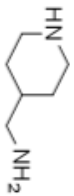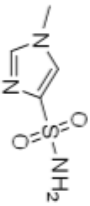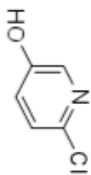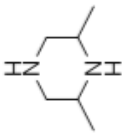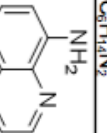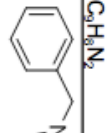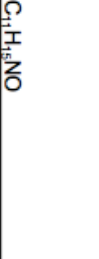
#	A Structure	B Name	C Molecular Weight (Da)
1	$C_7H_{11}NO_2S$ (4-prop-2-ynyl-1λ^6,4-thiazinane-1,1-dione)	4-PROP-2-YNYL-1LAMBDA6,4-THIAZINANE-1,1-DIONE	173.2
9	$C_6H_5N_3$ (1H-imidazo[4,5-b]pyridine)	1H-IMIDAZO[4,5-B]PYRIDINE	119.1
10	$C_{12}H_{13}ClN_2$ (phenyl(2-pyridyl)methylamine · HCl)	PHENYL(2-PYRIDYL)METHYLAMINE HYDROCHLORIDE	220.7
11	$C_9H_9NOS_2$ (2-(2-benzothiazolylthio)-ethanol)	2-(2-BENZOTHIAZOLYLTHIO)-ETHANOL	211.3
12	C_7H_6ClN (4-ethynylpyridine · HCl)	4-ETHYNYLPYRIDINE HYDROCHLORIDE	139.6
13	$C_{11}H_{15}NO$ (2-(1-piperidino)phenol)	2-(1-PIPERIDINO)PHENOL	177.2
14			
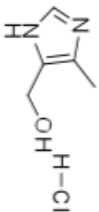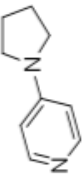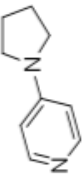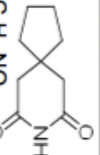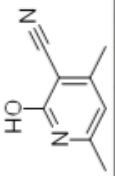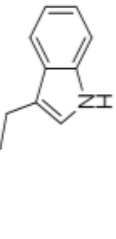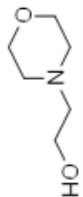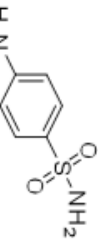
	A	B	C
1	**Structure**	**Name**	**Molecular Weight (Da)**
15	C$_{12}$H$_{17}$NO$_4$S	BOC-L-2-THIENYLALANINE	271.3
16	C$_5$H$_3$N$_5$O	8-AZAHYPOXANTHINE, 98%	149.2
17	C$_9$H$_6$F$_2$N$_2$S	2-AMINO-4-(3,4-DIFLUOROPHENYL)THIAZOLE	212.2
18	C$_{12}$H$_{14}$ClFN$_2$O	5-FLUORO-3-(4-PIPERIDINYL)-1,2-BENZISOXAZOLE HYDROCHLORIDE	256.7
19	C$_8$H$_{10}$ClN$_3$O	4-(6-CHLOROPYRIDAZIN-3-YL)MORPHOLINE	199.6
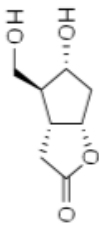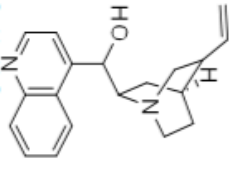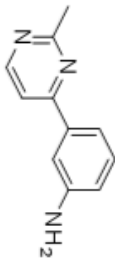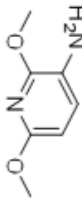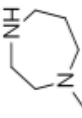
	A	B	C
1	Structure	Name	Molecular Weight (Da)
20	$C_{15}H_{18}N_2O$	5-AMINO-2-(4-TERT-BUTYLPHENOXY)PYRIDINE	242.3
21	$C_{10}H_{14}N_2O$	4-HYDROXY-1-(PYRIDIN-4-YL)-PIPERIDINE	178.2
22	$C_5H_{11}N_3O$	1-(2-AMINOETHYL)IMIDAZOLIDIN-2-ONE	129.2
23	$C_7H_6N_2$	7-AZAINDOLE	118.1
24	$C_{12}H_{16}N_2O$	4'-PIPERAZINOACETOPHENONE	204.3
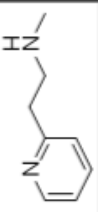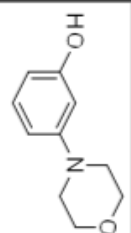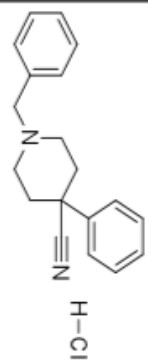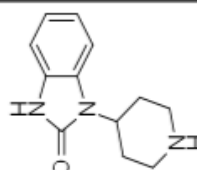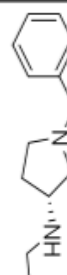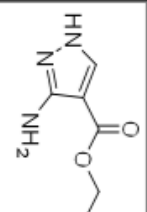
	A	B	C
1	Structure	Name	Molecular Weight (Da)
25	C$_5$H$_3$ClN$_4$	6-CHLOROPURINE	154.6
26	C$_6$H$_5$BrN$_2$O	5-BROMONICOTINAMIDE	201.0
27	C$_6$H$_{14}$N$_2$O	4-(2-AMINOETHYL)MORPHOLINE	130.2
28	C$_{10}$H$_{20}$N$_2$	4-PIPERIDINOPIPERIDINE	168.3
29	C$_7$H$_{10}$N$_2$	2-(2-AMINOETHYL)PYRIDINE	122.2
30	C$_5$H$_9$NO$_2$	(S)-(+)-5-(HYDROXYMETHYL)-2-PYRROLIDINONE	115.1
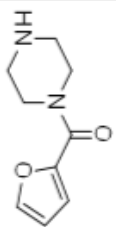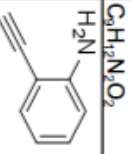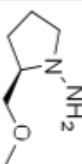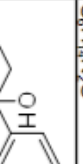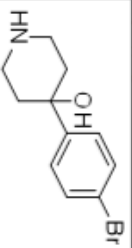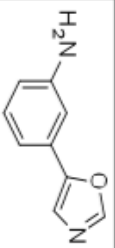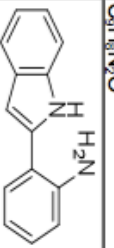
	A	B	C
1	**Structure**	**Name**	**Molecular Weight (Da)**
31	$C_{10}H_7NO_2$	QUINALDIC ACID	173.2
32	$C_{11}H_{18}N_2O_4S$	BOC-D-4-THIAZOLYLALANINE	272.3
33	$C_6H_{14}N_2$	N-(2-AMINOETHYL)PYRROLIDINE	114.2
34	$C_{13}H_{14}N_2$	2-BENZYLAMINO-4-METHYLPYRIDINE	198.3
35	$C_{10}H_{20}N_2$	1-CYCLOHEXYLPIPERAZINE	168.3
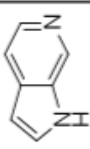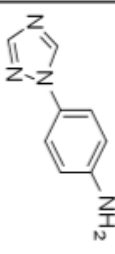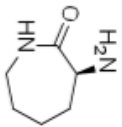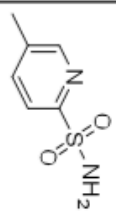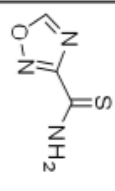
	A	B	C
	Structure	Name	Molecular Weight (Da)
1			
36	C$_6$H$_{14}$N$_2$	4-(AMINOMETHYL)PIPERIDINE	114.2
37	C$_4$H$_7$N$_3$O$_2$S	1-METHYL-1H-IMIDAZOLE-4-SULFONAMIDE	161.2
38	C$_5$H$_4$ClNO	2-CHLORO-5-HYDROXYPYRIDINE	129.5
39	C$_6$H$_{14}$N$_2$	2,6-DIMETHYLPIPERAZINE	114.2
40	C$_9$H$_8$N$_2$	8-AMINOQUINOLINE	144.2
41	C$_{11}$H$_{15}$NO	1-BENZYL-3-PYRROLIDINOL	177.2
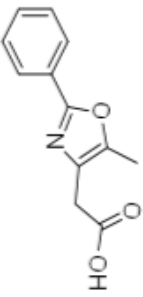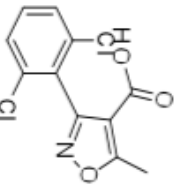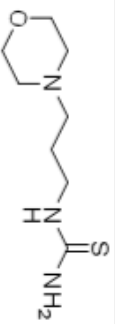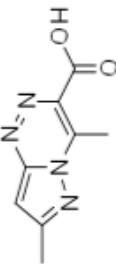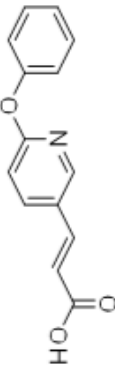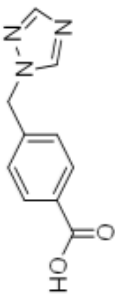
	A	B	C
1	Structure	Name	Molecular Weight (Da)
42	C₅H₉ClN₂O	4-METHYL-5-IMIDAZOLEMETHANOL HYDROCHLORIDE	148.6
43	C₉H₁₂N₂	4-PYRROLIDINOPYRIDINE	148.2
44	C₉H₁₃NO₂	TETRAMETHYLENE GLUTARIMIDE	167.2
45	C₈H₈N₂O	3-CYANO-4,6-DIMETHYL-2-HYDROXYPYRIDINE	156.2
46	C₁₂H₁₅NO₂	HOMOTRYPTOPHOL	204.3
47	C₆H₁₃NO₂	N-(2-HYDROXYETHYL)MORPHOLINE	131.2
48	C₆H₈N₂O₂S	SULFANILAMIDE	172.2
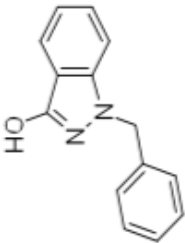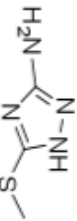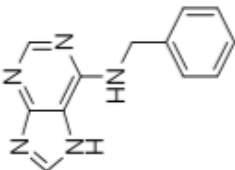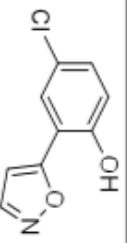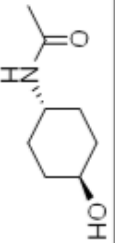
	A	B	C
1	Structure	Name	Molecular Weight (Da)
49	C₉H₁₂O₄	(3AR,4S,5R,6AS,)-(-)-HEXAHYDRO-5-HYDROXY-4-(HYDROXYMETHYL)-2H-CYCLOPENTA(b)FURAN-2-ONE	172.2
50	C₁₉H₂₂N₂O	(-)-CINCHONIDINE	294.4
51	C₁₁H₁₁N₃	4-(3-AMINOPHENYL)-2-METHYLPYRIMIDINE	185.2
52	C₇H₁₀N₂O₂	2,6-DIMETHOXYPYRIDIN-3-AMINE	154.2
53	C₇H₁₆N₂O	4-(3-AMINOPROPYL)MORPHOLINE	144.2
54	C₆H₁₄N₂	1-METHYLHOMOPIPERAZINE	114.2
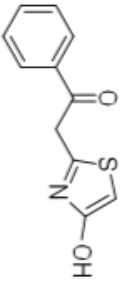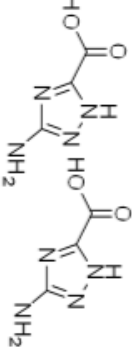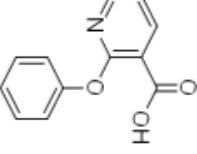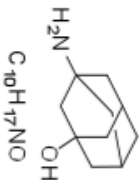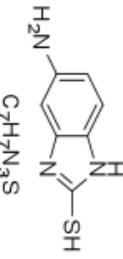
	A	B	C
1	Structure	Name	Molecular Weight (Da)
55 C$_9$H$_{12}$N$_2$		2-(B-METHYLAMINOETHYL)-PYRIDINE	136.2
56 C$_{10}$H$_{13}$NO$_2$		3-(4-MORPHOLINO)PHENOL	179.2
57 C$_{19}$H$_{21}$ClN$_2$		1-BENZYL-4-CYANO-4-PHENYLPIPERIDINE HYDROCHLORIDE	312.8
58 C$_{12}$H$_{15}$N$_3$O		4-(2-KETO-1-BENZIMIDAZOLINYL)-PIPERIDINE	217.3
59 C$_{13}$H$_{20}$N$_2$		(3R)-(-)-1-BENZYL-3-(ETHYLAMINO)PYRROLIDINE	204.3
60 C$_6$H$_9$N$_3$O$_2$		3-AMINO-4-CARBETHOXYPYRAZOLE	155.2
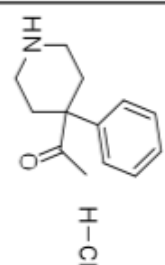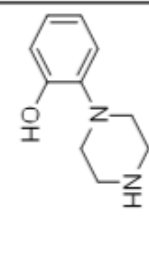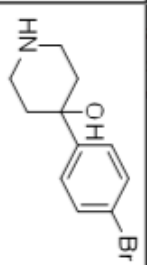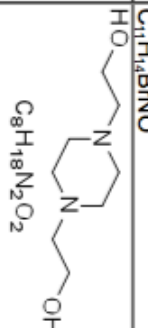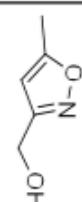
	A	B	C
1	Structure	Name	Molecular Weight (Da)
61	C$_9$H$_{12}$N$_2$O$_2$	1-(2-FUROYL)PIPERAZINE	180.2
62	C$_8$H$_7$N	2-ETHYNYLANILINE	117.1
63	C$_6$H$_{14}$N$_2$O	(R)-(+)-1-AMINO-2-(METHOXYMETHYL)PYRROLIDINE	130.2
64	C$_{11}$H$_4$BrNO	4-(4'-BROMOPHENYL)-4-HYDROXYPIPERIDINE	256.1
65	C$_9$H$_8$N$_2$O	3-(1,3-OXAZOL-5-YL)ANILINE	168.2
66	C$_{14}$H$_{12}$N$_2$	2-(2-AMINOPHENYL)INDOLE	208.3
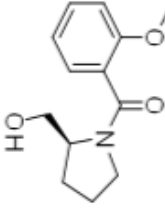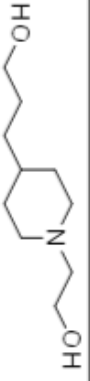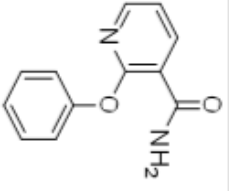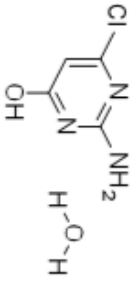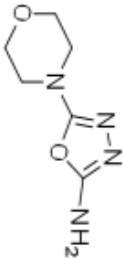
	A Structure	B Name	C Molecular Weight (Da)
1			
67 C$_7$H$_6$N$_2$		6-AZAINDOLE	118.1
68 C$_8$H$_8$N$_4$		4-(1H-1,2,4-TRIAZOL-1-YL)ANILINE	160.2
69 C$_7$H$_{16}$CINO		1-AMINOMETHYL-1-CYCLOHEXANOL HYDROCHLORIDE	165.7
70 C$_{10}$H$_{11}$NO$_2$		(S)-4-BENZYL-2-OXAZOLIDINONE	177.2
71 C$_6$H$_{13}$CIN$_2$O		L(-)-ALPHA-AMINO-EPSILON-CAPROLACTAM HYDROCHLORIDE	164.6
72 C$_6$H$_8$N$_2$O$_2$S		5-METHYLPYRIDINE-2-SULFONAMIDE	172.2
73 C$_3$H$_3$N$_3$OS		1,2,4-OXADIAZOLE-3-CARBOTHIOAMIDE	129.1

115
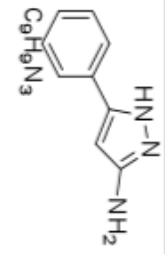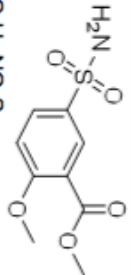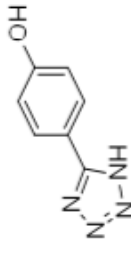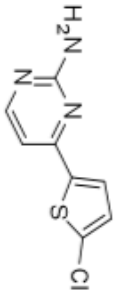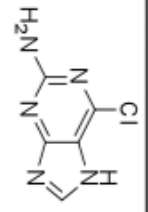
	A	B	C
1	Structure	Name	Molecular Weight (Da)
74 C$_{12}$H$_{11}$NO$_3$		2-(5-METHYL-2-PHENYL-1,3-OXAZOL-4-YL)ACETIC ACID	217.2
75 C$_{11}$H$_7$Cl$_2$NO$_3$		2-(5-METHYL-2-PHENYL-1,3-OXAZOL-4-YL)ACETIC ACID	272.1
76 C$_8$H$_{17}$N$_3$OS		1-(3-MORPHOLINOPROPYL)-2-THIOUREA	203.3
77 C$_8$H$_8$N$_4$O$_2$		4,7-DIMETHYLPYRAZOLO[5,1-C][1,2,4]TRIAZINE-3-CARBOXYLIC ACID	192.2
78 C$_{14}$H$_{11}$NO$_3$		3-(6-PHENOXY-3-PYRIDYL)ACRYLIC ACID	241.2
79 C$_{10}$H$_9$N$_3$O$_2$		4-(1H-1,2,4-TRIAZOL-1-YL)BENZOIC ACID	203.2
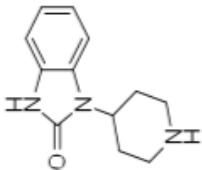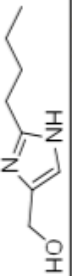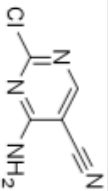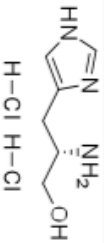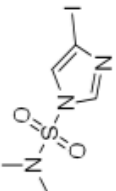
	A	B	C
1	Structure	Name	Molecular Weight (Da)
80 C₉H₁₂N₂O		1-BENZYL-3-HYDROXY-1H-INDAZOLE	224.3
81 C₃H₆N₄S		3-AMINO-5-METHYLTHIO-1H-1,2,4-TRIAZOLE	130.2
82 C₁₂H₁₁N₅		6-BENZYLAMINOPURINE	225.2
83 C₉H₆ClNO₂		4-CHLORO-2-(5-ISOXAZOLYL)PHENOL	195.6
84 C₈H₁₅NO₂		TRANS-4-ACETAMIDOCYCLOHEXANOL	157.2
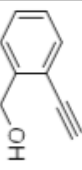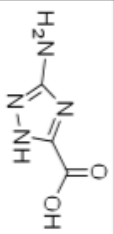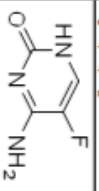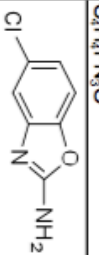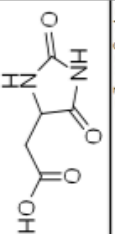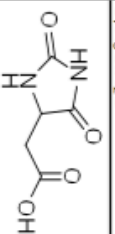
	A	B	C
1	Structure	Name	Molecular Weight (Da)
85	C₁₁H₉NO₂S	2-(4-HYDROXY-1,3-THIAZOL-2-YL)-1-PHENYLETHAN-1-ONE	219.3
86	C₆H₁₀N₆O₅ · H₂O	3-AMINO-1,2,4-TRIAZOLE-5-CARBOXYLIC ACID HEMIHYDRATE	274.2
87	C₁₂H₉NO₃	2-PHENOXYNICOTINIC ACID	215.2
88	C₁₀H₁₇NO	3-AMINO-1-ADAMANTANOL	167.2
89	C₇H₇N₃S	5-AMINO-2-MERCAPTOBENZIMIDAZOLE	165.2
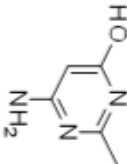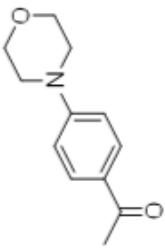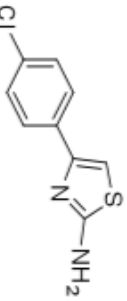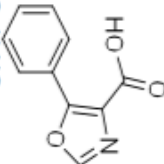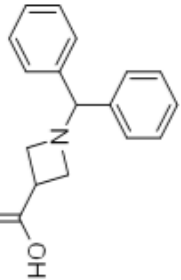
A Structure	B Name	C Molecular Weight (Da)
1		
90 C$_{13}$H$_{18}$ClNO (H–Cl)	4-ACETYL-4-PHENYLPIPERIDINE HYDROCHLORIDE	239.7
91 C$_{10}$H$_{14}$N$_2$O	N-(2-HYDROXYPHENYL)PIPERAZINE	178.2
92 C$_{11}$H$_{14}$BrNO	4-(4-BROMOPHENYL)-4-PIPERIDINOL	256.1
93 C$_8$H$_{18}$N$_2$O$_2$	N,N'-BIS(2-HYDROXYETHYL)PIPERAZINE	174.2
94 C$_5$H$_7$NO$_2$	(5-METHYL-3-ISOXAZOLYL)METHANOL	113.1
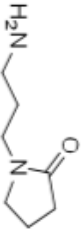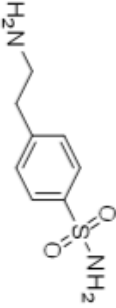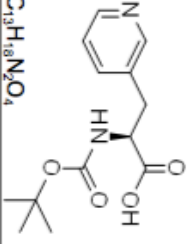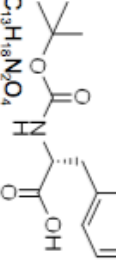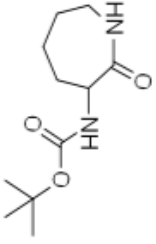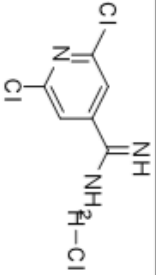
	A	B	C
1	**Structure**	**Name**	**Molecular Weight (Da)**
95	$C_{13}H_{17}NO_3$	(S)-(-)-1-(2-METHOXYBENZOYL)-2-PYRROLIDINEMETHANOL	235.279
96	$C_{10}H_{21}NO_2$	1-(2-HYDROXYETHYL)-4-(3-HYDROXYPROPYL)PIPERIDINE	187.279
97	$C_{12}H_{10}N_2O_2$	2-PHENOXYNICOTINAMIDE	214.22
98	$C_4H_6ClN_3O_2$	2-AMINO-6-CHLORO-4-PYRIMIDINOL MONOHYDRATE	163.562
99	$C_6H_{10}N_4O_2$	5-MORPHOLINE-4-YL-1,3,4-OXADIAZOL-2-YLAMINE	170.169
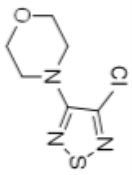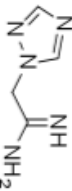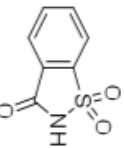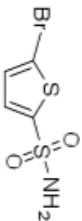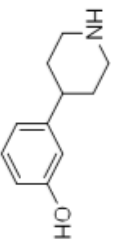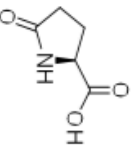
	A	B	C
1	Structure	Name	Molecular Weight (Da)
100	$C_9H_9N_3$	3-AMINO-5-PHENYLPYRAZOLE	159.188
101	$C_9H_{11}NO_5S$	METHYL-2-METHOXY-5-SULFAMOYL-BENZOATE,	245.252
102	$C_7H_6N_4O$	5-(4-HYDROXYPHENYL)TETRAZOLE	162.149
103	$C_8H_6ClN_3S$	4-(5-CHLORO-2-THIENYL)-2-PYRIMIDINAMINE	211.671
104	$C_5H_4ClN_5$	2-AMINO-6-CHLOROPURINE	169.572
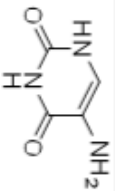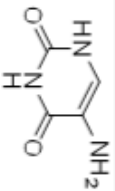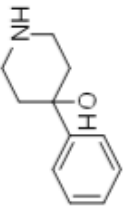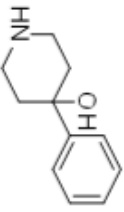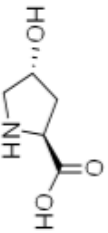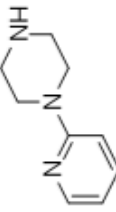
	A	B	C
1	Structure	Name	Molecular Weight (Da)
105	C12H15N3O	4-(2-KETO-1-BENZIMIDAZOLINYL)PIPERIDINE	217.267
106	C8H14N2O	(2-BUTYL-1H-IMIDAZOL-4-YL)METHANOL	154.21
107	C5H3ClN4	4-AMINO-2-CHLORO-PYRIMIDINE-5-CARBONITRILE,	154.557
108	C6H13Cl2N3O	L-HISTIDINOL DIHYDROCHLORIDE	214.093
109	C5H8IN3O2S	N,N-DIMETHYL-4-IODO-1H-IMIDAZOLE-1-SULFONAMIDE	301.105
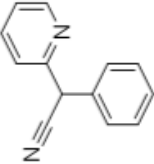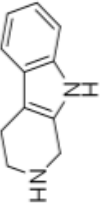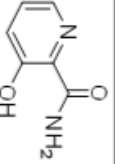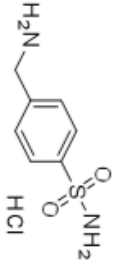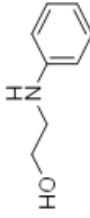
	A	B	C
1	Structure	Name	Molecular Weight (Da)
110 C$_9$H$_8$O		2-ETHYNYLBENZYL ALCOHOL	132.159
111 C$_3$H$_4$N$_4$O$_2$		3-AMINO-1,2,4-TRIAZOLE-5-CARBOXYLIC ACID	128.089
112 C$_4$H$_4$FN$_3$O		5-FLUOROCYTOSINE	129.092
113 C$_7$H$_5$ClN$_2$O		2-AMINO-5-CHLOROBENZOXAZOLE	168.58
114 C$_5$H$_6$N$_2$O$_4$		5-HYDANTOINACETIC ACID	158.12
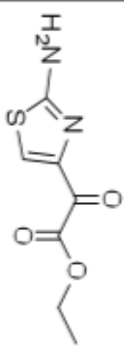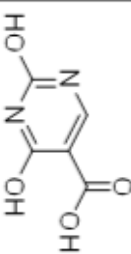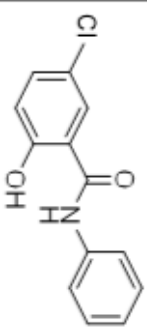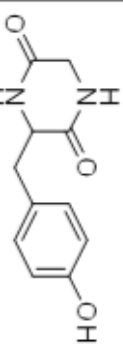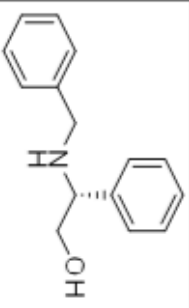
	A	B	C
1	Structure	Name	Molecular Weight (Da)
115 C5H7N3O		4-AMINO-6-HYDROXY-2-METHYLPYRIMIDINE	125.129
116 C12H15NO2		4'-MORPHOLINOACETOPHENONE	205.253
117 C9H7ClN2S		2-AMINO-4-(4-CHLOROPHENYL)THIAZOLE	210.683
118 C10H7NO3		5-PHENYL-1,3-OXAZOLE-4-CARBOXYLIC ACID	189.167
119 C17H17NO2		1-BENZHYDRYLAZETANE-3-CARBOXYLIC ACID	267.322

124
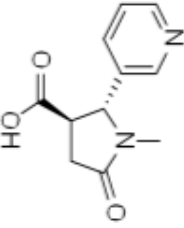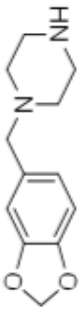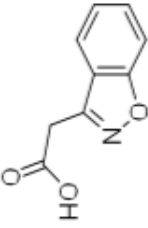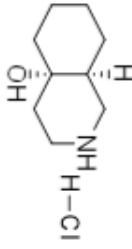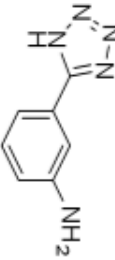
	A	B	C
1	Structure	Name	Molecular Weight (Da)
120	$C_7H_{14}N_2O$	1-(3-AMINOPROPYL)-2-PYRROLIDINONE	142.199
121	$C_8H_{12}N_2O_2S$	4-(2-AMINOETHYL)BENZENESULFONAMIDE	200.258
122	$C_{13}H_{18}N_2O_4$	BOC-ALA(3'-PYRIDYL)-OH	266.293
123	$C_{13}H_{18}N_2O_4$	BOC-3-(3-PYRIDYL)-D-ALA-OH	266.293
124	$C_{11}H_{20}N_2O_3$	(+/-)-N-ALPHA-BOC-AMINO-EPSILON-CAPROLACTAM	228.288
125	$C_6H_6Cl_3N_3$	2,6-DICHLOROPYRIDINE-4-CARBOXIMIDAMIDE HYDROCHLORIDE	226.491
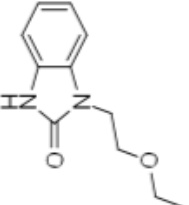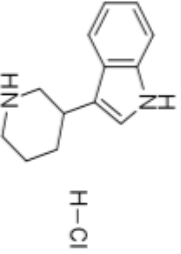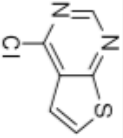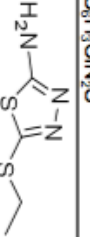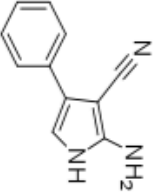
125

A		B	C
1	Structure	Name	Molecular Weight (Da)
126 C₆H₈ClN₃OS		3-CHLORO-4-MORPHOLINO-1,2,5-THIADIAZOLE	205.665
127 C₄H₇N₅		2-(1H-1,2,4-TRIAZOL-1-YL)ETHANIMIDAMIDE	125.132
128 C₇H₅NO₃S		SACCHARIN	183.185
129 C₄H₄BrNO₂S₂		5-BROMOTHIOPHENE-2-SULFONAMIDE	242.114
130 C₁₁H₁₅NO		4-(3-HYDROXYPHENYL)PIPERIDINE	177.243
131 C₅H₇NO₃		L-2-PYRROLIDONE-5-CARBOXYLIC ACID	129.114

A		B	C
1	Structure	Name	Molecular Weight (Da)
126 $C_6H_8ClN_3OS$		3-CHLORO-4-MORPHOLINO-1,2,5-THIADIAZOLE	205.665
127 $C_4H_7N_5$		2-(1H-1,2,4-TRIAZOL-1-YL)ETHANIMIDAMIDE	125.132
128 $C_7H_5NO_3S$		SACCHARIN	183.185
129 $C_4H_4BrNO_2S_2$		5-BROMOTHIOPHENE-2-SULFONAMIDE	242.114
130 $C_{11}H_{15}NO$		4-(3-HYDROXYPHENYL)PIPERIDINE	177.243
131 $C_5H_7NO_3$		L-2-PYRROLIDONE-5-CARBOXYLIC ACID	129.114
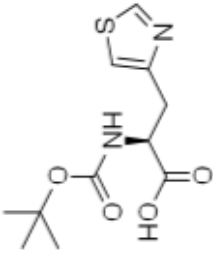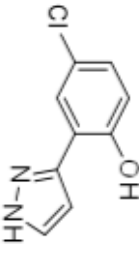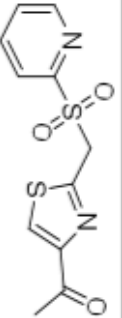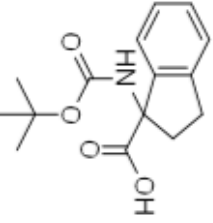
	A	B	C
1	Structure	Name	Molecular Weight (Da)
132	C₄H₅N₃O₂	5-AMINOURACIL	127.101
133	C₁₂H₁₇NO	4-BENZYL-4-HYDROXYPIPERIDINE	191.269
134	C₁₁H₁₅NO	4-HYDROXY-4-PHENYLPIPERIDINE	177.243
135	C₅H₉NO₃	TRANS-4-HYDROXY-L-PROLINE	131.13
136	C₉H₁₃N₃	1-(2-PYRIDYL)PIPERAZINE	163.22
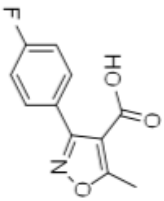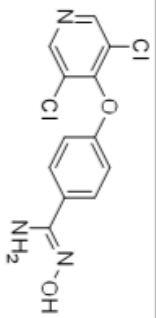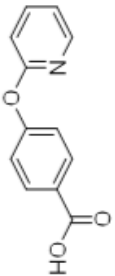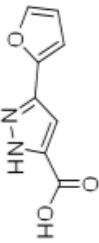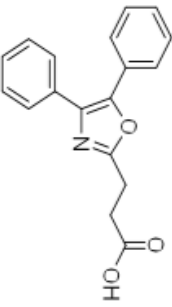
	A	B	C
1	Structure	Name	Molecular Weight (Da)
137	$C_{13}H_{10}N_2$	PHENYL-2-PYRIDYLACETONITRILE	194.232
138	$C_{11}H_{12}N_2$	1,2,3,4,-TETRAHYDRO-9H-PYRIDO[3,4-b]INDOLE	172.226
139	$C_6H_6N_2O_2$	3-HYDROXYPICOLINAMIDE	138.124
140	$C_8H_{18}N_2O_2$	1-(2-(2-HYDROXYETHOXY)ETHYL)PIPERAZINE	174.241
141	$C_7H_{11}ClN_2O_2S$	HOMOSULFAMINE HYDROCHLORIDE	222.692
142	$C_8H_{11}NO$	2-ANILINOETHANOL	137.179
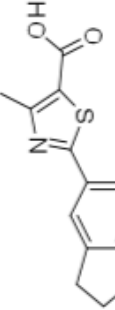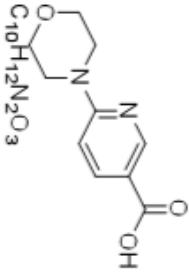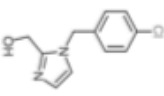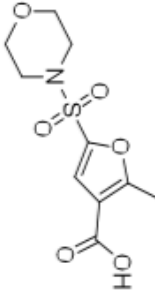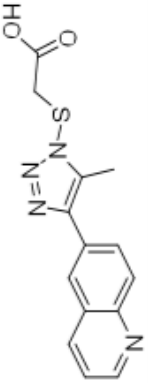
	A	B	C
1	Structure	Name	Molecular Weight (Da)
143	$C_7H_8N_2O_3S$	ETHYL 2-AMINO-4-THIAZOLEGLYOXYLATE,	200.215
144	$C_5H_4N_2O_4$	2,4-DIHYDROXYPYRIMIDINE-5-CARBOXYLIC ACID	156.096
145	$C_{13}H_{10}ClNO_2$	5-CHLOROSALICYLANILIDE	247.677
146	$C_{11}H_{12}N_2O_3$	CYCLO(GLY-TYR)	220.225
147	$C_{15}H_{17}NO$	(R)-(-)-N-BENZYL-2-PHENYLGLYCINOL	227.302
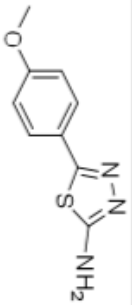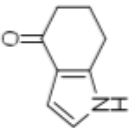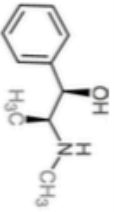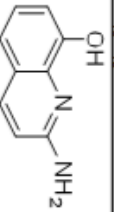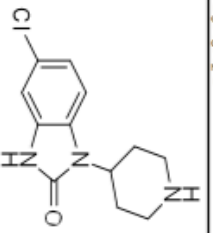
A		B	C
	Structure	**Name**	**Molecular Weight (Da)**
1			
148 C₁₁H₁₂N₂O₃		TRANS-4-COTININE CARBOXYLIC ACID	220.225
149 C₁₂H₁₆N₂O₂		1-PIPERONYLPIPERAZINE	220.268
150 C₉H₇NO₃		2-(1,2-BENZISOXAZOL-3-YL)ACETIC ACID	177.157
151 C₉H₁₈ClNO		(4AS,8AS)-OCTAHYDROISOQUINOLIN-4A(2H)-OL-HYDROCHLORIDE	191.698
152 C₇H₇N₅		5-(3-AMINOPHENYL)TETRAZOLE	161.164

130
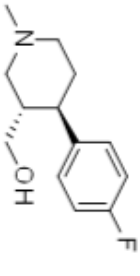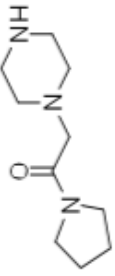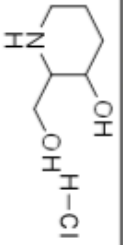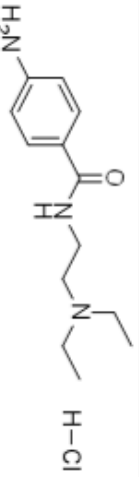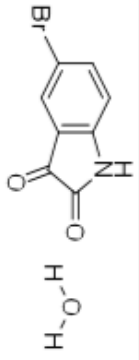
	A	B	C
1	Structure	Name	Molecular Weight (Da)
153	$C_{11}H_4N_2O_2$	2-ETHOXYETHYL-BENZIMIDAZOLINONE	206.241
154	$C_{13}H_{17}ClN_2$	3-(PIPERIDIN-3-YL)-1H-INDOLE HYDROCHLORIDE	236.74
155	$C_6H_3ClN_2S$	4-CHLOROTHIENO[2,3-D]PYRIMIDINE	170.619
156	$C_4H_7N_3S_2$	2-AMINO-5-(ETHYLTHIO)-1,3,4-THIADIAZOLE	161.248
157	$C_{11}H_9N_3$	2-AMINO-4-PHENYL-1H-PYRROLE-3-CARBONITRILE	183.209
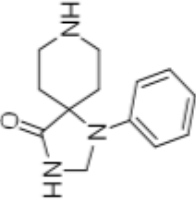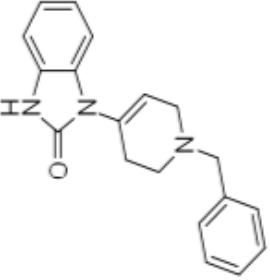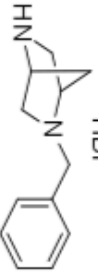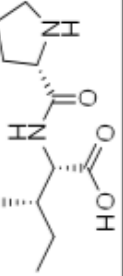
	A		B	C
1	Structure		Name	Molecular Weight (Da)
158	C₁₁H₁₆N₂O₄S		(S)-N-BOC-4-THIAZOYLALANINE	272.321
159	C₉H₇ClN₂O		4-CHLORO-2-(1H-PYRAZOL-3-YL)PHENOL	194.618
160	C₁₁H₁₀N₂O₃S₂		1-{2-[(2-PYRIDYLSULFONYL)METHYL]-1,3-THIAZOL-4-YL}ETHAN-1-ONE	282.339
161	C₁₅H₁₉NO₄		BOC-(R,S)-1-AMINOINDANE-1-CARBOXYLIC ACID	277.316
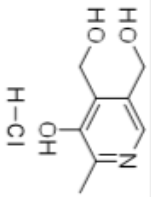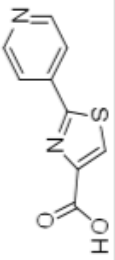
	A	B	C
1	Structure	Name	Molecular Weight (Da)
162	$C_{11}H_8FNO_3$	3-(4-FLUOROPHENYL)-5-METHYL-4-ISOXAZOLECARBOXYLIC ACID	221.185
163	$C_{12}H_9Cl_2N_3O_2$	(Z)-4-((3,5-DICHLOROPYRIDIN-4-YL)OXY)-N'-HYDROXYBENZIMIDAMIDE	298.125
164	$C_{12}H_9NO_3$	4-(PYRID-2-YLOXY)BENZOIC ACID	215.205
165	$C_8H_6N_2O_3$	5-FURAN-2-YL-2H-PYRAZOLE-3-CARBOXYLIC ACID	178.145
166	$C_{18}H_{15}NO_3$	OXAPROZIN	293.317

	A	B	C
1	Structure	Name	Molecular Weight (Da)
167 $C_{13}H_{11}NO_3S$		2-(2,3-DIHYDRO-1-BENZOFURAN-5-YL)-4-METHYL-2-PHENYL-THIAZOLE-5-CARBOXYLIC ACID	261.296
168 $C_{10}H_{12}N_2O_3$		6-MORPHOLINONICOTINIC ACID	208.2
169 $C_{11}H_{11}ClN_2O$		1-(4-CHLOROBENZYL)-2-(HYDROXYMETHYL)IMIDAZOLE	222.7
170 $C_{10}H_{13}NO_6S$		2-METHYL-5-(MORPHOLINOSULFONYL)-3-FUROIC ACID	275.278
171 $C_{14}H_{12}N_4O_2S$		4-METHYL-5-(QUINOL-6-YL)TRIAZOLE-3-THIOACETIC ACID	300.336

134

	A	B	C
1	Structure	Name	Molecular Weight (Da)
172 C₉H₉N₃OS		5-(4-METHOXY-PHENYL)-[1,3,4]THIADIAZOL-2-YLAMINE	207.252
173 C₈H₉NO		1,5,6,7-TETRAHYDRO-4H-INDOL-4-ONE	135.163
174 C₁₀H₁₅NO		(1R,2S)-(-)-EPHEDRINE	165.232
175 C₉H₈N₂O		2-AMINO-8-HYDROXYQUINOLINE	160.173
176 C₁₂H₁₄ClN₃O		5-CHLORO-1-(4-PIPERIDINYL)-2-BENZIMIDAZOLIDINONE	251.712

135

	Structure	Name	Molecular Weight (Da)
A		**B**	**C**
1	**Structure**	**Name**	**Molecular Weight (Da)**
177 $C_{13}H_{18}FNO$		(3S,4R)-4-(4-FLUOROPHENYL)-1-METHYL-3-PIPERIDINEMETHANOL	223.287
178 $C_{10}H_{19}N_3O$		PIPERAZINOACETIC ACID-PYRROLIDIDE	197.277
179 $C_6H_{14}ClNO_2$		3-HYDROXY-2-PIPERIDINEMETHANOL HYDROCHLORIDE	167.634
180 $C_{13}H_{22}ClN_3O$		PROCAINAMIDE HYDROCHLORIDE	271.786
181 $C_8H_6BrNO_3$		5-BROMOISATIN MONOHYDRATE	244.042

136

1	A	B	C
	Structure	Name	Molecular Weight (Da)
182 C$_{13}$H$_{17}$N$_3$O		1-PHENYL-1,3,8-TRIAZASPIRO(4.5)DECAN-4-ONE	231.294
183 C$_{19}$H$_{19}$N$_3$O		1-(1-BENZYL-1,2,3,6-TETRAHYDRO-PYRIDIN-4-YL)-1,3-DIHYDRO-BENZOIMIDAZOL-2-ONE	305.374
184 C$_{12}$H$_{18}$Br$_2$N$_2$		(1S,4S)-2,5-DIAZABICYCLO[2.2.1]HEPTANEDIHYDROBROMIDE	350.093
185 C$_{11}$H$_{20}$N$_2$O$_3$		L-PROLYL-L-ISOLEUCINE	228.288

	A	B	C
	Structure	Name	Molecular Weight (Da)
1			
186 C$_8$H$_{12}$ClNO$_3$		PYRIDOXINE HYDROCHLORIDE	205.639
187 C$_9$H$_6$N$_2$O$_2$S		2-(4-PYRIDYL)THIAZOLE-4-CARBOXYLIC ACID	206.221

Chapter 3: Article 2 (Published 2017)

Title : **Type IV secretion system core component VirB8 interacts via the β1-strand with VirB10**

Authors : Mahzad Sharifahmadian, Ingrid U. Nlend, Lauriane Lecoq, James G. Omichinski and Christian Baron*

Affiliation : Université de Montréal, Faculty of Medicine, Department of Biochemistry and Molecular Medicine

Corresponding Author: Christian Baron

E-mail: christian.baron@umontreal.ca

Phone: (514) 343-6300

Abstract

In this work, we provide evidence for the interactions between VirB8 and VirB10, two core components of type IV secretion system (T4SS). Using Nuclear Magnetic Resonance (NMR) experiments, we identified residues on the β1-strand of *Brucella* VirB8 that undergo chemical shift changes in the presence of VirB10. Bacterial two-hybrid experiments confirm the importance of the β1-strand whereas phage display experiments suggest that the α2-helix of VirB8 may also contribute to the interaction with VirB10. Conjugation assays using the VirB8 homolog TraE as a model show that several residues on the β1-strand of TraE are important for T4SS function. Together, our results suggest that the β1-strand of VirB8-like proteins is essential for their interaction with VirB10 in the T4SS complex.

Introduction

Gram-negative bacteria use type IV secretion systems (T4SS) to translocate macromolecules across the cell envelope. A typical T4SS contains 12 conserved VirB proteins that form a macromolecular complex that spans the inner and the outer membrane of both Gram-negative [1-3] and Gram-positive bacteria [4]. A high-resolution substructure containing the core complex and outer membrane portion of the T4SS comprising homologs of VirB7, VirB9 and the C-terminal domain of VirB10 from plasmid pKM101 was determined using single-particle electron microscopy and X-ray crystallography [5, 6]. The localization of VirB4 in the inner membrane part of the complex was also determined using single particle electron microscopy [7]. Despite these advancements, the interactions between the proteins from the inner membrane part of the complex (e.g. VirB3, VirB6, VirB8 and VirB10) remain to be defined at both the structural and functional level.

VirB8-like proteins undergo several protein-protein interactions that impact both the functionality and assembly of the T4SS complex [8-14]. VirB8 from *Brucella suis* (VirB8s) is comprised of an 18 kDa periplasmic domain, a single transmembrane helix and a 5 kDa cytoplasmic N-terminus. The crystal structures of the periplasmic domain of VirB8 homologs from Gram-negative and from Gram-positive bacteria have similar folds that consist of a single α-helical region and a single β-sheet domain [15-19]. VirB8 proteins from Gram-negative bacteria were shown to dimerize through this α-helical region of the periplasmic domain [16, 20, 21], but the molecular basis of VirB8 interactions with other VirB proteins in the context of the T4SS complex remains unknown.

VirB10 is an essential component of the T4SS that spans the inner and the outer membrane and is required for the translocation of substrates [22]. The crystal structure of the outer membrane core complex from pKM101 showed that the C-terminal domain of TraF (homologue of VirB10) interacts in the outer membrane complex with TraN and TraO (homologues of VirB7 and VirB9) [6]. The ATPase activities of VirD4 and VirB11 are required for conformational changes in VirB10 that may be linked to substrate translocation [23]. A dynamic model for the sequence of interactions between VirB8, VirB9 and VirB10 forming the periplasmic core complex assembly has been suggested [14], but there is little information on the interaction sites of VirB8 with either VorB9 or VirB10. The analysis of variants of *B. suis* VirB8 (R230D, T201A and T201Y) on the solvent-exposed β-sheet interface showed that substituting for these amino acids lead to reduced intracellular growth in macrophages [11]. Changing T201 (T201A and T201Y) also decreased the interaction with VirB10 *in vitro* [11], suggesting that the β-sheet interface may be the site of interaction. In this work, we analyze the interaction of the periplasmic domain of VirB8s (VirB8sp) with the periplasmic domain of VirB10 from *B. suis* (VirB10sp) using a combination of biochemical and genetic approaches. In addition, we analyze variants of the VirB8 homologue TraE from pKM101 to assess the effects of changes of the protein sequence in the natural biological context. Our results suggest that VirB8 interacts with VirB10 via the β1-sheet.

Materials and Methods

Cloning and protein expression. The strains and plasmids used in this study are presented in Table 1. Plasmids pHTVirB8sp and pHTVirB10sp were transformed into *E. coli* strain BL21 star (DE3) for protein expression. For Nuclear Magnetic Resonance (NMR) experiments, ^{15}N-labeled VirB8sp was produced as previously described [21].

Protein purification. Hexa-histidine-tagged *B. suis* VirB8sp (residues 77–239) and VirB10sp (residues 53–391) were initially purified by metal ion affinity chromatography, followed by cleavage of the His-tag with TEV protease and final purification by gel filtration as described [24, 25].

NMR assignments and chemical shift perturbation experiments. All NMR experiments were carried out at 300 K on a Bruker 500 MHz spectrometer (at Université de Montréal) equipped with z-pulsed-field gradient units and triple resonance probes. NMR data were processed using NMRPipe [26] and analyzed by CCPNMR [27]. Signal peaks in heteronuclear single quantum coherence (HSQC) experiments were referenced based on the assignment of VirB8sp (BMRB accession no. 26852) [21]. HSQC spectra of VirB8sp were collected at the concentration of 0.2 mM as described [21] and VirB10sp was added to a final concentration of 0.2 mM. Chemical shift changes were calculated from ^{1}H-^{15}N HSQC experiments using the formula $\Delta\delta=[(0.17\Delta NH)^2+(\Delta HN)^2]^{\frac{1}{2}}$.

Bacterial two-hybrid assay. The interactions between variants of VirB8s with VirB10s were examined using the bacterial two-hybrid assay as described [14, 24, 28]. The steady state levels of adenylate cyclase T18 and T25 domain fusion proteins in the cells were assessed by Western blot using VirB8s- and VirB10s-specific antisera [20].

Phage Display. Purified VirB10sp in 0.1 M $NaHCO_3$ (pH 8.6) at a concentration of 100 μg/mL was adsorbed onto polystyrene microtiter plates (Thermo Scientific), and incubated at 4°C for 16 h, followed by phage display analysis (Ph.D.-12 and Ph.D.-C7C libraries, New England Biolabs) as described [24, 29, 30]. The sequences of VirB10sp-binding peptides were aligned with the VirB8sp protein sequence using the Relic server's MATCH program [31].

Bacterial conjugation assay. Conjugation experiments between *E. coli* strains FM433 pKM101 (donor, ampicillin-resistant) and a non-polar *traE* transposon insertion variant of pKM101 and WL400 (recipient, chloramphenicol-resistant) were conducted as described [16, 32]. Complementation of the *traE* insertion was conducted with plasmid pTrc200 expressing TraE and its variants (Table 1). Conjugation frequencies were calculated as the mean of three biological replicates and one-way ANOVA was performed to determine statistical significance (GraphPad Prism version 7.00, La Jolla, USA).

144

Results

NMR analysis suggests that interaction with VirB10sp causes conformational changes of VirB8sp

In previous work, we showed that changing T201 of VirB8s to other amino acids reduced its binding affinity to VirB10 [11]. In order to obtain higher resolution information on the VirB10 binding interface on VirB8, we performed NMR chemical shift perturbation experiments with VirB8sp and VirB10sp. ^{1}H-^{15}N HSQC (heteronuclear single quantum coherence) spectra were recorded with ^{15}N-labeled VirB8sp both in the absence and in the presence of one molar equivalent of VirB10sp (Fig. 1A). Changes in both ^{1}H and ^{15}N chemical shifts of VirB8sp are observed for several signals following the addition of VirB10sp (Fig. 1A). The signals exhibiting the most significant and clearly measured chemical shift changes ($\delta\Delta > 0.03$) correspond to residues S157 and V166 (Fig. 1B). We also observe significant chemical shift changes of residues G174, R179, T201 and Q205, but the precise determination of their chemical shift perturbation is somewhat ambiguous due to their overlap with other signals following addition of VirB10sp (Fig. 1A and 1B). Interestingly, all of the residues showing significant changes are located on the surface of VirB8sp and primarily within the β-sheet domain (Fig. 1C).

Phage display reveals a domain of VirB8sp that may interact with VirB10sp

As an independent approach to obtain insights into the VirB8-VirB10 interaction, we performed phage display analysis to identify interacting regions using randomized libraries of peptides

displayed on the surface of phages [24, 29, 30]. Purified VirB10sp was used as bait for peptides displayed on the surface of M13 phages from two randomized peptide libraries (Ph.D.-12 and Ph.D.-C7C, NEB). Analysis of the sequence of binding phages reveals the sequences of peptides that have the capacity to bind to VirB10sp. Alignment of the binding peptides with the sequence of VirB8sp identifies 10 peptides that have significant sequence similarity (Fig. 2A). Two clusters of peptides localize onto the sequence of VirB8sp, one to the inward-oriented α2-helix (residues 129-135) and the second to the surface-exposed β1-strand (residues 159−169) (Fig. 2B). The latter sequence includes residue V166, which displayed the most significant chemical shift changes in the VirB8-VirB10 NMR experiments (Fig. 1C), providing further evidence that the β1-strand is part of the VirB8 binding interface to VirB10.

Identification of residues of VirB8s involved in the interaction with VirB10s using the bacterial two-hybrid assay

To assess the importance of the β1-strand and of other potential interacting regions of VirB8 on the VirB8s-VirB10s interaction *in vivo*, we used the bacterial two-hybrid (BTH) assay [28]. Proteins are fused to enzymatically inactive domains of adenylate cyclase (AC), and in the case of an interaction this leads to restoration of cAMP production, triggering a signalling cascade and the production of β-galactosidase in an AC-deficient reporter strain. VirB8 residues on the β1-strand (V159 to V169) as well as adjacent surface-exposed residues (G174, T201 and Q205) that show chemical shift changes upon interaction with VirB10 were changed to alanine (Fig. 3A). Analysis of the interactions of AC fusions to VirB8s and its variants with VirB10s AC fusions shows that changes of all β1-strand residues lead to significant reductions in the

146

interaction, and the V163A and S167A changes have the strongest effects (Fig. 3B). Also, the

G174A, T201A and Q205A changes lead to significant reductions of β-galactosidase activity in

the BTH assay. Western blot analyses show reduced levels of many VirB8s variants in the cell as

compared to wild type, and the levels of VirB10s are equally reduced in these strains (Fig. 3B).

The amount of the S167A fusion is the lowest correlating well with the BTH assay data.

Conjugation assays demonstrate the functional importance of the β-1 strand surface for functionality of the T4SS

To assess the importance of the VirB8s residues identified above for T4SS functionality, we

studied the impacts of corresponding changes in the VirB8 homolog TraE on conjugative

plasmid transfer of pKM101. The structure of TraE is very similar to VirB8s [16], and we

changed residues on the β1-strand and adjacent residues corresponding to G174, Q205 and T201

in VirB8s to alanine (Fig. 4A and C). We then tested complementation of plasmid transfer of a

non-polar pKM101::*traE* transposon insertion mutant [32] by TraE wild type protein and

variants. Changes of the β1-strand residues N162A and S163A result in significant decreases of

conjugation, and no plasmid transfer is observed in the case of V164A (Fig. 4B). In addition, the

G171A, I198A and E202A changes inhibit conjugation and the effect is very strong for the

G171A and E202A variants (Fig. 4B). Western blot analysis shows that TraE and its variants are

present at comparable levels in the cell (Fig. 4B), suggesting that the changes inhibit their

interaction with the T4SS, presumably with the VirB10 homolog TraF, but not their overall

stability.

147

Discussion

It was previously reported that VirB8, VirB9 and VirB10 interact and form part of the core T4SS [9, 14]. In this work, we provide evidence for the molecular basis of the interaction between VirB8 and VirB10. We used NMR chemical shift perturbation experiments to identify residues of VirB8 involved in the interaction and mapping these residues onto the crystal structure of VirB8sp [15] showed that they localize primarily to a surface in the β-sheet domain (V166, R179, T201, and Q205). These results are consistent with previous studies showing the importance of T201 for the interaction of VirB8s with VirB10s *in vitro* and for T4SS function in *Brucella* [11]. The assignments of some of the NMR chemical shift changes were ambiguous due to signal overlap following addition of VirB10. However, NMR spectroscopy greatly aided in the identification of the interaction site and the following results in cell-based assays showed that indeed all these residues are likely part of the binding site to VirB10. As independent approach to identify the interaction site, we performed phage display analysis and the isolated peptides do also point to the β-sheet domain, notably to the β1-strand (V159-V169), as the likely interaction site with VirB10sp.

To assess the importance of the residues identified as important in the VirB8-VirB10 interaction *in vitro* in an *in vivo* assay, we changed them by site-directed mutagenesis to alanine and analyzed the interaction of VirB8s and of its variants with VirB10s using the BTH assay. These experiments showed that changes at most residues on the β1-strand of VirB8s significantly reduces its interaction with VirB10s. In addition, changes of adjacent surface residues (G174, T201 and Q205) to alanine also reduce the interaction, providing additional support for the

localization of the interaction site. It was interesting to note that the levels of fusion proteins in the cell correlated with the results of the BTH assay. The VirB8s-VirB10s interaction probably stabilizes both proteins in the *E. coli* strain used for the BTH assay that lacks other interaction partners from the T4SS. When this interaction is weakened by changes at the interaction site, this apparently reduces the stability of the VirB8s and VirB10s fusion proteins, which is similar to previous observations we made studying interactions between other components of the T4SS complex using the BTH assay [24]. Interestingly, residues V166, G174 and Q205 also undergo chemical shift changes during monomer-to-dimer transition of VirB8s [21], indicating that binding to VirB10s may influence VirB8s self-association during T4SS assembly.

To assess the functional importance of the identified VirB8-VirB10 interaction site, we studied conjugative plasmid DNA transfer mediated by the T4SS from pKM101 as a model. The *Brucella* and the pKM101 T4SS share eleven VirB protein homologs and the structures of VirB8s and of its homolog TraE are very similar [15, 16]. This enabled us to identify the residues in TraE corresponding to the β1-strand (V159-V169) as well as adjacent surface residues G174, T201 and Q205 in VirB8s. Changes of the β1-strand residues N162 and S163 of TraE to alanine lead to significant decreases in conjugation, and it was essentially abolished in cells expressing the V164A variant. These residues are the equivalents of residues V166, S167 and I168 in the β1-strand of VirB8s. In addition, the G171A and E202A changes in TraE strongly inhibit conjugation and they are the equivalents of G174 and Q205 in VirB8sp, which display significant chemical shift changes upon interaction with VirB10sp. In the case of residues I161 and I198 from TraE (equivalent to I165 and T201 in VirB8s, respectively), the reduction of conjugation is relatively modest, but taken together, the results with the pKM101

conjugation assay confirm the functional significance of the VirB10 interaction site identified in VirB8s.

Despite a significant degree of conservation between the components of the *Brucella* VirB T4SS and the pKM101 Tra T4SS as well as the conservation in the overall structure of VirB8s and TraE, we cannot assume with certainty that each equivalent amino acid is involved in the same interactions in the two systems. However, the fact that we identified several functionally important residues that localize to the β1-strand of VirB8s and TraE, or closely adjacent, suggests that we have identified a functionally significant site for the interaction between VirB8 and VirB10 homologs. In contrast to the results of the BTH assay, disruption of the interaction does not affect the levels of TraE variants in the cell and this may be due to the presence of other components of the T4SS stabilizing the protein. The changes in TraE may also affect binding to other T4SS components, e.g. with the VirB4-homolog TraB [11], explaining the strong effects on bacterial conjugation as compared to the more moderate effects on the protein-protein interaction in the BTH assay. VirB10 was shown to bind VirB6 [24] and VirB8 and VirB6 are also believed to interact [22], suggesting that a sub-complex composed of VirB6, VirB8 and VirB10 may constitute the inner membrane part of the T4SS. However, until now no detailed information on the structure of the inner membrane part of the T4SS was available [7]. Our work therefore sheds light on this important open question.

Figures
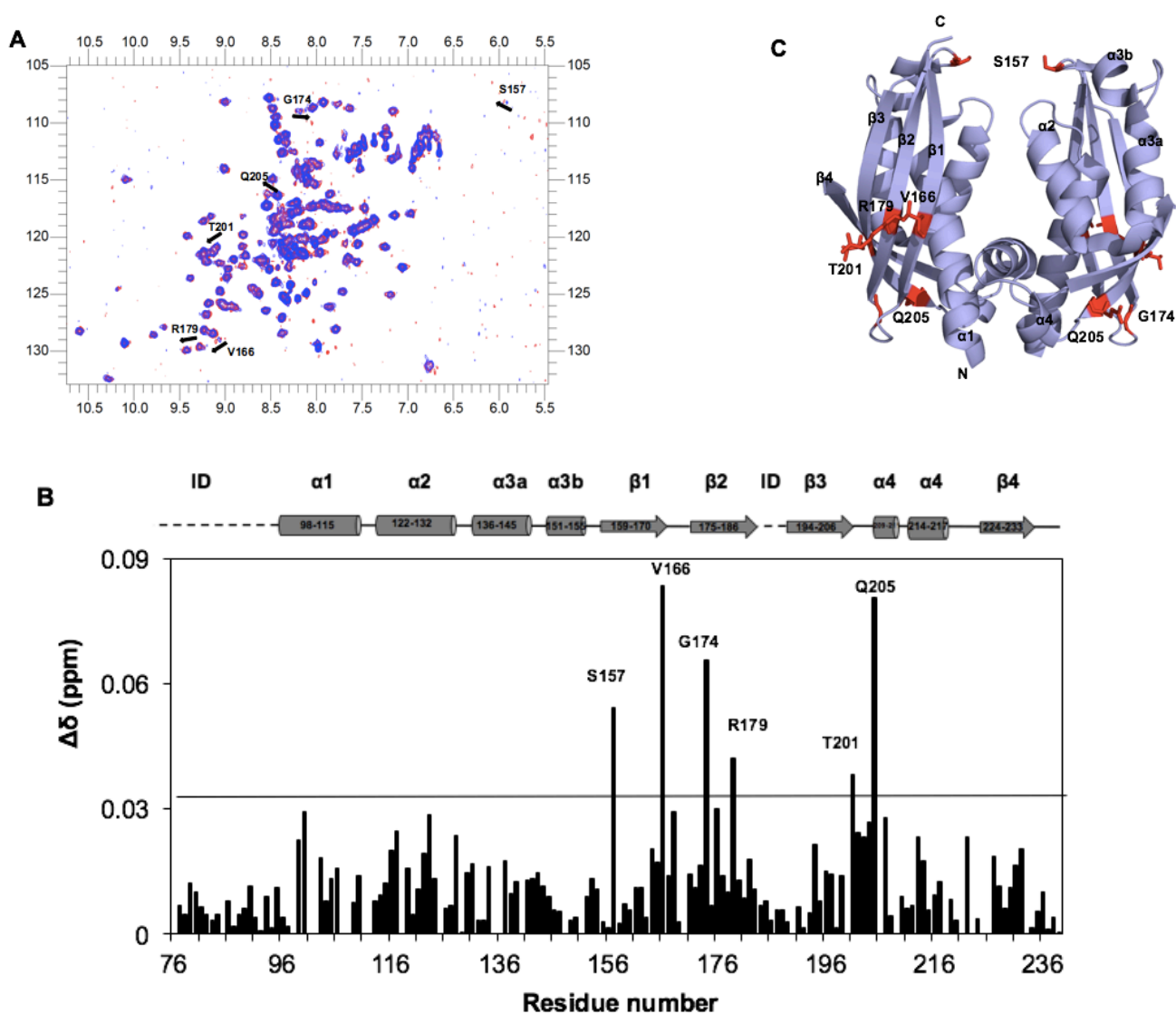
Figure 1. Mapping of chemical shift changes of VirB8sp in the presence of VirB10sp. (A) Overlay of ^{1}H-^{15}N HSQC spectra of VirB8sp in the absence (blue) and presence (red) of one molar equivalent of VirB10sp; arrows indicate the signals that display significant changes in chemical shifts. (B) Histogram of the variation in chemical shifts [$\Delta\delta$ (ppm)] observed in ^{1}H-^{15}N HSQC spectra of ^{15}N-labeled VirB8sp and after addition of VirB10sp. The chemical shift perturbations were calculated with the formula $\Delta\delta=[(0.17\Delta NH)^2 +(\Delta HN)^2]^{\frac{1}{2}}$, and are given in

parts per million. ΔδHN values above the horizontal line are considered significant (average of changes plus one standard deviation). On top of the histogram, the secondary structural contents of VirB8sp are presented as previously described [21] (C) Mapping of the residues with significant chemical shift changes (shown in red as stick format) on the cartoon structure of VirB8sp (PDB code 2BHM)[15].
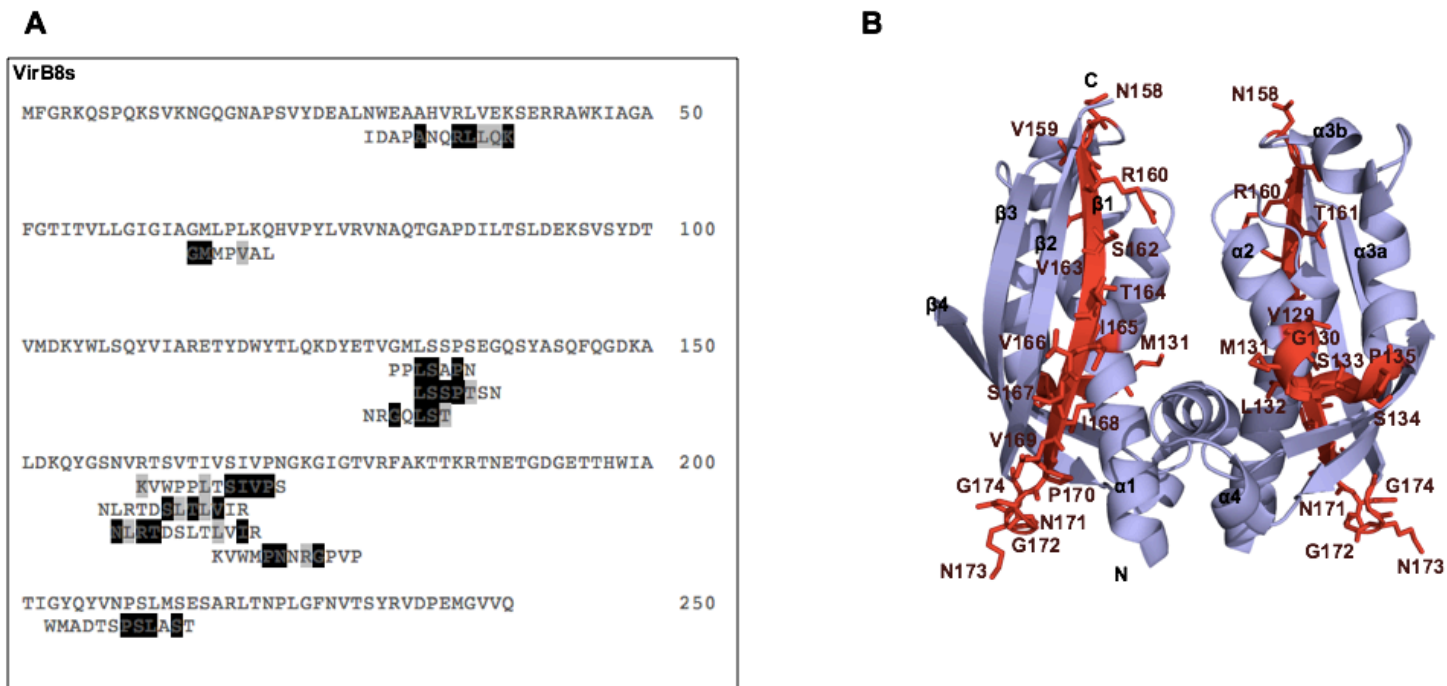
Figure 2. Phage display to identify the VirB10sp binding site on VirB8s. (A) The sequence of VirB8s is displayed and aligned with VirB10sp affinity-selected peptides from phage display libraries [Ph.D.-C7C and Ph.D.-12 (NEB)]. Identical residues in the protein and peptide sequences are highlighted in black, and conserved residues are highlighted in gray. (B) VirB8sp residues (red) identified by phage display as potential VirB10sp interaction sites are mapped on a cartoon representation of the crystal structure of VirB8sp (PDB code 2BHM) [15].
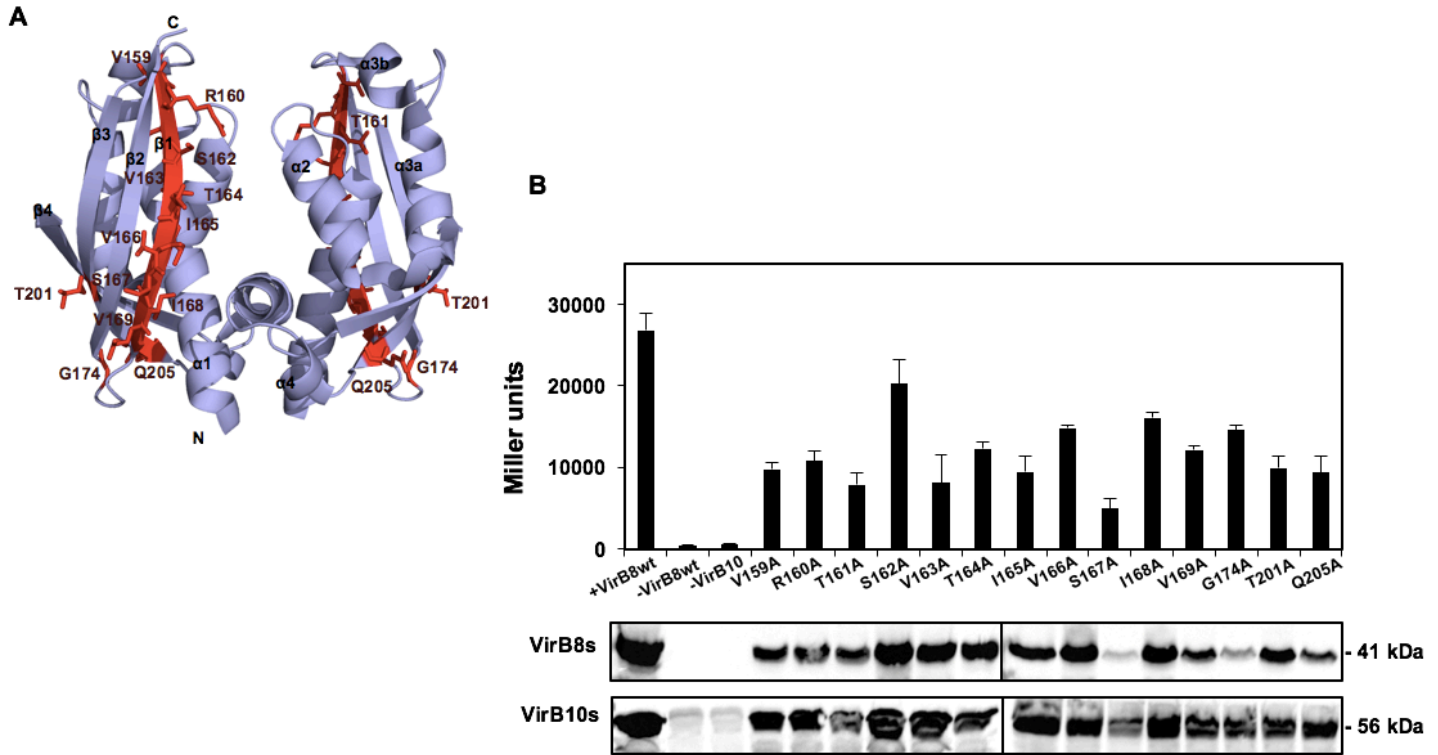
Figure 3. Bacterial two-hybrid assay to assess the interactions of VirB10s with variants of VirB8s. (A) The residues in VirB8s that were changed to alanine are mapped (labelled in red) on a cartoon representation of the crystal structure of VirB8sp (PDB code 2BHM) [15]. (B) Analysis of the interactions between VirB10s, VirB8s and VirB8s alanine variants using the BTH assay; negative controls without expression of VirB8s or VirB10s. Values and standard deviations were calculated from three independent experiments. Analysis of the expression of fusion proteins by Western blotting with VirB8sp- and VirB10sp-specific antisera. Signals correspond to the predicted molecular masses of VirB8s and VirB10s fusion proteins to domains of AC.
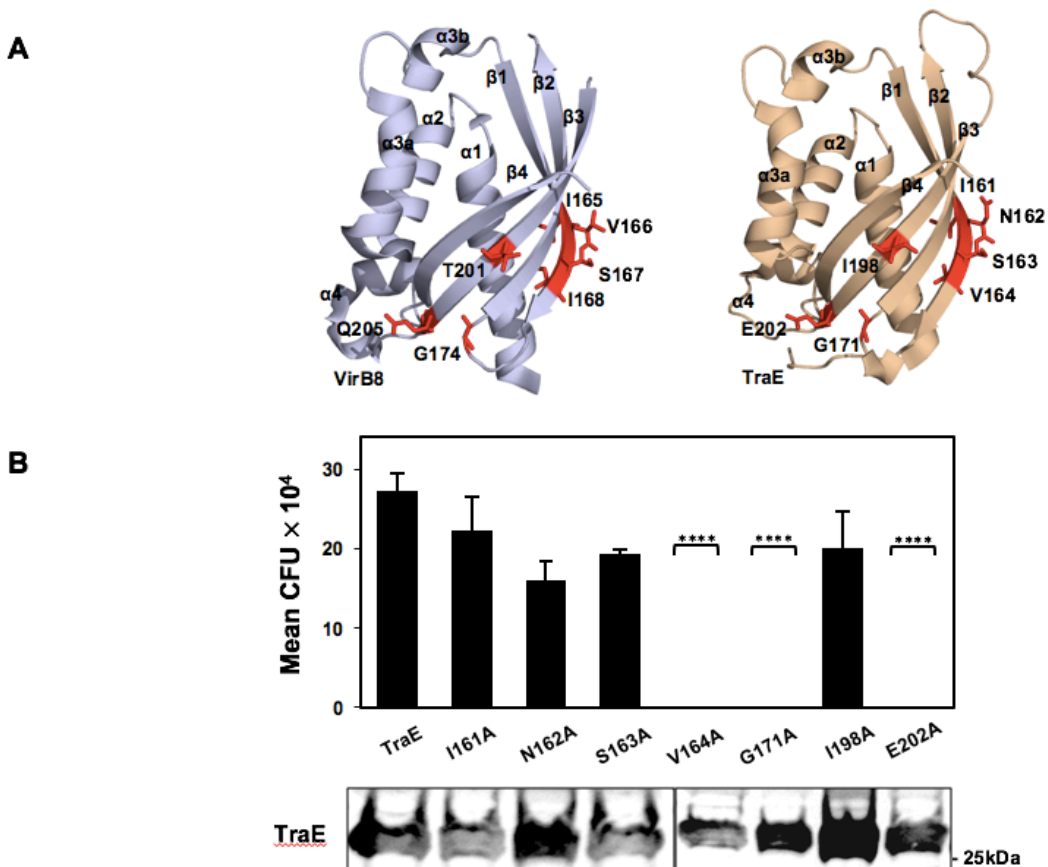
Figure 4. Impact of changes of the β-strand region of TraE on pKM101 conjugation. (A) Cartoon representation of the changed amino acids (labelled in red) mapped on the crystal structures of VirB8sp [15] and TraE [16]. (B) Conjugation assays showing effects of changes on the capacity of TraE and TraE variants to complement a pKM101::*traE* transposon insertion deletion (CFU, colony forming units of recipient strain). Averages and standard error of the mean of three biological replicate cultures of each variant are represented ($p < 0.0001$, $n = 3$; stars added to variants with significant p value). The lower panel represents a Western blot showing expression of TraE and TraE variants using TraE-specific antiserum. (C) Sequence alignment of the β-strand regions of VirB8s and TraE. Conserved and similar residues are indicated and changes at TraE residues labelled in red were studied using the conjugation assay.

Acknowledgements

Tables

Table 1. Bacterial strains and plasmids.

Strain	Genotype or Description	Source or Reference
JM109	*endA1 gyr96 thi hsdR71 supE44 recA1 relA1 (Δlac-proAB) (F'traD36 proAB+lacIqlacZΔM15)*	[33]
BL21(DE3)star	*F– ompT hsdSB(rB–, mB–) gal dcm rne131 (DE3)*	Invitrogen
BTH101	*F- cya-99, araD139, galE15, galK16, rpsL1 (str^r), hsdR2, mcrA1, mcrB1*	[28]
FM433	Spcr araD139 Δ(argF-lac)U169 ptsF25 deoC1 relA1 flbB5301 rpsE13 Δ(srl-recA)306::Tn10, conjugation donor	[34]
WL400	Cmr Strr araD139 Δ(argF-lac)U169, ptsF25 deoC1 relA1 flbB5301 rpsL150 ΔselD204::cat, conjugation recipient	Leinfelder, W. Unpublished data.
Plasmids		
pHTVirB8sp	kan^r T7 promoter vector for the expression of 6xHis-tagged periplasmic domain of *B. suis* VirB8	[25]
pHTVirB10sp	kan^r pHT harboring 1017 bp *virB10* fragment from *B. suis* (encoding 339 amino acid periplasmic domain)	[24]
pUT18C	pUC19 derivative including the T18 fragment (amino acids 225-399 of *B. pertussis* CyaA) C-terminal to the multiple cloning site	[28]
pKT25	pSU40 derivative including the T25 fragment (amino acids 1-224 of *B. pertussis* CyaA) C-terminal to the multiple cloning site	[28]
pKT25B10	kan^r, pKT25 harboring 1176 bp XbaI/KpnI *virB10* fragment from *B. suis* (encoding full-length VirB10)	[20]
pUT18CB8	amp^r , pUT18C harboring 720 bp XbaI/KpnI *virB8* from *B. suis* (encoding full-length VirB8)	[20]
pUT18CB8 V159A	amp^r , pUT18C harboring 720 bp XbaI/KpnI *virB8* from *B. suis* with amino acid change V159A	This work

pUT18CB8 R160A	amp^r , pUT18C harboring 720 bp XbaI/KpnI *virB8* from *B. suis* with amino acid change R160A	This work
pUT18CB8 T161A	amp^r , pUT18C harboring 720 bp XbaI/KpnI *virB8* from *B. suis* with amino acid change T161A	This work
pUT18CB8 S162A	amp^r , pUT18C harboring 720 bp XbaI/KpnI *virB8* from *B. suis* with amino acid change S162A	This work
pUT18CB8 V163A	amp^r , pUT18C harboring 720 bp XbaI/KpnI *virB8* from *B. suis* with amino acid change V163A	This work
pUT18CB8 T164A	amp^r , pUT18C harboring 720 bp XbaI/KpnI *virB8* from *B. suis* with amino acid change T164A	This work
pUT18CB8 I165A	amp^r , pUT18C harboring 720 bp XbaI/KpnI *virB8* from *B. suis* with amino acid change I165A	This work
pUT18CB8 V166A	amp^r , pUT18C harboring 720 bp XbaI/KpnI *virB8* from *B. suis* with amino acid change V166A	This work
pUT18CB8 S167A	amp^r , pUT18C harboring 720 bp XbaI/KpnI *virB8* from *B. suis* with amino acid change S167A	This work
pUT18CB8 I168A	amp^r , pUT18C harboring 720 bp XbaI/KpnI *virB8* from *B. suis* with amino acid change I168A	This work
pUT18CB8 V169A	amp^r , pUT18C harboring 720 bp XbaI/KpnI *virB8* from *B. suis* with amino acid change V169A	This work
pUT18CB8 G174A	amp^r , pUT18C harboring 720 bp XbaI/KpnI *virB8* from *B. suis* with amino acid change G174A	This work
pUT18CB8 T201A	amp^r , pUT18C harboring 720 bp XbaI/KpnI *virB8* from *B. suis* with amino acid change T201A	This work

pUT18CB8 Q205A	amp^r , pUT18C harboring 720 bp XbaI/KpnI *virB8* from *B. suis* with amino acid change Q205A	This work
pTrc200	Strr , Spcr , pVS1 derivative, LacIq , trc promoter expression vector	[35]
pTrc200TraE	pTrc200, traE PCR fragment cloned downstream of the *trae* promoter	[16]
pTrc200TraE I161A	pTrc200TraE modified to encode TraE with amino acid change I161A	This work
pTrc200TraE N162A	pTrc200TraE modified to encode TraE with amino acid change N162A	This work
pTrc200TraE S163A	pTrc200TraE modified to encode TraE with amino acid change S163A	This work
pTrc200TraE V164A	pTrc200TraE modified to encode TraE with amino acid change V164A	This work
pTrc200TraE G171A	pTrc200TraE modified to encode TraE with amino acid change G171A	This work
pTrc200TraE I198A	pTrc200TraE modified to encode TraE with amino acid change I198A	This work
pTrc200TraE E202A	pTrc200TraE modified to encode TraE with amino acid change E202A	This work

References

1. Chandran Darbari, V. & Waksman, G. (2015) Structural Biology of Bacterial Type IV Secretion Systems, *Annu Rev Biochem.* **84**, 603-29.

2. Trokter, M., Felisberto-Rodrigues, C., Christie, P. J. & Waksman, G. (2014) Recent advances in the structural and molecular biology of type IV secretion systems, *Current opinion in structural biology.* **27C**, 16-23.

3. Fronzes, R., Christie, P. J. & Waksman, G. (2009) The structural biology of type IV secretion systems, *Nature reviews Microbiology.* **7**, 703-14.

4. Goessweiner-Mohr, N., Arends, K., Keller, W. & Grohmann, E. (2013) Conjugative type IV secretion systems in Gram-positive bacteria, *Plasmid.* **70**, 289-302.

5. Fronzes, R., Schafer, E., Wang, L., Saibil, H. R., Orlova, E. V. & Waksman, G. (2009) Structure of a type IV secretion system core complex, *Science.* **323**, 266-8.

6. Chandran, V., Fronzes, R., Duquerroy, S., Cronin, N., Navaza, J. & Waksman, G. (2009) Structure of the outer membrane complex of a type IV secretion system, *Nature.* **462**, 1011-5.

7. Low, H. H., Gubellini, F., Rivera-Calzada, A., Braun, N., Connery, S., Dujeancourt, A., Lu, F., Redzej, A., Fronzes, R., Orlova, E. V. & Waksman, G. (2014) Structure of a type IV secretion system, *Nature.* **508**, 550-3.

8. Fercher, C., Probst, I., Kohler, V., Goessweiner-Mohr, N., Arends, K., Grohmann, E., Zangger, K., Meyer, N. H. & Keller, W. (2016) VirB8-like protein TraH is crucial for DNA transfer in Enterococcus faecalis, *Sci Rep.* **6**, 24643.

9. Das, A. & Xie, Y.-H. (2000) The *Agrobacterium* T-DNA transport pore proteins VirB8, VirB9 and VirB10 interact with one another, *J Bacteriol.* **182**, 758-763.

10. Yuan, Q., Carle, A., Gao, C., Sivanesan, D., Aly, K., Höppner, C., Krall, L., Domke, N. & Baron, C. (2005) Identification of the VirB4-VirB8-VirB5-VirB2 pilus assembly sequence of type IV secretion systems, *J Biol Chem.* **280**, 26349-26359.

11. Paschos, A., Patey, G., Sivanesan, D., Gao, C., Bayliss, R., Waksman, G., O'Callaghan, D. & Baron, C. (2006) Dimerization and interactions of *Brucella suis* VirB8 with VirB4 and VirB10 are required for its biological activity, *Proc Natl Acad Sci USA.* **103**, 7252-7257.

12. Bourg, G., Sube, R., O'Callaghan, D. & Patey, G. (2009) Interactions between *Brucella suis* VirB8 and its homolog TraJ from the plasmid pSB102 underline the dynamic nature of type IV secretion systems, *J Bacteriol.* **191**, 2985-92.

13. Villamil Giraldo, A. M., Sivanesan, D., Carle, A., Paschos, A., Smith, M. A., Plesa, M., Coulton, J. & Baron, C. (2012) Type IV secretion system core component VirB8 from *Brucella* binds to the globular domain of VirB5 and to a periplasmic domain of VirB6, *Biochemistry.* **51**, 3881-90.

14. Sivanesan, D., Hancock, M. A., Villamil Giraldo, A. M. & Baron, C. (2010) Quantitative analysis of VirB8-VirB9-VirB10 interactions provides a dynamic model of type IV secretion system core complex assembly, *Biochemistry.* **49**, 4483-93.

15. Terradot, L., Bayliss, R., Oomen, C., Leonard, G., Baron, C. & Waksman, G. (2005) Crystal Structures of the periplasmic domains of two core subunits of the bacterial type IV secretion system, VirB8 from *Brucella suis* and ComB10 from *Helicobacter pylori, Proc Natl Acad Sci USA.* **102**, 4596-4601.

16. Casu, B., Smart, J. P., Hancock, M. A., Smith, M., Sygusch, J. & Baron, C. (2016) Structural analysis and inhibition of TraE from the pKM101 type IV secretion system, *J Biol Chem*, PMID: 27634044

17. Bailey, S., Ward, D., Middleton, R., Grossmann, J. G. & Zambryski, P. (2006) *Agrobacterium tumefaciens* VirB8 structure reveals potential protein-protein interactions sites, *Proc Natl Acad Sci USA.* **103**, 2582-2587.

18. Goessweiner-Mohr, N., Grumet, L., Arends, K., Pavkov-Keller, T., Gruber, C. C., Gruber, K., Birner-Gruenberger, R., Kropec-Huebner, A., Huebner, J., Grohmann, E. & Keller, W. (2013) The 2.5 A structure of the enterococcus conjugation protein TraM resembles VirB8 type IV secretion proteins, *The Journal of biological chemistry.* **288**, 2018-28.

19. Gillespie, J. J., Phan, I. Q., Scheib, H., Subramanian, S., Edwards, T. E., Lehman, S. S., Piitulainen, H., Sayeedur Rahman, M., Rennoll-Bankert, K. E., Staker, B. L., Taira, S., Stacy, R., Myler, P. J., Azad, A. F. & Pulliainen, A. T. (2015) Structural Insight into How Bacteria Prevent Interference between Multiple Divergent Type IV Secretion Systems, *MBio.* **6**.

20. Paschos, A., den Hartigh, A., Smith, M. A., Atluri, V. L., Sivanesan, D., Tsolis, R. M. & Baron, C. (2011) An In Vivo High-Throughput Screening Approach Targeting the Type IV Secretion System Component VirB8 Identified Inhibitors of *Brucella abortus 2308* Proliferation, *Infect Immun.* **79**, 1033-43.

21. Sharifahmadian, M., Arya, T., Bessette, B., Lecoq, L., Ruediger, E., Omichinski, J. G. & Baron, C. (2017) Monomer-to-dimer transition of *Brucella suis* type IV secretion system component VirB8 induces conformational changes, *The FEBS journal.* **284**, 1218-1232.

22. Cascales, E. & Christie, P. J. (2004) Definition of a bacterial type IV secretion pathway for a DNA substrate, *Science.* **304**, 1170-1173.

23. Cascales, E. & Christie, P. J. (2004) *Agrobacterium* VirB10, an ATP energy sensor required for type IV secretion, *Proc Natl Acad Sci USA.* **101**, 17228-17233.

24. Villamil Giraldo, A. M., Mary, C., Sivanesan, D. & Baron, C. (2015) VirB6 and VirB10 from the *Brucella* type IV secretion system interact via the N-terminal periplasmic domain of VirB6, *FEBS letters*. **589**, 1883-9.

25. Smith, M. A., Coincon, M., Paschos, A., Jolicoeur, B., Lavallee, P., Sygusch, J. & Baron, C. (2012) Identification of the Binding Site of *Brucella* VirB8 Interaction Inhibitors, *Chem Biol*. **19**, 1041-8.

26. Delaglio, F., Grzesiek, S., Vuister, G. W., Zhu, G., Pfeifer, J. & Bax, A. (1995) NMRPipe: a multidimensional spectral processing system based on UNIX pipes, *J Biomol NMR*. **6**, 277-93.

27. Vranken, W. F., Boucher, W., Stevens, T. J., Fogh, R. H., Pajon, A., Llinas, M., Ulrich, E. L., Markley, J. L., Ionides, J. & Laue, E. D. (2005) The CCPN data model for NMR spectroscopy: development of a software pipeline, *Proteins*. **59**, 687-96.

28. Karimova, G., Dautin, N. & Ladant, D. (2005) Interaction network among *Escherichia coli* membrane proteins involved in cell division as revealed by bacterial two-hybrid analysis, *J Bacteriol*. **187**, 2233-2243.

29. Oudouhou, F., Casu, B., Dopgwa Puemi, A. S., Sygusch, J. & Baron, C. (2017) Analysis of Novel Interactions between Components of the Selenocysteine Biosynthesis Pathway, SEPHS1, SEPHS2, SEPSECS, and SECp43, *Biochemistry*.

30. Carter, D. M., Gagnon, J. N., Damlaj, M., Mandava, S., Makowski, L., Rodi, D. J., Pawelek, P. D. & Coulton, J. W. (2006) Phage display reveals multiple contact sites between FhuA, an outer membrane receptor of Escherichia coli, and TonB, *Journal of molecular biology*. **357**, 236-51.

31. Mandava, S., Makowski, L., Devarapalli, S., Uzubell, J. & Rodi, D. J. (2004) RELIC--a bioinformatics server for combinatorial peptide analysis and identification of protein-ligand interaction sites, *Proteomics.* **4**, 1439-60.

32. Winans, S. C. & Walker, G. C. (1985) Conjugal transfer system of the N incompatibility plasmid pKM101, *J Bacteriol.* **161**, 402-410.

33. Yanisch-Perron, C., Viera, J. & Messing, J. (1985) Improved M13 phage cloning vectors and host strains: nucleotide sequence of the M13mp18 and pUC18 vectors, *Gene.* **33**, 103-119.

34. Zinoni, F., Heider, J. & Böck, A. (1990) Features of the formate dehydrogenase mRNA necessary for decoding of the UGA codon as selenocysteine, *Proc Natl Acad Sci USA.* **87**, 4660-4664.

35. Schmidt-Eisenlohr, H., Domke, N. & Baron, C. (1999) TraC of IncN plasmid pKM101 associates with membranes and extracellular high molecular weight structures in *Escherichia coli*, *J Bacteriol.* **181**, 5563-5571.

Chapter 4: Discussion

4.1 General goals of the thesis

Many pathogenic bacteria secrete virulence factors across their envelope into the host cell or into the extracellular environment. Several of them use type IV secretion systems as major virulence factor and a wide range of hosts are being infected by these pathogenic bacteria. These bacteria cause plant diseases by transfer of oncogenic DNA (e.g. crown gall tumors induced by *Agrobacterium tumefaciens*) and human diseases by secreting virulence factors, such as bacillary angiomatosis (*Bartonella henselae*), whooping cough (*Bordetella pertussis*), Brucellosis (*Brucella spp.*), Q-fever (*Coxiella burnetii),* gastritis and peptic ulcer (*Helicobacter pylori*) and Legionnaire's disease (*Legionella pneumophila*) (Baron, 2005; Christie, et al., 2005). Many bacteria use T4SSs for conjugation to transfer plasmids leading to the spread of antibiotic resistance genes (Waters, 1999; Molin, & Tolker-Nielsen, 2003). The world health organization (WHO) has called antimicrobial resistance the major public health threat of the current century (www.who.int/drugresistance/documents/surveillancereport). As part of the strategy to address this challenge, identifying molecular details of T4SS assembly and function will provide new targets for the development of drugs that disarm the bacterial pathogens without killing them. The goal of this research is to provide insights into the molecular basis of protein-protein interactions and its role for assembly and function of T4SSs. My research was focused on the VirB8 protein, an essential assembly factor for the T4SS multiprotein complex (Sivanesan, Hancock, Villamil Giraldo & Baron, 2010). I used structural and chemical biology approaches to gain insights into the structural dynamics and function of

VirB8. I have conducted structural analyses using NMR studies on the VirB8 protein from *B. suis* to identify conformational changes of VirB8 in complex with other VirB proteins. In addition, I have used *in vivo* interaction assays such as the bacterial two-hybrid assay and the measurement of conjugative DNA transfer to identify and to characterize the importance of interaction sites of VirB8 with other T4SS components and with small molecules that could be developed into inhibitors of VirB8 protein functions. The ultimate goal of our work is to propose a model for the interactions of VirB8 in the T4SS complex. The results of this thesis provide novel insights into the structure and interactions of VirB8 contributing to better understanding of its role in T4SS assembly and function.

4.2 Article 1: Monomer-to-dimer transition of *Brucella suis* type IV secretion system component VirB8 induces conformational changes

4.2.1 Overview of investigations on the structure and dynamics of VirB8

The crystal structure of the periplasmic domain of VirB8 from *B. suis* (PDB code 2BHM) has been resolved. The analysis of the crystal structure and subsequent functional analysis suggested that VirB8s forms homodimers (Terradot et al., 2005; Paschos et al., 2006). Similar to the crystallography work, I conducted NMR analysis of the purified periplasmic domain of VirB8 (VirB8sp: missing the 49 amino acids of the cytoplasmic N-terminus and the 18 amino acids of the transmembrane domain). Studying VirB8sp by solution NMR analysis provided information on the dynamics and conformational changes of the protein, which had not previously been observed by X-ray crystallography.

4.2.2 Evidence for an effect of the membrane on the conformation of VirB8

As reported in the first article, the amino acid backbone assignment of VirB8sp was obtained from NMR spectra of the protein in CHAPS micelles. The presence of CHAPS micelles stabilized the protein and many peaks appeared in HSQC spectra only in presence of CHAPS resulting in the best quality of signals on the spectra. Whereas this was not primary goal of this work, it was interesting to note that a membrane mimicking condition like CHAPS micelles stabilized the structure of the periplasmic domain of VirB8. Interestingly, in the presence of CHAPS micelles the HSQC spectra of VirB8sp at the monomeric (15 μM) and mostly dimeric concentrations (200 μM) were similar. This observation suggests that the micelles change the monomer-dimer equilibrium favoring the dimer conformation. This raises the possibility that the plasma membrane has an effect on the conformation and interactions of the full length protein. In future studies, comparing the NMR spectra of full length VirB8s to those of the periplasmic domain VirB8sp will provide insights into the effects of the membrane environment on the conformation of the protein.

4.2.3 Analysis of VirB8 dimerization by NMR spectroscopy

Previous studies reported the functional importance of dimerization of VirB8 (Paschos et al., 2006). In addition, analysis of the VirB8sp crystal structure suggested that the helical regions (α-1 and α-4) of VirB8sp constitute the dimer interface and that residues M102, Y105 and E214 play a particular role for dimerization. In order to understand the molecular mechanism of monomer-to-dimer transition, I monitored the conformational changes of VirB8sp at monomeric- (15 μM) and primarily dimeric (200 μM) concentrations by HSQC experiments. Comparing chemical shift changes in the HSQC spectra revealed changes at

different sites of VirB8sp. Significant chemical shift changes were observed for residues D103, Q109, S210 and L211. Interestingly, these residues are located in the same regions on the α-1 and α-4 helices, which comprised the dimer interface in the X-ray structure. In addition, it was noticeable that several peaks appeared on the HSQC spectrum only at dimeric concentration. This observation suggests that similar to the presence of CHAPS, dimerization stabilized the protein. For example, I observed significant chemical shift changes for residues S157 and S210 located in a loop and in the α-4 helix during monomer-to-dimer transition and in the presence of the CHAPS micelle. Since most of VirB8 proteins share similar overall structure (Terradot et al., 2005; Bailey, et al., 2006 ; Casu et al., 2016; Porter et al., 2012 ; Goessweiner-Mohr et al., 2013), the identified changes by NMR during monomer-to-dimer transition may be pertinent in other VirB8 proteins. In accord with this notion, it was shown that the equivalents of *Brucella* VirB8 residues M102, Q109 and T121 are involved in dimerization of *Bartonella* VirB8 (Gillespie et al., 2015).

4.2.4 Structural analysis of a monomeric variant of VirB8sp

The functional importance of dimerization suggested that it is pertinent to conduct structural analysis of the VirB8sp^{M102R} variant. We previously reported that the change M102R strongly reduces dimerization and this variant has a K_D higher than 1 mM (Figure 19, from: Sivanesan, Hancock, Villamil Giraldo & Baron, 2010). To understand how a single amino acid change disrupts dimerization we analyzed the structure of VirB8sp^{M102R} by NMR spectroscopy. Comparison of the HSQC spectra showed a substantial number of differences between the variant and the wild-type protein. Chemical shifts of several residues (24 individual amino acids) were strongly changed, which impeded tracing of their signal peaks. Therefore, these

residues could not be assigned. Significant chemical shift changes localized primarily in the α-helical regions (α-1 and α-4) that are also important for dimerization. We also studied this variant by X-ray crystallography as a complementary approach to understand the molecular basis for reduced dimerization of VirB8sp^{M102R}.
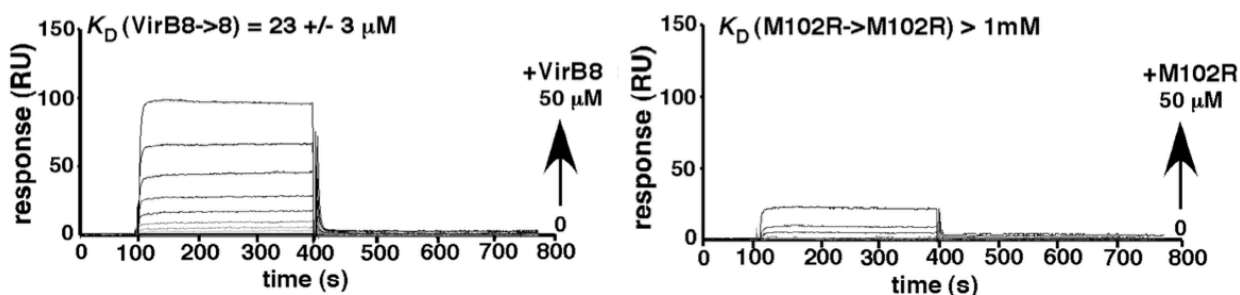
Figure 19. Surface plasmon resonance (SPR) analysis of VirB8sp. VirB8sp was passed over a surface carrying immobilized VirB8sp (left). VirB8sp^{M102R} was passed over a surface with immobilized VirB8sp^{M102R} (right). The figure is adapted from (Sivanesan, Hancock, Villamil Giraldo & Baron, 2010).

Analysis of the crystal structure revealed that the overall fold of VirB8sp^{M102R} is similar to the wild-type except for a significant change in the orientation of the α-4 helix. This is consistent with the results of NMR studies that also showed significant chemical shift changes of several residues of VirB8sp^{M102R} located in the α-4 helix. The orientation of the proteins in the crystal packing also reflected structural differences. In the case of wild-type VirB8sp, the M102 residues of two proteins are facing each other in the dimer. In contrast, in the case of VirB8sp^{M102R}, the R102 residues face away from each other in the X-ray structure. The

repulsion of the positive charges between the arginine residues of VirB8sp^{M102R} may prevent crystallization like the wild type. The identified structural differences (NMR and X-ray crystal analyses) support the notion that the α-helical regions (α-1 and α-4) are important for the functionality of VirB8. Further studies on the structures and interactions of VirB8 variants on the α-helical regions (α-1 and α-4) will provide complementary information on the functional dynamics of VirB8 structure in the T4SS complex.

4.2.5 Identification of fragments that bind to the VirB8s dimer

Dimerization of VirB8 has been the main target for inhibitors. In previous work from our team, a small molecule inhibitor of *Brucella* VirB8 was identified that reduced dimerization and inhibited *Brucella abortus 2308* in an infection assay (Paschos et al., 2011). Further structural studies of this molecule by co-crystallisation and X-ray analysis revealed that it binds to a surface groove of VirB8 that is opposite to the dimerization interface (Smith et al., 2012). This study identified that residues E115 and K182 are critical for inhibitor binding, while residues R114, Y229 and L151 also contribute to binding of the inhibitor. In order to identify novel small molecule inhibitors of dimerization of *Brucella* VirB8, we conducted a screen of a library of 186 fragments assessing their effect on wild-type VirB8sp and its monomeric variant VirB8sp^{M102R}. Differential scanning fluorimetry (DSF) was used to determine the melting temperature of the proteins; binding of the fragments changes the conformation and consequently the melting temperature of the protein. Most of the fragments in this screen had no or very similar effects on the melting temperatures (ΔT_m values) of the wild-type and VirB8sp ^{M102R}, except for two molecules (II and VIII) that had differential effects. Fragment II significantly changed the T_m value of the wild-type, while it had a moderate effect on the T_m

value of VirB8sp^{M102R}. Fragment II is a salicylanilide and its structure is similar to B8I-2 (salicylidene acylhydrazide) (Figure 20), an inhibitor of VirB8s dimerization (Smith et al., 2012). *In silico* docking showed that fragment II may bind to the surface groove of both VirB8sp and VirB8sp^{M102R}, which is the same site suggested for binding of B8-I2 (Smith et al., 2012). Fragment VIII is a benzimidazole and induced almost no changes of the melting temperature of the wild-type. However, it significantly changed the T$_m$ value of VirB8sp^{M102R}. Docking analysis suggested that fragment VIII localized in the B8-I2-binding groove of VirB8sp^{M102R} and at a different site on the wild-type far from the surface groove.
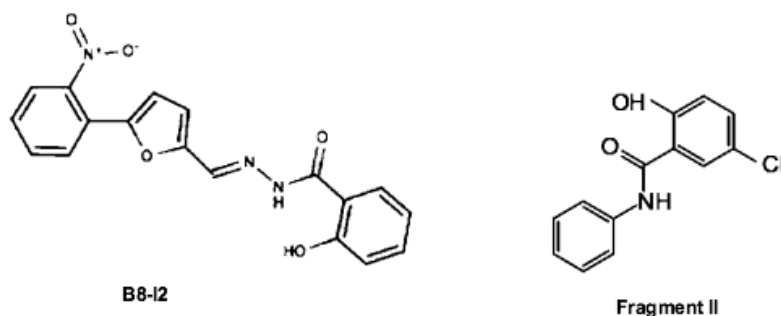
Figure 20. The structure of B8I-2, a salicylidene acylhydrazide, and of fragment II, a salicylanilide.

Our NMR studies show that several residues of VirB8sp^{M102R} have different conformations than the wild-type in the B8I-2 binding surface groove (e. g. L151, K182, and E114) and on the α-1 helix that links the dimerization interface to the surface groove. Therefore, the conformation of the groove and consequently the binding of inhibitors to this site may be different for VirB8sp^{M102R} and the wild-type. We have indeed identified two

molecules by DSF that serve as chemical probes for the different conformations of VirB8sp and its monomeric variant VirB8sp[M102R]. The results of this study support the importance of this groove and of its conformation for the binding and effectiveness of VirB8-specific inhibitors. This knowledge could be exploited for the design of more effective inhibitors in future.

4.2.6 The VirB8 surface groove as a target site for future drug design

We did not obtain high-resolution structural data on the binding site of the fragments to VirB8sp and VirB8sp[M102R]. However, fragments II and VIII share the chemical structures of salicylanilides and benzimidazoles, respectively, which are known for their antibacterial and antiviral properties (Delaglio et al., 1995; Paschos et al., 2011). Their similarity to the structure of antimicrobial molecules and binding to the target raised the possibility that VirB8s dimerization inhibitors based on the fragments II and VIII could be designed in future. Studying the effect of these fragments and of derivates on the dimerization of full-length VirB8s will be very interesting for future work and this may reveal the contribution of the membrane and of the transmembrane domain to dimerization of VirB8s.

4.3 Article 2: Type IV secretion system core component VirB8 interacts via the β1-strand with VirB10

4.3.1   Overview of the characterization of interactions of VirB8 with VirB10

After analyzing the conformational dynamics of VirB8 and residues involved in dimerization, I next investigated the interactions of VirB8 with VirB10. VirB10 is the only subunit of the T4SS complex that spans the outer and inner membranes and it probably acts as a scaffold of the complex. It was reported that VirB8 participates in a series of probably transient interactions with several other VirB proteins of the T4SS complex. Previous studies provided evidence for direct interactions of VirB8 with VirB4, VirB5 and VirB6 (Cascales & Christie, 2004a; Yuan et al., 2005; Villamil Giraldo et al., 2012; Villamil Giraldo et al., 2015). Based on the fact that VirB8 is essential for the T4SS, it was suggested that VirB8 transiently interacts with other VirB proteins and works as an assembly factor (Sivanesan, Hancock, Villamil Giraldo & Baron, 2010). VirB8 and VirB10 are both essential for the functionality of the complex and early studies showed that these proteins interact (Ding et al., 2002 ; Das & Xie, 2000; Sivanesan, Hancock, Villamil Giraldo & Baron, 2010).

4.3.2 Structural analysis of the interactions of VirB8 with VirB10

The only structural information on the site of interaction of VirB8 with VirB10 comes from a previous study by our group suggesting that VirB8 residue T201 is needed for the interaction. It was also shown that changes of this residue reduced the virulence of *Brucella suis 1330* (Paschos et al., 2006). T201 is located on the highly conserved β-sheet domain of VirB8. In order to identify the structural basis of the VirB8-VirB10 interaction, I conducted

NMR studies and biochemical assays. The NMR experiments on the purified periplasmic domain VirB8sp revealed chemical shift changes of several residues upon addition of the purified periplasmic domain VirB10sp. Most of these identified residues (i.e. V166, R179, T201 and Q205) located on the surface of the VirB8sp β-sheet domain. Subsequently, the importance of these residues for the interaction with VirB10 was assessed using an *in vivo* interaction assay (bacterial two hybrid assay) and a cell-based T4SS functional assay (plasmid conjugation). In parallel, phage display analysis suggested that 11 residues from the β-sheet domain (β1-strand V159-V169) of VirB8 are likely part of the interface for interaction with VirB10.

4.3.3 Characterizing the VirB8 interaction interface with VirB10

To further investigate the molecular basis of the VirB8-VirB10 interaction, we studied the effects of changes of the residues identified by NMR and phage display. In the bacterial two hybrid assay (BTH assay) changes of most residues on the β1-strand of VirB8s reduced the interaction with VirB10s. The levels of the fusion proteins to VirB8s and VirB10s in the cell correlated with the level of interaction determined in the BTH assay. Similar to observations made in a previous BTH study of the VirB10-VirB6 interaction (Villamil Giraldo et al., 2015), it is likely that the interaction stabilizes the fusion proteins in the cell.

In case of residues V166, G174 and Q205 that are adjacent to the β1-strand we observed chemical shift changes in NMR experiments upon interaction with VirB10. Changes of these residues also led to reduced VirB8-VirB10 interaction in the BTH assay. As presented in article 1, residues V166, G174 and Q205 of VirB8s undergo chemical shift changes during monomer-to-dimer transition. Based on these results, it can be hypothesized that binding to VirB10s may

174

influence VirB8s self-association during T4SS assembly. Future analyses of VirB10s will show whether the interaction with VirB8 leads to structural changes as well that may contribute to the assembly and function of the T4SS.

4.3.4 Changes of the VirB8-VirB10 interaction site affect T4SS function

A conjugation assay was used to study the effects of changes at the VirB8-VirB10 interaction in a natural biological context. I studied changes of residues at the likely interaction site identified by NMR, phage display and the BTH assay. The T4SS from plasmid pKM101 was used as a model to monitor conjugative transfer. The conjugative plasmid pKM101 from *E. coli*, carries a T4ASS similar to the VirB system from *Brucella* sharing eleven VirB protein homologs. TraE from pKM101 is the homologue of *Brucella* VirB8s and has a very similar overall structure (Terradot et a., 2005; Casu et al., 2016). I investigated the effects of changes at the β-sheet domain of TraE. Conjugation assays testing the complementation by TraE variants at positions corresponding to VirB8 residues on the β1-strand (V159-V169) and adjacent surface residues G174, T201 and Q205 showed strong effects on the efficacy of conjugation in several cases. Changes of TraE at β1-strand residues I161, N162, S163 and V164 (homologues of I165, V166, S167 and I168 in VirB8s) led to decreased conjugation. In case of I161A, we noticed a slight reduction, whereas in case of N162A, S163A and V164A significant reductions or even complete loss of conjugation was observed. In the case of variants adjacent to the β1-strand including TraE G171A and E202A and I198A (homologues of G174, T201 and Q205 in VirB8s) we also observed a reduction of conjugation. Variation at G171 and E202 of TraE strongly suppressed conjugation while I198A slightly reduced conjugation.

Results of the conjugation assays showed that changes of the VirB8 (TraE) interaction site with VirB10 (TraF) affect the functionality of the T4SS. However, the Western blot analysis showed that there were no apparent changes of the level of TraE protein variants. This result differs from observations made in case of the VirB8 fusions in the BTH assay, indicating that TraE and its variants may be stabilized by other components of the T4SS complex in the natural biological context. It was previously shown that changes of R230 located on the β4-strand of VirB8s reduced the interaction with VirB4s (Paschos et a., 2006), suggesting that the β-sheet may be the site of interaction with different T4SS components. Considering the role of VirB8/TraE for T4SS assembly, it is possible that the changes of the β1-strand and of adjacent residues affected the conformation of TraE and its interactions with other components of the T4SS complex. Further studies on the VirB8s β1-strand is required to support the role of this region in VirB8's interactions with other VirB proteins of the T4SS complex. In addition, despite similar overall structure of VirB8s and TraE, the sequence similarity between them is not very high. Therefore, we cannot assume with certainty that each equivalent amino acid is involved in the same interactions in the two T4SSs. Nevertheless, we have identified several residues of VirB8s and TraE that are important for the functionality of T4SSs and that may play a role for transient interactions between VirB8 and VirB10 homologues.

4.3.5 The potential impact of the membrane domain on VirB8 interactions

In this study, we focused on the periplasmic domain of VirB8s and its interaction with VirB10s. A previous study suggested that the transmembrane domain of VirB8s plays a role for its interaction with VirB10s (Andrieux et al., 2011). This study demonstrated that variations at the transmembrane helix of VirB8 strengthened the self-association and cross-interactions of

VirB8s with VirB10s (Andrieux et al., 2011). In addition, we showed in article 1 that a membrane-mimicking condition (addition of CHAPS) induced changes in the conformation of VirB8sp and stabilized the dimeric state of the protein. This may indicate that even the periplasmic region is influenced by association with the membrane. Further studies are needed to understand the contribution of the transmembrane domains of VirB8s and VirB10s to T4SS function and assembly. In spite of important achievements in resolving the structure of the outer membrane complex of the T4SS (Low et al., 2014) the interactions and structure of the inner membrane complex have yet to be discovered. Given the fact that the currently available information on T4SS complex structure was resulted from overexpression and purification of a subassembly of T4SS (VirB$_{3-10}$), it is expected that an *in situ* study with electron cryotomography on structure of T4SS complex can result to profound information on the stoichiometry and conformation of the complex while all the VirB proteins are present in their natural biological context. Combining our results with findings on the interactions of VirB6 with VirB8 and VirB10 (Villamil Giraldo et al., 2012; Villamil Giraldo et al., 2015) provides the basis for understanding the interactions in the inner membrane part of the T4SS complex.

Chapter 5: Appendix

5.1 Overview of VirB8 interactions with VirB5 in the T4SS

VirB5 is the minor pilin subunit and VirB2 is the major subunit of the T-pilus in *A. tumefaciens* (Schmidt-Eisenlohr, Domke, & Baron, 1999). VirB5 interacts with VirB8 and VirB10 (Yuan et al., 2005 ; Villamil Giraldo et al., 2012). VirB8 is believed to transiently interact with VirB5 to translocate it to the cell surface for pilus assembly. The X-ray crystal structure of a VirB5 homolog (TraC from the IncN plasmid pKM101) was solved, showing that TraC is a single domain protein with a three-helices bundle and a globular domain (Yeo, Yuan, Beck, Baron & Waksman, 2003). It was reported that the globular domain of VirB5 interacts with VirB8, but there is no information available on the interaction site on VirB8 (Villamil Giraldo et al., 2012).

5.2 Structural analysis of the interaction of VirB8 with VirB5

In order to identify the interaction site on VirB8, I conducted NMR HSQC experiments adding purified VirB5s to ^{15}N-labelled VirB8sp. Similar to the experimental procedure explained in articles 1 and 2, I assessed the chemical shift changes in the VirB8sp spectrum upon addition of VirB5s. Purified VirB5s at 200 µM concentration was added to ^{15}N-labelled VirB8sp at 200 µM concentration (mostly dimeric state). Analysis of the spectra revealed significant chemical shift changes or several residues including E127, Y141, S157, V166, I168, G174, R179, G203 and D232 (Fig. 21A&B). It was noticeable that most of these residues

178

(V166, I168, G174, R179, G203, D232) locate on the surface of the β-sheet domain (Fig.21C). In the NMR study presented in article 2, residues V166, G174 and R179 were part of the putative VirB8sp-VirB10sp interaction site. Conjugation studies also showed that the changes of residues from the β-sheet domain reduce T4SS function. The interaction site with VirB5s identified here strongly supports the notion that the exposed β-sheet surface plays are role for transient interactions of VirB8 with other T4SS components. In future, variants of VirB5 and of VirB8 should be studied in order to assess the biological significance of this interaction, e.g. by measuring the effects of changes on T-pilus formation.
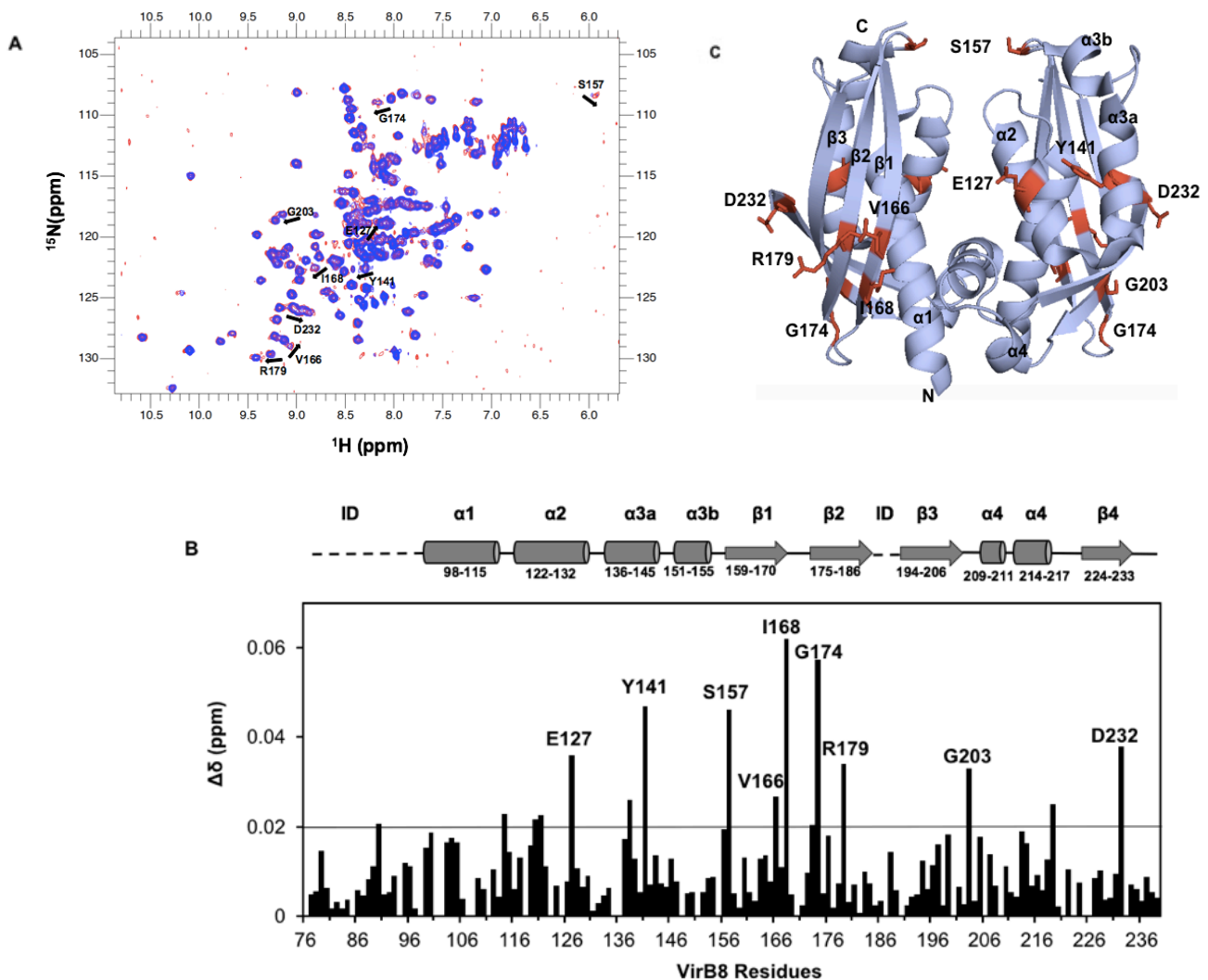
Figure 21. Mapping of chemical shift changes of VirB8sp in the presence of VirB5s. (A) Overlay of ^{1}H-^{15}N HSQC spectra of VirB8sp in the absence (blue) and in the presence (red) of one molar equivalent of VirB5s. (B) Histogram of the variations of chemical shifts [$\Delta\delta$ (ppm)] observed in ^{1}H-^{15}N HSQC spectra of ^{15}N-labeled VirB8sp after addition of VirB5s. The chemical shift perturbations were calculated with the formula $\Delta\delta=[(0.17\Delta NH)^2+(\Delta HN)^2]^{1/2}$, and are given in parts per million. $\Delta\delta HN$ values above the horizontal line are considered significant (average of changes plus one standard deviation). On top of the histogram, the secondary structural motifs of VirB8sp are presented (C) Mapping of the residues with significant chemical shift changes (shown in red as stick format) on the cartoon structure of VirB8sp (PDB code 2BHM) (Terradot et al., 2005).

Chapter 6: Concluding remarks

The focus of this thesis was to gain further insights into the role of VirB8 proteins for the assembly and function of type IV secretion systems from Gram-negative bacteria. I worked extensively on components of the VirB system from *B. suis* and I also worked on TraE from the pKM101 conjugative plasmid. Through the studies presented here, we assessed the structural dynamics of VirB8 and its interactions by combining NMR studies, X-ray crystallography and *in silico* docking with quantitative biochemical studies including thermal shift assays (DSF), the bacterial two hybrid and conjugation assays.

The first project presented in paper 1 characterized the dynamics of the periplasmic domain of *Brucella* VirB8s. First, solution NMR analyses identified VirB8sp residues that undergo chemical shift changes during monomer-to-dimer transition. Comparison of the wild-type protein with VirB8sp^{M102R} by NMR and X-ray crystallography showed the structural differences at the helical region (α-1 and α-4). Together with previous studies on VirB8 dimer inhibitors, we provided evidence for the importance of the conformation of the inhibitor-binding groove.

In the second project described in paper 2, the interaction of VirB8 with VirB10 was investigated *in vitro* and in the pKM101 type IV secretion system from *E.coli*. Using NMR experiments, we showed chemical shift changes of VirB8sp residues upon interaction with VirB10sp. The NMR results together with the results of phage display analysis identified the β1-strand region of VirB8s as the binding site for VirB10s. Subsequently, the impact of

changes of the identified residues was assessed using the BTH assay. Finally, *in vivo* conjugation assays showed the effect of changes of the β1-strand region of VirB8 homolog TraE on plasmid pKM101 conjugation.

In the appendix chapter, I present structural information on the interaction of VirB8s with VirB5s. The NMR analysis identified several residues from the β-sheet surface of VirB8sp that may contribute to the interaction. Interestingly, some of these residues were also identified by NMR as contributing to the VirB8sp-VirB10sp interaction. In article 2, several biochemical approaches were used to verify that the β-sheet region (the β1-strand in particular) is the interaction interface of VirB8 with VirB10. Analysis of the VirB8-VirB5 require similar approaches in future.

Several studies can be designed as the future work based on the finding of this research to better understand the T4SS function. The role of VirB8 α4 helix in dimerization is identified in this work and provides the basis to study the dynamics of VirB8 in the T4SS complex. The functionality of the T4SS complex should be studied for variants of VirB8 at the α4 helix. In addition, these VirB8 variants at α4 helix can be studied through fragment screening for design and development of inhibitors specific to dimer VirB8. The conformation of the VirB8's surface groove was important for binding of fragments, therefore the surface groove of VirB8 can be studied as a new target site for fragment screening and inhibition studies. Most of the findings in this research are resulted from studies on periplasmic fragment of VirB8. The roles of the inner membrane and VirB8's membrane domain on VirB8's interactions in T4SS complex are not identified. These questions should be addressed by studies on full-length VirB8 and comparisons

with the results from periplasmic VirB8. NMR studies on full-length VirB8 should be carried out in presence of micelles or liposomes to mimic the membrane environment. Co-crystallization of full-length VirB8 in complex with VirB10 or VirB6 will complement our current knowledge on VirB8 interactions and the interfaces. In this study, VirB8 β-sheet has been suggested as the potential interface for interactions with VirB5. This hypothesis should be addressed by conducting studies based on VirB8 variants at the interface and the resulted effect on the functionality of the complex and pilus formation. Since VirB8 β-sheet is the interface for interactions with VirB10 and VirB5, it is important to study the role of this interface for interactions within the inner membrane part of T4SS complex and its interaction with VirB6 and VirB3. These interactions can be studied through NMR analysis and SPR experiments on VirB8 variants at the β-sheet in complex with VirB6 and/or ViB3.

The overall findings presented in this thesis emphasize on the importance of VirB8 as assembly factor that interacts with other components of the complex. As presented in Figure 22, this research provides important information on the dynamic contributions of VirB8 to T4SS assembly and function. Moreover, the results presented in this thesis provide novel information on the basis of interactions between inner membrane T4SS compartments thereby contributing to understanding the structure and assembly of the T4SS inner membrane complex.
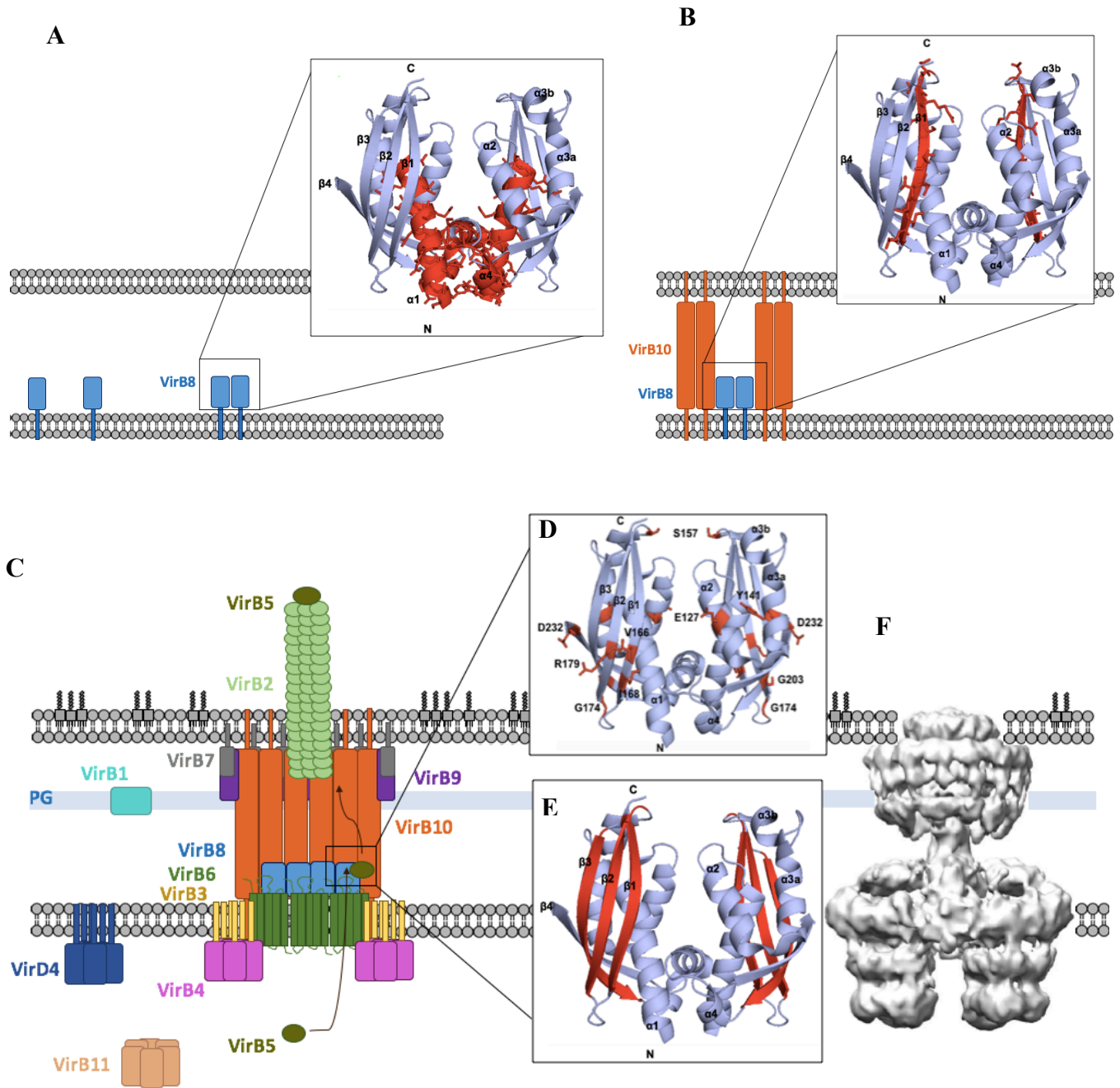
Figure 22. A model for the dynamics of VirB8 during T4SS assembly. A) Changes in dynamics of VirB8 structure upon dimerization, important identified regions (α-1 and α-4 helices) are shown in red. B) Changes in dynamics of VirB8 structure upon interaction with VirB10, the identified region (β1-strand) is shown in red. C) Changes in dynamics of VirB8 structure in the T4SS complex. D) VirB8sp residues changing their conformations upon interaction with VirB5

are shown in red. E) β-sheet surface of VirB8 (shown in red) is the potential interface for interactions with other VirB proteins, e.g. with VirB10 and VirB5. F) The reconstituted structure of a T4SS$_{3-10}$ complex is shown (Low et al., 2014).

References

Adcox, H. E., Vasicek, E. M., Dwivedi, V., Hoang, K. V., Turner, J., & Gunn, J. S. (2016). *Salmonella* extracellular matrix components influence biofilm formation and gallbladder colonization. *Infect. Immun.*, *84*(11), 3243-3251.

Alvarez-Martinez, C. E., & Christie, P. J. (2009). Biological diversity of prokaryotic type IV secretion systems. *Microbiol Mol Biol Rev, 73*(4), 775-808.

Aly, K., & Baron, C. (2007). VirB5 initiates T-pilus assembly in *Agrobacterium tumefaciens* and localizes at the pilus tip. *Microbiol., 153*, 3766-3775.

Andrieux, L., Bourg, G., Pirone, A., O'Callaghan, D., & Patey, G. (2011). A single amino acid change in the transmembrane domain of the VirB8 protein affects dimerization, interaction with VirB10 and *Brucella suis* virulence. *FEBS let.*, *585*(15), 2431-2436.

Atmakuri, K., Cascales, E., & Christie, P. J. (2004). Energetic components VirD4, VirB11 and VirB4 mediate early DNA transfer reactions required for bacterial type IV secretion. *Mol. Microbiol., 54*, 1199-1211.

Austin, J. W., Sanders, G., Kay, W. W., & Collinson, S. K. (1998). Thin aggregative fimbriae enhance *Salmonella enteritidis* biofilm formation. *FEMS Microbiol Lett, 162*(2), 295-301.

Bailey, S., Ward, D., Middleton, R., Grossmann, J. G., & Zambryski, P. (2006). *Agrobacterium tumefaciens* VirB8 structure reveals potential protein-protein interactions sites. *Proc. Natl. Acad. Sci. USA, 103*(8), 2582-2587.

Balakrishnan, L., Hughes, C., & Koronakis, V. (2001). Substrate-triggered recruitment of the TolC channel-tunnel during type I export of hemolysin by *Escherichia coli*. *J Mol Biol, 313*(3), 501-510.

Baron, C. (2005). From bioremediation to biowarfare: On the impact and mechanism of type IV secretion systems. *FEMS Microbiol. Lett., 253*, 163-170.

Baron, C., Thorstenson, Y. R., & Zambryski, P. C. (1997). The lipoprotein VirB7 interacts with VirB9 in the membranes of *Agrobacterium tumefaciens*. *J. Bacteriol., 179*, 1211-1218.

Berger, B. R., & Christie, P. J. (1994). Genetic complementation analysis of the *Agrobacterium tumefaciens* virB operon: virB2 through virB11 are essential virulence genes. *J. Bacteriol., 176*, 3646-3660.

Blocker, A., Jouihri, N., Larquet, E., Gounon, P., Ebel, F., Parsot, C., ... & Allaoui, A. (2001). Structure and composition of the *Shigella flexneri* 'needle complex', a part of its type III secreton. *Mol. Microbial.*, *39*(3), 652-663.

Bourg, G., Sube, R., O'Callaghan, D., & Patey, G. (2009). Interactions between *Brucella suis* VirB8 and its homolog TraJ from the plasmid pSB102 underline the dynamic nature of type IV secretion systems. *J Bacteriol, 191*(9), 2985-2992.

Boyer, F., Fichant, G., Berthod, J., Vandenbrouck, Y., & Attree, I. (2009). Dissecting the bacterial type VI secretion system by a genome wide in silico analysis: what can be learned from available microbial genomic resources?. *BMC genomics*, *10*(1), 104.

Busch, A., & Waksman, G. (2012). Chaperone–usher pathways: diversity and pilus assembly mechanism. *Phil. Trans. R. Soc. B*, *367*(1592), 1112-1122.

Cascales, E., & Christie, P. J. (2004a). Definition of a bacterial type IV secretion pathway for a DNA substrate. *Science*, *304*(5674), 1170-1173.

Cascales, E., & Christie, P. J. (2004b). Agrobacterium VirB10, an ATP energy sensor required for type IV secretion. *Proc. Natl. Acad. Sci. USA*, *101*(49), 17228-17233.

Casu, B., Smart, J. P., Hancock, M. A., Smith, M., Sygusch, J. & Baron, C. (2016) Structural analysis and inhibition of TraE from the pKM101 type IV secretion system, *J. Biol. Chem*, PMID: 27634044

Chandran, V., Fronzes, R., Duquerroy, S., Cronin, N., Navaza, J., & Waksman, G. (2009). Structure of the outer membrane complex of a type IV secretion system. *Nature, 29*, 29.

Christie, P. J. (2001). Type IV secretion: intercellular transfer of macromolecules by systems ancestrally related to conjugation machines. *Mol. Microbiol., 40*, 294- 305.

Christie, P. J. (2004). Type IV secretion: the *Agrobacterium* VirB/D4 and related conjugation systems. *Biochim. Biophys. Acta, 1694*, 219-234.

Christie, P. J., Atmakuri, K., Krishnamoorthy, V., Jakubowski, S., & Cascales, E. (2005). Biogenesis, Architecture, and Function of Bacterial Type IV Secretion Systems. *Annu. Rev. Microbiol., 59*, 415-485.

Christie, P. J., Whitaker, N., & González-Rivera, C. (2014). Mechanism and structure of the bacterial type IV secretion systems. *Biochim. Biophys. Acta (BBA)*, *1843*(8), 1578-1591.

Cianfanelli, F. R., Monlezun, L., & Coulthurst, S. J. (2016). Aim, load, fire: the type VI secretion system, a bacterial nanoweapon. *Trends in microbial.*, *24*(1), 51-62.

Costa, T. R., Felisberto-Rodrigues, C., Meir, A., Prevost, M. S., Redzej, A., Trokter, M., & Waksman, G. (2015). Secretion systems in Gram-negative bacteria: structural and mechanistic insights. *Nat. Rev. Microbiol.*, *13*(6), 343-359.

Das, A., & Xie, Y.-H. (2000). The *Agrobacterium* T-DNA transport pore proteins VirB8, VirB9 and VirB10 interact with one another. *J. Bacteriol., 182*, 758-763.

Delaglio, F., Grzesiek, S., Vuister, G. W., Zhu, G., Pfeifer, J., and Bax, A. (1995) NMRPipe: a multidimensional spectral processing system based on UNIX pipes, *J Biomol NMR 6*, 277-293.

Deng, W., Marshall, N. C., Rowland, J. L., McCoy, J. M., Worrall, L. J., Santos, A. S., ... & Finlay, B. B. (2017). Assembly, structure, function and regulation of type III secretion systems. *Nat. Rev. Microbiol.*, *15*(6), 323-337.

Desvaux, M., Hebraud, M., Talon, R., & Henderson, I. R. (2009). Secretion and subcellular localizations of bacterial proteins: a semantic awareness issue. *Trends Microbiol, 17*(4), 139-145.

Ding, Z., Zhao, Z., Jakubowski, S., Krishnamohan, A., Margolin, W., & Christie, P. J. (2002). A novel cytology-based, two-hybrid screen for bacteria applied to protein- protein interaction studies of a type IV secretion system. *J. Bacteriol., 184*(20), 5572-5582.

Du, D., Wang, Z., James, N. R., Voss, J. E., Klimont, E., Ohene-Agyei, T., ... & Luisi, B. F. (2014). Structure of the AcrAB-TolC multidrug efflux pump. *Nature*, *509*(7501), 512-515.

Eisenbrandt, R., Kalkum, M., Lai, E. M., Lurz, R., Kado, C. I., & Lanka, E. (1999). Conjugative pili of IncP plasmids, and the Ti plasmid T pilus are composed of cyclic subunits. *J. Biol. Chem.*, *274*(32), 22548-22555.

Fernandez, D., Dang, T. A. T., Spudich, G. M., Zhou, X.-R., Berger, B. R., & Christie, P. J. (1996). The *Agrobacterium tumefaciens* virB7 gene product, a proposed component of the T-complex transport apparatus, is a membrane-associated lipoprotein exposed at the periplasmic surface. *J. Bacteriol., 178*, 3156-3167.

Fernandez, D., Spudich, G. M., Zhou, X.-R., & Christie, P. J. (1996). The *Agrobacterium tumefaciens* virB7 lipoprotein is required for stabilization of VirB proteins during assembly of the T-complex transport apparatus. *J. Bacteriol., 178*, 3168-3176.

Fronzes, R., Schafer, E., Wang, L., Saibil, H. R., Orlova, E. V., & Waksman, G. (2009). Structure of a type IV secretion system core complex. *Science, 323*(5911), 266- 268.

Fullner, K. J., Lara, J. C., & Nester, E. W. (1996). Pilus assembly by *Agrobacterium* T-DNA transfer genes. *Science*, *273*(5278), 1107.

Gerlach, R. G., & Hensel, M. (2007). Protein secretion systems and adhesins: the molecular armory of Gram-negative pathogens. *Int. J. Med. Microbiol.*, *297*(6), 401-415.

Ghosal, D., Chang, Y. W., Jeong, K. C., Vogel, J. P., & Jensen, G. J. (2017). In situ structure of the Legionella Dot/Icm type IV secretion system by electron cryotomography. *EMBO rep.*, *18*(5), 726-732.

Gibson, D. L., White, A. P., Rajotte, C. M., & Kay, W. W. (2007). AgfC and AgfE facilitate extracellular thin aggregative fimbriae synthesis in *Salmonella enteritidis*. *Microbiol.*, *153*(4), 1131-1140.

Gillespie, J. J., Phan, I. Q., Scheib, H., Subramanian, S., Edwards, T. E., Lehman, S. S., ... & Taira, S. (2015). Structural insight into how bacteria prevent interference between multiple divergent type IV secretion systems. *MBio*, *6*(6), e01867-15.

Goessweiner-Mohr, N., Arends, K., Keller, W., & Grohmann, E. (2013). Conjugative type IV secretion systems in Gram-positive bacteria. *Plasmid*, *70*(3), 289-302.

Goyal, P., Krasteva, P. V., Van Gerven, N., Gubellini, F., Van den Broeck, I., Troupiotis-Tsaïlaki, A., ... & Hultgren, S. J. (2014). Structural and mechanistic insights into the bacterial amyloid secretion channel CsgG. *Nature*, *516*(7530), 250-253.

Green, E. R., & Mecsas, J. (2016). Bacterial secretion systems–an overview. *Microbiol. Spect.*, *4*(1).

Guglielmini, J., Néron, B., Abby, S. S., Garcillán-Barcia, M. P., la Cruz, F. D., & Rocha, E. P. (2014). Key components of the eight classes of type IV secretion systems involved in bacterial conjugation or protein secretion. *Nucl. acids res.*, *42*(9), 5715-5727.

Hammer, N. D., McGuffie, B. A., Zhou, Y., Badtke, M. P., Reinke, A. A., Brännström, K., ... & Chapman, M. R. (2012). The C-terminal repeating units of CsgB direct bacterial functional amyloid nucleation. *J. Mol. Biol.*, *422*(3), 376-389.

Hapfelmeier, S., Domke, N., Zambryski, P. C., & Baron, C. (2000). VirB6 is required for stabilization of VirB5, VirB3 and formation of VirB7 homodimers in *Agrobacterium tumefaciens*. *J. Bacteriol., 182*, 4505-4511.

Henderson, I. R., Cappello, R., & Nataro, J. P. (2000). Autotransporter proteins, evolution and redefining protein secretion. *Trends Microbiol, 8*(12), 529-532.

Ho, B. T., Dong, T. G., & Mekalanos, J. J. (2014). A view to a kill: the bacterial type VI secretion system. *Cell host & microbe*, *15*(1), 9-21.

Höppner, C., Liu, Z., Domke, N., Binns, A. N., & Baron, C. (2004). VirB1 orthologs from *Brucella suis* and pKM101 complement defects of the lytic transglycosylase required for efficient type IV secretion from *Agrobacterium tumefaciens*. *J. Bacteriol., 186*, 1415-1422.

Höppner, C., Carle, A., Sivanesan, D., Hoeppner, S., & Baron, C. (2005). The putative lytic transglycosylase VirB1 from *Brucella suis* interacts with the type IV secretion system core components VirB8, VirB9 and VirB11. *Microbiology, 151*, 3469-3482.

Hospenthal, M. K., Costa, T., & Waksman, G. (2017). Pilus biogenesis at the inner and outer membranes of Gram-negative bacteria. *Nat. Rev. Microb*.

Houben, E. N., Korotkov, K. V., & Bitter, W. (2014). Take five—Type VII secretion systems of Mycobacteria. *Bioch. Biophys. Acta (BBA)*, *1843*(8), 1707-1716.

Jakubowski, S. J., Krishnamoorthy, V., Cascales, E., & Christie, P. J. (2004). *Agrobacterium tumefaciens* VirB6 domains direct the ordered export of a DNA substrate through a type IV secretion System. *J. Mol. Biol., 341*, 961-977.

Jakubowski, S. J., Cascales, E., Krishnamoorthy, V., & Christie, P. J. (2005). *Agrobacterium tumefaciens* VirB9, an outer-membrane-associated component of a type IV secretion system, regulates substrate selection and T-Pilus biogenesis. *J. Bacteriol., 187*, 3486-3495.

Jones, A. L., Shirasu, K., & Kado, C. I. (1994). The product of the *virB4* gene of *Agrobacterium tumefaciens* promotes accumulation of VirB3 protein. *J. Bacteriol., 176*, 5255-5261.

Judd, P. K., Kumar, R. B., & Das, A. (2005a). Spatial location and requirements for the assembly of the *Agrobacterium tumefaciens* type IV secretion apparatus. *Proc. Natl. Acad. Sci. USA*(102), 11498-11503.

Judd, P. K., Kumar, R. B., & Das, A. (2005b). The type IV secretion apparatus protein VirB6 of *Agrobacterium tumefaciens* localizes to a cell pole. *Mol. Microbiol., 55*, 115-124.

Kerr, J. E., & Christie, P. J. (2010). Evidence for VirB4-mediated dislocation of membrane-integrated VirB2 pilin during biogenesis of the *Agrobacterium* VirB/VirD4 type IV secretion system. *J. Bacteriol.*, *192*(19), 4923-4934.

Korotkov, K. V., Sandkvist, M., & Hol, W. G. (2012). The type II secretion system: biogenesis, molecular architecture and mechanism. *Nat. Rev. Microbiol.*, *10*(5), 336-351.

Korotkova, N., Freire, D., Phan, T. H., Ummels, R., Creekmore, C. C., Evans, T. J., ... & Korotkov, K. V. (2014). Structure of the *Mycobacterium tuberculosis* type VII secretion system chaperone EspG5 in complex with PE25–PPE41 dimer. *Mol. Microbiol., 94*(2), 367-382.

Kube, S., Kapitein, N., Zimniak, T., Herzog, F., Mogk, A., & Wendler, P. (2014). Structure of the VipA/B type VI secretion complex suggests a contraction-state-specific recycling mechanism. *Cell reports*, *8*(1), 20-30.

Kubori, T., Matsushima, Y., Nakamura, D., Uralil, J., Lara-Tejero, M., Sukhan, A., ... & Aizawa, S. I. (1998). Supramolecular structure of the *Salmonella typhimurium* type III protein secretion system. *Science*, *280*(5363), 602-605.

Kubori, T., Koike, M., Bui, X. T., Higaki, S., Aizawa, S. I., & Nagai, H. (2014). Native structure of a type IV secretion system core complex essential for *Legionella* pathogenesis. *Proc. Natl. Acad. Sci. U.S.A.*, *111*(32), 11804-11809.

Kuldau, G. A., Vos, G., Owen, J., McCaffrey, G., & Zambryski, P. (1990). The virB operon of *Agrobacterium tumefaciens* pTiC58 encodes 11 open reading frames. *Mol. Gen. Gen. MGG*, *221*(2), 256-266.

Kumar, R. B., & Das, A. (2001). Functional analysis of the *Agrobacterium tumefaciens* T-DNA transport pore protein VirB8. *J. Bacteriol., 183*, 3636-3641.

Lai, E. M., Chesnokova, O., Banta, L. M., & Kado, C. I. (2000). Genetic and Environmental Factors Affecting T-Pilin Export and T-Pilus Biogenesis in Relation to Flagellation of *Agrobacterium tumefaciens*. *J. Bacteriol.*, *182*(13), 3705-3716.

Lai, E. M., Eisenbrandt, R., Kalkum, M., Lanka, E., & Kado, C. I. (2002). Biogenesis of T pili in *Agrobacterium tumefaciens* requires precise VirB2 propilin cleavage and cyclization. *J. Bacteriol*, *184*(1), 327-330.

Leo, J. C., Grin, I., & Linke, D. (2012). Type V secretion: mechanism (s) of autotransport through the bacterial outer membrane. *Phil. Trans. R. Soc. B*, *367*(1592), 1088-1101.

Lillington, J., Geibel, S., & Waksman, G. (2014). Biogenesis and adhesion of type 1 and P pili. *Biochim. Biophys Acta (BBA)*, *1840*(9), 2783-2793.

Low, H. H., Gubellini, F., Rivera-Calzada, A., Braun, N., Connery, S., Dujeancourt, A., ... & Waksman, G. (2014). Structure of a type IV secretion system. *Nature*, *508*(7497), 550-553.

Lycklama Nijeholt, J. A. L., & Driessen, A. J. (2012). The bacterial Sec-translocase: structure and mechanism. *Phil. Trans. R. Soc. B*, *367*(1592), 1016-1028.

Ma, L. S., Lin, J. S., & Lai, E. M. (2009). An IcmF family protein, ImpLM, is an integral inner membrane protein interacting with ImpKL, and its walker a motif is required for type VI secretion system-mediated Hcp secretion in *Agrobacterium tumefaciens*. *J. Bacteriol.*, *191*(13), 4316-4329.

Mandava, S., Makowski, L., Devarapalli, S., Uzubell, J., & Rodi, D. J. (2004). RELIC–A bioinformatics server for combinatorial peptide analysis and identification of protein-ligand interaction sites. *Proteomics*, *4*(5), 1439-1460.

Marlovits, T. C., & Stebbins, C. E. (2010). Type III secretion systems shape up as they ship out. *Curr. Opin. Microbiol.*, *13*(1), 47-52.

Middleton, R., Sjölander, K., Krishnamurthy, N., Foley, J., & Zambryski, P. (2005). Predicted hexameric structure of the *Agrobacterium* VirB4 C terminus suggests VirB4 acts as a docking site during type IV secretion. *Proc. Natl. Acad. Sci. USA, 102*, 1685-1690.

Molin, S., & Tolker-Nielsen, T. (2003). Gene transfer occurs with enhanced efficiency in biofilms and induces enhanced stabilisation of the biofilm structure. *Curr. Opin. Biotechn.*, *14*(3), 255-261.

Mota, L. J., & Cornelis, G. R. (2005). The bacterial injection kit: type III secretion systems. *Ann Med, 37*(4), 234-249.

Mudrak, B., & Kuehn, M. J. Specificity of the type II secretion systems of enterotoxigenic *Escherichia coli* and *Vibrio cholerae* for heat-labile enterotoxin and cholera toxin. *J Bacteriol, 2010*, 22.

Murakami, S., Nakashima, R., Yamashita, E., & Yamaguchi, A. (2002). Crystal structure of bacterial multidrug efflux transporter AcrB. *Nature*, *419*(6907), 587-593.

Nagai, H., & Kubori, T. (2011). Type IVB secretion systems of Legionella and other Gram-negative bacteria. *Front. Microbiol.*, *2*.

Nakashima, R., Sakurai, K., Yamasaki, S., Nishino, K., & Yamaguchi, A. (2011). Structures of the multidrug exporter AcrB reveal a proximal multisite drug-binding pocket. *Nature*, *480*(7378), 565-569.

Nans, A., Kudryashev, M., Saibil, H. R., & Hayward, R. D. (2015). Structure of a bacterial type III secretion system in contact with a host membrane in situ. *Nat. commu.*, *6*, 10114.

Nivaskumar, M., & Francetic, O. (2014). Type II secretion system: a magic beanstalk or a protein escalator. *Biochim. Biophys Acta (BBA)*, *1843*(8), 1568-1577.

O´Callaghan, D., Cazevieille, C., Allardet-Servent, A., Boschiroli, M. L., Bourg, G., Foulongne, V., et al. (1999). A homologue of the *Agrobacterium tumefaciens* VirB and *Bordetella pertussis* Ptl type IV secretion systems is essential for intracellular survival of *Brucella suis*. *Mol. Microbiol., 33*, 1210-1220.

Palmer, T., & Berks, B. C. (2012). The twin-arginine translocation (Tat) protein export pathway. *Nat. Rev. Microbiol.*, *10*(7), 483-496.

Paschos, A., Patey, G., Sivanesan, D., Bayliss, R., Waksman, G., O'Callaghan, D., et al. (2006). Dimerization and interactions of *Brucella suis* VirB8 with VirB4 and VirB10 are required for its biological activity. *Proc Natl Acad Sci U S A, 103*(19), 7252-7257.

Paschos, A., Den Hartigh, A., Smith, M. A., Atluri, V. L., Sivanesan, D., Tsolis, R. M., & Baron, C. (2011). An in vivo high-throughput screening approach targeting the type IV secretion system component VirB8 identified inhibitors of *Brucella abortus 2308* proliferation. *Infect. Immun.*, *79*(3), 1033-1043.

Patey, G., Qi, Z., Bourg, G., Baron, C., & O'Callaghan, D. (2006). Swapping of periplasmic domains between *Brucella suis* VirB8 and a pSB102 VirB8 homologue allows heterologous complementation. *Infect. Immun*, *74*(8), 4945-4949.

Piddock, L. J. (2006). Multidrug-resistance efflux pumps? not just for resistance. *Nat. Rev. Microbiol.*, *4*(8), 629-636.

Porter, C. J., Bantwal, R., Bannam, T. L., Rosado, C. J., Pearce, M. C., Adams, V., ... & Rood, J. I. (2012). The conjugation protein TcpC from *Clostridium perfringens* is structurally related to the type IV secretion system protein VirB8 from Gram-negative bacteria. *Mol. Microbiol*, *83*(2), 275-288.

Rambow-Larsen, A. A., Petersen, E. M., Gourley, C. R., & Splitter, G. A. (2009). *Brucella* regulators: self-control in a hostile environment. *Trends Microbiol, 17*(8), 371-377.

Redzej, A., Waksman, G., & Orlova, E. (2015). Structural studies of T4S systems by electron microscopy. *AIMS Biophysics*, *2*(2), 184-199.

Reichow, S. L., Korotkov, K. V., Hol, W. G., & Gonen, T. (2010). Structure of the cholera toxin secretion channel in its closed state. *Nat. struct. & mol. Boil.*, *17*(10), 1226-1232.

Roggenkamp, A., Ackermann, N., Jacobi, C. A., Truelzsch, K., Hoffmann, H., & Heesemann, J. (2003). Molecular analysis of transport and oligomerization of the *Yersinia enterocolitica* adhesin YadA. *J. Bacteriol.*, *185*(13), 3735-3744.

Roman-Hernandez, G., Peterson, J. H., & Bernstein, H. D. (2014). Reconstitution of bacterial autotransporter assembly using purified components. *Elife*, *3*, e04234.

Sagulenko, E., Sagulenko, V., Chen, J., & Christie, P. J. (2001). Role of *Agrobacterium* VirB11 ATPase in T-pilus assembly and substrate selection. *J. Bacteriol*, *183*(20), 5813-5825.

Schmidt-Eisenlohr, H., Domke, N., Angerer, C., Wanner, G., Zambryski, P. C., & Baron, C. (1999). Vir proteins stabilize VirB5 and mediate its association with the T pilus of *Agrobacterium tumefaciens*. *J. Bacteriol., 181*, 7485-7492.

Schmidt-Eisenlohr, H., Domke, N., & Baron, C. (1999). TraC of IncN plasmid pKM101 associates with membranes and extracellular high molecular weight structures in *Escherichia coli*. *J. Bacteriol., 181*, 5563-5571.

Seubert, A., Hiestand, R., de la Cruz, F., & Dehio, C. (2003). A bacterial conjugation machinery recruited for pathogenesis. *Mol. Microbiol., 49*, 1253-1266.

Sivanesan, D., & Baron, C. (2011). The dimer interface of *Agrobacterium tumefaciens* VirB8 is important for type IV secretion system function, stability, and association of VirB2 with the core complex. *J. Bacteriol*, *193*(9), 2097-2106.

Sivanesan, D., Hancock, M. A., Villamil Giraldo, A. M., & Baron, C. (2010). Quantitative Analysis of VirB8− VirB9− VirB10 Interactions Provides a Dynamic Model of Type IV Secretion System Core Complex Assembly. *Biochemistry*, *49*(21), 4483-4493.

Villamil Giraldo, A. M., Sivanesan, D., Carle, A., Paschos, A., Smith, M. A., Plesa, M., ... & Baron, C. (2012). Type IV secretion system core component VirB8 from *Brucella* binds to the globular domain of VirB5 and to a periplasmic domain of VirB6. *Biochem.*, *51*(18), 3881-3890.

Stanley, S. A., Raghavan, S., Hwang, W. W., & Cox, J. S. (2003). Acute infection and macrophage subversion by *Mycobacterium tuberculosis* require a specialized secretion system. *Proc. Natl. Acad. Sci. USA*, *100*(22), 13001-13006.

Sutherland, M. C., Binder, K. A., Cualing, P. Y., & Vogel, J. P. (2013). Reassessing the role of DotF in the *Legionella pneumophila* type IV secretion system. *PloS one*, *8*(6), e65529.

Tato, I., Zunzunegui, S., De La Cruz, F., & Cabezon, E. (2005). TrwB, the coupling protein involved in DNA transport during bacterial conjugation, is a DNA-dependent ATPase. *Proc. Natl. Acad. Sci. USA.*, *102*(23), 8156-8161.

Terradot, L., Bayliss, R., Oomen, C., Leonard, G., Baron, C., & Waksman, G. (2005). Crystal Structures of the periplasmic domains of two core subunits of the bacterial type IV secretion system, VirB8 from *Brucella suis* and ComB10 from *Helicobacter pylori*. *Proc. Natl. Acad. Sci. USA, 102*, 4596-4601.

Thanassi, D. G., Bliska, J. B., & Christie, P. J. (2012). Surface organelles assembled by secretion systems of Gram-negative bacteria: diversity in structure and function. *FEMS Microbiol. Rev.*, *36*(6), 1046-1082.

Trokter, M., Felisberto-Rodrigues, C., Christie, P. J., & Waksman, G. (2014). Recent advances in the structural and molecular biology of type IV secretion systems. *Curr. Opin. Struct Biol*, *27*, 16-23.

Villamil Giraldo, A. M., Sivanesan, D., Carle, A., Paschos, A., Smith, M. A., Plesa, M., ... & Baron, C. (2012). Type IV secretion system core component VirB8 from *Brucella* binds to the globular domain of VirB5 and to a periplasmic domain of VirB6. *Biochemistry*, *51*(18), 3881-3890.

Villamil Giraldo, A. M. V., Mary, C., Sivanesan, D., & Baron, C. (2015). VirB6 and VirB10 from the *Brucella* type IV secretion system interact via the N-terminal periplasmic domain of VirB6. *FEBS letters*, *589*(15), 1883-1889.

Vincent, C. D., Friedman, J. R., Jeong, K. C., Buford, E. C., Miller, J. L., & Vogel, J. P. (2006). Identification of the core transmembrane complex of the *Legionella* Dot/Icm type IV secretion system. *Mol. Microbiol.*, *62*(5), 1278-1291.

Voth, D. E., Broederdorf, L. J., & Graham, J. G. (2012). Bacterial Type IV secretion systems: versatile virulence machines. *Future Microbiol*, *7*(2), 241-257.

Walldén, K., Williams, R., Yan, J., Lian, P. W., Wang, L., Thalassinos, K., ... & Waksman, G. (2012). Structure of the VirB4 ATPase, alone and bound to the core complex of a type IV secretion system. *Proc. Natl. Acad. Sci. USA,109*(28), 11348-11353.

Ward, D., Draper, O., Zupan, J. R., & Zambryski, P. C. (2002). Peptide linkage mapping of the *A. tumefaciens* vir-encoded type IV secretion system reveals novel protein subassemblies. *Proc. Natl. Acad. Sci. USA, 99*, 11493-11500.

Waters, M. G., & Pfeffert, S. R. (1999). Membrane tethering in intracellular transport. *Curr. Opin. Cell Biol.*, *11*(4), 453-459.

Wright, K. J., Seed, P. C., & Hultgren, S. J. (2007). Development of intracellular bacterial communities of uropathogenic *Escherichia coli* depends on type 1 pili. *Cell. Microbiol*, *9*(9), 2230-2241.

Yeo, H.-J., Yuan, Q., Beck, M. R., Baron, C., & Waksman, G. (2003). Structural and functional characterization of the VirB5 protein from the type IV secretion system encoded by the conjugative plasmid pKM101. *Proc. Natl. Acad. Sci. USA, 100*, 15947-15962.

Yeo, H. J., Savvides, S. N., Herr, A. B., Lanka, E., & Waksman, G. (2000). Crystal structure of the hexameric traffic ATPase of the *Helicobacter pylori* type IV secretion system. *Mol. Cell, 6*, 1461-1472.

Yuan, Q., Carle, A., Gao, C., Sivanesan, D., Aly, K., Höppner, C., et al. (2005). Identification of the VirB4-VirB8-VirB5-VirB2 pilus assembly sequence of type IV secretion systems. *J. Biol. Chem., 280*, 26349-26359.

Zahrl, D., Wagner, M., Bischof, K., Bayer, M., Zavecz, B., Beranek, A., et al. (2005a). Peptidoglycan degradation by specialized lytic transglycosylases associated with type III and type IV secretion systems. *Microbiol., 151*, 3455-3467.

Zupan, J., Muth, T. R., Draper, O., & Zambryski, P. C. (2000). The transfer of DNA from *Agrobacterium tumefaciens* into plants: A feast of fundamental insights. *Plant J., 23*, 11-28.